Exploring Electrophysiological Features of Pain in Freely Moving Mice

Heidelberg University

Presented by

Jiaojiao Zhang

October 2020

Dissertation

submitted to the

Combined Faculty of Natural Sciences and Mathematics

of the Ruperto Carola University Heidelberg, Germany

for the degree of

Doctor of Natural Sciences

Presented by

Jiaojiao Zhang, M. Sc.

Born in Xuzhou, China

Oral-examination: October 22nd, 2020

Exploring electrophysiological features of pain in freely moving mice

Referees:

Prof. Dr. med. Andreas Draguhn

Prof. Dr. Hilmar Bading

Declaration of authorship

Declarations according to the doctoral regulations, I hereby declare that:

- I have written this dissertation by myself, and I have used no other sources of materials than those indicated in the dissertation.
- Regarding the experiments and analysis jointly performed in Chapter 3.1 with Simon Ponsel has been annotated in this respect; Analysis in Chapter 3.1.4 has been annotated as performed by Maximilian Pilz.
- Regarding the custom built apparatus in Chapter 3.2, the construction has been annotated as supported by Lee Embray (electronics) and Jürgen Schmitt (mechanics).
- I have not applied to be examined at any other institution, nor have I submitted the dissertation to any other faculty.

Heidelberg, August 04, 2020

……

Jiaojiao Zhang

Contents

Abstract

Multiple brain regions are involved in pain processing, contributing to a complex pattern of neuronal activation in specific brain structures referred to as pain matrix. Activation of this system may lead to a specific pain signature which remains, however, to be identified. As a step towards this end, I recorded local field potentials from multiple brain regions of the mouse under different pain-inducing conditions to explore specific electrophysiological features of this state.

In a first series of experiments, acute pain was induced by capsaicin, and neuronal network oscillations were recorded from different relevant brain regions: primary somatosensory cortex (S1), the anterior cingulate cortex (ACC), the ventral posterolateral thalamic nucleus (VPL), the posterior insula (Ins), the central nucleus of the amygdala (AMYG), the olfactory bulb (OB) and parietal cortex (PAC). Pain-specific alterations were most prominent in higher-order phenomena of neuronal network oscillations like interregional coherence. By selecting parameters from these multi-dimensional with logistic regression, acute pain states could be successfully classified in our data set.

As a second, methodological step, I constructed an apparatus for sensory testing of evoked potentials in freely moving mice. Using this custom built apparatus, evoked laser-light and mechanical stimulations were performed in both naïve mice and in mice with inflammatory pain. Enhanced peak amplitudes of evoked potentials were observed in multiple brain regions in different pain conditions, with specific and different patterns.

These results together reveal specific alterations of neuronal activity across brain regions, in different pain conditions. Although the mechanisms of pain processing in different types of pain may differ, they all share common sensory, affective and behavioral aspects. These lead to specific electrophysiological characteristics which may help shedding light on the mechanism study of pain, as well as to develop physiological markers for specific pain conditions.

Zusammenfassung

Mehrere Hirnregionen sind an der Schmerzverarbeitung beteiligt und führen so zu einem komplexen Muster der neuronalen Aktivierung bei Schmerzen. Diese „Schmerzmatrix“ kann zu einer spezifischen funktionellen Signatur von Schmerzen führen, die jedoch bisher nicht bekannt ist. Ich habe in meiner Arbeit lokale Feldpotenziale in mehreren Hirnregionen der Maus in verschiedenen Zuständen von Schmerzwahrnehmung gemessen, um solche spezifischen elektrophysiologischen Merkmale zu identifizieren.

Im ersten Projekt habe ich veränderte Netzwerk-Aktivität bei akuten, durch Capsaicin induzierten Schmerzen gemessen, und dazu von folgenden Hirnregionen in vivo abgeleitet: Primärer somatosensorischer Kortex (S1), vorderer cingulärer cortex (ACC), ventraler posterolateraler thalamischer Kerns (VPL), hintere Insula (Ins), zentraler Kerns der Amygdala (AMYG), olfaktorischer Kortex (OB) und parietaler Kortex (PAC). Veränderungen zeigten sich vor Allem bei Phänomenen höherer Ordnung wie der interregionalen Kohärenz von Netzwerk-Oszillationen. Mittels logistischer Regression wurden systematisch Parameter ausgewählt, mit denen letztlich eine Klassifizierung der Aktivität bei Schmerz gegenüber Kontrolldaten gelang.

In einem zweiten Projektteil habe ich einen Versuchsaufbau entwickelt und angewandt, mit dem evozierte Potenziale bei frei beweglichen Mäusen untersucht werden können. Dieses Gerät wurden angewandt, um elektrophysiologische und Verhaltens-Antworten auf Stimulation mit Laser (schmerzhaft) und mechanische Reizung (nicht schmerzhaft) zu untersuchen. Dabei ergaben sich klare Unterschiede zwischen beiden Reizen sowie zwischen naiven Mäusen und Mäusen mit entzündlichen Schmerzen, insbesondere erhöhte Empfindlichkeit gegenüber mechanischer Reizung und erhöhte Amplituden der evozierten Potenziale als Ausdruck der Hyperalgesie.

Diese Ergebnisse zeigen zusammen spezifische Veränderungen der neuronalen Aktivität unter verschiedenen Schmerzbedingungen, die in mehreren relevanten Hirnregionen verteilt auftreten.. Obwohl die Mechanismen der Schmerzverarbeitung bei verschiedenen Schmerzarten unterschiedlich sein können, umfassen sie gemeinsame sensorische, affektive und Verhalttens-Aspekte. Dies ermöglicht, spezifische elektrophysiologische Signaturen zu bestimmen. Damit können zugrunde liegende Mechanismen aufgeklärt und potenziell auch objektive Marker für bestimmte Schmerzzustände entwickelt werden.

Abbreviations

ACC	Anterior cingulate cortex
AMYG	Central nucleus of the amygdala
AUC	Areas under curve
BL	Baseline
c	Contralateral
Caps	capsaicin
CFA	Complete Freund's adjuvant
CFC	Cross-frequency coupling
i	Ipsilateral
Ins	Posterior insula
LFP	Local field potential
MI	modulation index
N1	The first negative peak
N2	The second negative peak
OB	Olfactory bulb
P2	The second positive peak
P2-N1	Vertex peak-to-peak amplitude
PAC	Posterior parietal cortex
PSD	Power spectrol density
S1	Primary somatosensory cortex
Sal	Saline
TAC	Mechanical tactile stimulus
VPL	Ventral posterolateral thalamic nucleus

1. Introduction

1.1 Pain and different types of pain

As defined by the International Association for the Study of Pain (IASP), pain is "An unpleasant sensory and emotional experience associated with, or resembling that associated with, actual or potential tissue damage" (IASP, 2020). Pain is a major health concern in most developed countries (Debono, Hoeksema, and Hobbs 2013) and it can impact general functioning and quality of individual life (Breivik et al. 2008).

According to its duration relative to an actual disease, pain can be divided into two types: acute pain and chronic pain. In humans, acute pain is short-term pain lasting for fewer than six months. It is normally caused by tissue injury and vanishes as the injury is gone (Merskey 1986). Chronic pain, in contrast, lasts for more than six months, sometimes for years, and even after the original injury heals (Merskey 1986). Chronic pain can result from past injuries, but it can also occur without a clear reason (Deuis, Dvorakova, and Vetter 2017). Yet the correlation between injury and 'adequate' duration of pain can be arbitrary and is controversial. Due to the complex mechanisms of pain processing, there are also further sub-types of pain, such as inflammatory pain, which is a prolonged sub-chronic hypersensitivity state accompanying inflammation.

On the other hand, based on the cause of pain, it can be classified into nociceptive pain and neuropathic pain. Nociceptive pain arises from non-neural tissue damage which activates the nociceptors, which are free nerve endings of the peripheral somatosensory nervous system transducing noxious stimuli into electrical signals (IASP, 2020). Nociceptive pain is commonly observed in daily life and can result from multiple reasons like skin lesions, bone fractures, inflammatory arthritis and so on. In contrast to nociceptive pain, neuropathic pain results from a lesion or disease of the nervous system itself (IASP, 2020). For instance, neuropathic pain is found in spinal cord injury, stroke and multiple sclerosis, a disease in which myelination of axons is damaged (Foley et al. 2013).

Chronic and neuropathic pain is usually maladaptive (Deuis, Dvorakova, and Vetter 2017). However, acute and sub-chronic, nociceptive pain serves to protect an individual from harm and avoid further tissue damage. Its protective role is prominent in a syndrome called congenital insensitivity to pain (Cox et al. 2006). Although with intact nervous system, individuals with this syndrome are insensitive to nociceptive stimuli and thus can hardly avoid potential harm. And pain by definition is not just a sensory process but a complex integration of information from both sensory and affective aspects. The experience of pain results from central nervous processes within the so-called pain matrix.

1.2 Behavioral measurement of pain in rodents

In spite of the broad occurrence, there are difficulties in performing pain studies in humans as pain ratings are subjective and experiments ethically limited. As a result, animal models are widely applied to mimic the diverse clinical correlates of pain and to investigate underlying mechanisms and potential treatments, with mice and rats being the most commonly selected species (Mogil 2009).

Although nociception is a universal function in mammals and many other species, strictly speaking, pain cannot be directly measured in rodents, as they are unable to directly report the subjective experience. Instead, a variety of "pain-like" behaviors such as paw withdrawal from nociceptive stimuli are measured to indicate pain in animals (Sandkuhler 2009). In general, the behavioral methods for nociception measurements can be classified into stimulus evoked and non-stimulus evoked, or spontaneous pain, according to whether external stimuli are applied to elicit nociceptive response (Gregory et al. 2013).

1.2.1 Stimulus-evoked pain tests

According to the stimulus modality, stimulus-evoked pain responses can be provoked by mechanical, heat, cold or electrical stimuli. These stimuli activate localized nociceptors, which transduce nociceptive cues into electrical signals and conduct them into the central nervous system (for subsequent processes see chapter 1.3 and 1.4). Stimulus-evoked pain tests trigger stereotyped motor responses at the site of testing and can closely mimic human studies of hyperalgesia and allodynia. Hyperalgesia refers to enhanced responses to noxious stimuli, while allodynia is defined as hypersensitivity towards stimuli that normally do not induce pain (IASP, 2020). For example, in people with fibromyalgia, hyperalgesia is experienced as movement-evoked pain. Hence, stimulus-evoked pain tests may give insights to human pain responses.

Mechanical stimuli

Among all kinds of methods, mechanical stimuli have been most commonly used for allodynia and hyperalgesia measurement. A classical mechanical stimulus is determined by using von Frey filaments. This manual mechanical test was designed in 1896 by the

physiologist Maximilian von Frey and is the gold standard for determining mechanical threshold in rodents (Deuis, Dvorakova, and Vetter 2017). The test is performed by applying a monofilament perpendicularly to the tested region, usually the plantar surface of an animal's hind paw, which is placed in a small chamber with penetrable bottom. The filaments have different length, diameter and material such that they buckle elastically at varying forces, which can be taken to determine different thresholds of evoked pain. Despite the reliability of the manual von Frey test, it is time consuming due to large numbers of repeats, and thus induces an additional burden for the animals. The electronic von Frey hair test is applied under similar principles as the manual test, but with a single un-bending filament applied with increasing, defined force to the hind paw until its withdrawal. The paw withdrawal threshold can be recorded automatically by the electronic system and only 3-4 repeat measurements are sufficient (Ambalavanar et al. 2007; Deuis et al. 2014).

Heat stimuli

Heat stimuli are also widely applied in pain tests and contain various methods including the tail flick test, thermal probe test, hot plate test and Hargreaves test. Among these methods, Hargreaves is able to deliver heat stimulation to the hind paw of rodents, resulting in a localized measurement of heat hypersensitivity (Hargreaves et al. 1988). The Hargreaves test is normally carried out by aiming a radiant or infrared laser at the plantar surface of the hind paw, through a glass bottom that can be heated up with minimum heat sink effects. The time from stimulation to paw withdrawal is recorded as paw withdrawal latency, indicating the strength of pain. Compared to other kinds of heat-evoked pain tests, the Hargreaves test has advantages in providing experimental (stimulated paw) and control (non-stimulated paw) states in single trials, and in its applicability in unrestrained rodents which comes close to natural conditions (Deuis, Dvorakova, and Vetter 2017; Gregory et al. 2013). However, due to the relatively long withdrawal latency (in seconds), the Hargreaves test does not provide a sufficient analogy with laser-evoked pain tests in humans, where withdrawal latency are on a scale of tens of milliseconds.

1.2.2 Spontaneous pain tests

Contrary to stimulus-evoked pain measurements, spontaneous pain is tested without any temporally defined, specific stimulus. In recent years, spontaneous pain tests are increasingly developed and used due to concerns over the efficient translation of stimulus-evoked pain tests into the clinics (Mogil 2009; Tappe-Theodor and Kuner 2014). The spontaneous pain tests contain multidimensional measurements such as grimace scales, burrowing and weight bearing/gait analysis, which are correlated to facial expressions, self-motivated behaviors and imbalanced ambulation in humans with spontaneous pain (Deuis, Dvorakova, and Vetter 2017).

The most commonly used behavioral measurement of stimulus-evoked pain is paw withdrawal latency or withdrawal threshold. In spontaneous pain, in contrast, the behavioral readouts are more variable, such as spontaneous guarding, freezing, flinching and licking (Luger et al. 2002; Deuis, Dvorakova, and Vetter 2017). Guarding refers to the time of keeping hind paw lifted or putting less weight on the hind paw during movement. Freezing means the time of a stationary state where the only observable movement is respiration. Flinching is a fast shaking behavior of the animal's hind paw, and paw licking is an obvious indicator of strong ongoing pain. A quantitative pain rating can be gained by summing up the above-mentioned nociceptive readouts (Abdus-Saboor et al. 2019). Video records can facilitate the readout of spontaneous pain-like behaviors.

1.2.3 Disease models

A variety of animal models of disease have been developed to mimic clinical states of pain in patients with certain diseases.

Inflammatory pain models have been developed by applying different chemicals or drugs in specific rodent organs or regions like skin, paw or muscles, inducing an acute inflammatory pain and a subsequent sustained pain with recruitment of neutrophils and macrophages. Thus, inflammatory pain presents aspects of both, acute and sub-chronic pain conditions. Capsaicin injection can result in acute inflammatory-like pain, lasting for minutes to hours. It activates TRPV1-expressing nociceptors and leads to typical pain-like responses in stimulus-evoked pain tests such as von Frey (Knotkova, Pappagallo, and

Szallasi 2008). A method to introduce sub-chronic inflammatory pain is injection of complete Freund's adjuvant (CFA). CFA is solution of antigen emulsified in mineral oil and can induce inflammation. It is commonly used for modeling chronic inflammatory pain condition in patients with rheumatoid arthritis or tendonitis (Gregory et al. 2013). CFA injection is commonly applied in the rodent's hind paw, leading to hypersensitivity in stimulus-evoked pain tests. Depending on the dose of CFA and the depth of injection, nociceptive responses can be observed from one week to several months, making it possible to study different states of inflammatory pain.

Regarding to neuropathic pain, there are several longstanding classical rodent models such as spared nerve injury (SNI) and Chronic Constriction Injury (CCI) (Decosterd and Woolf 2000). Both models induce neuropathic pain by ligation of the sciatic nerve inducing a trauma in the peripheral sensory nervous system, which can be measured by mechanical allodynia, which is hypersensitivity towards non-noxious tactile stimuli (Costigan, Scholz, and Woolf 2009).

There are also other kinds of disease models such as cancer pain models, muscle pain models and visceral pain models, reflecting pain or nociception induced by inflammation in various organs (Gregory et al. 2013). Thus, experimentalists must select their model from a large variety of procedures mimicking acute, sub-chronic, chronic, nociceptive or neuropathic pain in different organs or conditions.

1.3 Pain circuitry across brain regions

Pain is both a sensory and a perceptual phenomenon. The neuronal processes underlying the subjective experience of pain involves encoding in localized nociceptors from a wide range of stimuli, transmission and modification through the peripheral nervous system, as well as projection and integration in a distributed brain regions with both sensory and emotional correlates (Basbaum et al. 2009; Bliss et al. 2016).

1.3.1 Brain regions involved in pain processing

The nociceptors, a subpopulation of peripheral nerve fibers, detect nociceptive stimuli like heat, mechanical and chemical irritants (Gold and Gebhart 2010). Two types of nociceptors are mainly involved, which are Aδ fibers and C fibers. Aδ fibers are medium diameter myelinated afferents transducing the well-localized 'first', or rapid pain sensation, while unmyelinated C fibers with small diameter mediate the poorly localized 'second', delayed pain. Thus, differences in velocity of nociceptive signal propagation are determined by the degree of myelination, leading to the fast transmission of Aδ fibers (3-30 m/s) and the slower transmission of C fibers (0.5-2 m/s).

Nociception signals are synaptically transmitted onto neurons of the dorsal horn of the spinal cord, and subsequently cross sides to project to defined brain structures (Gold and Gebhart 2010). The primary somatosensory cortex (S1) has been widely reported to participate in pain processing, mediating messages about the location and intensity of the noxious stimulus (Bushnell et al. 1999; Gross et al. 2007; Dowman, Rissacher, and Schuckers 2008; Zhang et al. 2012; Uhelski, Davis, and Fuchs 2012). Afferent signals reach S1 via the ventral posterolateral thalamus (VPL), which is one of the brain structures receiving projections from ascending pain pathways (Ab Aziz and Ahmad 2006) (Figure 1.3.1). In addition to S1, VPL can project to structures including insular cortex (Ins), anterior cingulate cortex (ACC) and amygdala (AMYG) (Treede et al. 2000; Bliss et al. 2016). There are also projections between these brain regions. For example, ACC can receive inputs from S1 and project to Ins (Bliss et al. 2016). Other studies indicate that nociceptive information reaches the insular cortex as well as ACC via connections from the parabrachial nucleus of the brain stem and the amygdala (AMYG) (Basbaum et al.

2009). ACC, Ins and AMYG have all been shown to contribute to the affective component of the pain experience. For example, the expectation of a painful stimulation can result in increased activity in both, ACC and AMYG (Lenz et al. 1998; Sawamoto et al. 2000; Bornhovd et al. 2002). AMYG has also emerged as an important center for learned fear, anxiety and depression (Neugebauer 2015). The anterior insular cortex is considered necessary for empathetic pain perception (Gu et al. 2012), as well as for modulating cognitive and affective information across cortical structures (Starr et al. 2009). The posterior parietal cortex (PAC), a major hub for perceptive and cognitive process like attention, memory, decision making, spatial representation and motor control, has also been implicated in the conscious appreciation of pain, including orientation and attention towards noxious stimuli (Duncan and Albanese 2003; Howard et al. 2016; Scheffzuk et al. 2011; Sestieri, Shulman, and Corbetta 2017; Hadjidimitrakis et al. 2019). However, the precise function of PAC in pain processing remains to be elucidated.

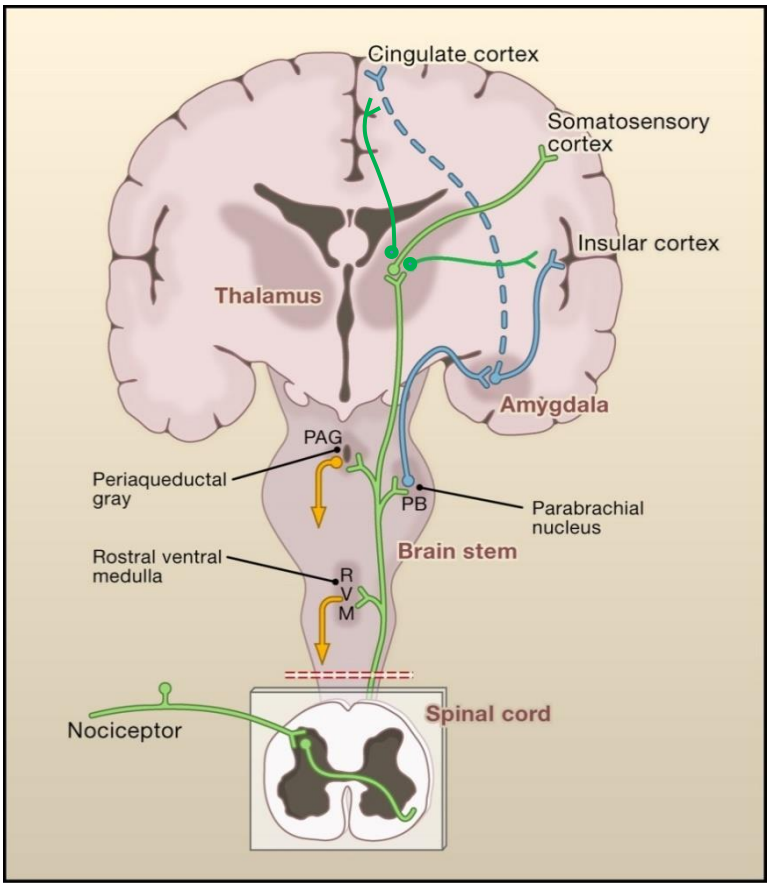

Figure 1.3.1 Pain circuity across multiple brain structures. Noxious information is transmitted to the thalamus through the dorsal horn of the spinal cord by nociceptors, and then is projected to multiple brain structures including the somatosensory cortex, the cingulate and insular cortices.

Besides, there are projections between these brain regions, such as a pathway to the insular and cingulate cortices through amygdala (Adapted and modified from Basbaum, 2009).

1.3.2 Pain matrix

Previous studies on pain circuity revealed that no single brain structure is essential for all aspects of pain processing. Instead, pain results from activity in discrete brain regions with both sensory and emotional correlates (Apkarian et al. 2005). As summarized in chapter 1.3.1, pain or nociception processing involves activation of a variety of brain regions including the ventral posterolateral thalamus (Ab Aziz and Ahmad 2006), the anterior cingulate cortex (Lieberman and Eisenberger 2015) somatosensory cortex (Gross et al. 2007; Dowman, Rissacher, and Schuckers 2008; Zhang et al. 2012), the insular cortex (Frot and Mauguiere 2003; Brooks and Tracey 2007; Isnard et al. 2011; Segerdahl et al. 2015) and the amygdala (Simons et al. 2014; Corder et al. 2019). This complex co-activated brain network pattern is referred to as the 'pain matrix' or 'pain network' (Melzack 1999). Due to the complexity of information processing on these broadly spread regions it is difficult to isolate the contribution of any single brain structure to pain processing (Mouraux et al. 2011; Davis et al. 2015; Wager et al. 2016). Rather, a multiregional approach to study the pain matrix seems to be more promising for elucidating the underlying mechanisms of pain.

1.4 Electrophysiology of pain

Pain is closely correlated with physiological and pathophysiological progress both in the peripheral and central nervous system. Thus, it is appropriate to investigate mechanisms of pain and nociception with electrophysiological techniques. To understand the generation of pain experiences in the pain matrix, a systematic neurophysiological signature of pain from neuronal activity patterns in multiple brain areas would be very desirable. Such an electrophysiological signature may further enable reliable diagnosis and distinction of different subclasses of pain (Davis et al. 2017), evaluation of pain in patients with communication disability (Benoit et al. 2017; Hartley et al. 2017) and development of biofeedback methods for pain monitoring (Jensen et al. 2013). Although *in vitro* methods such as patch clamp recording of brain slices can provide information on cellular mechanisms of pain processing, we need *in vivo* studies, especially in unrestrained animals, for studying pain processing in the pain matrix under natural conditions.

1.4.1 Local field potentials and network oscillaitons

In both human and animal studies, electroencephalography (EEG) is widely used for investigating electrical activity of the brain in pain processing. Yet, this recording method is limited to superficial cortical signals, making it hard to gain information on subcortical neural activity. Thus for a systematic establishment of the pain matrix in electrophysiological aspects, it is necessary to record network activity (local field potentials; LFPs) in both cortical and subcortical brain regions by using surface and depth electrodes. Brain LFPs are transient extracellular electrical signals resulting from summed and synchronous electrical activity of multiple neurons, mostly based on postsynaptic potentials (Legatt, Arezzo, and Vaughan 1980). In rodents, LFPs range from very low frequencies to very high frequencies with roughly classified frequency bands as follows:

(1) Slow Waves (< 1 Hz)

(2) Sharp Waves/Delta (1–4 Hz)

(3) Theta (4–12 Hz)

(4) Alpha (8-13 Hz)

(5) Beta (13-23 Hz)

(6) Gamma (low: 30–80 Hz, middle: 80–120 Hz, high: 120–160 Hz)

LFP recordings are widely used for pain studies, often looking for changes in power or amplitude of the LFPs. Most studies of electrical activity in pain report increased power of LFPs in various brain regions and in different frequency bands. For example, it has been shown that inflammatory pain leads to increased delta, theta, and alpha band activity (0–13 Hz) in anterior cingulate cortex in freely moving rats (Harris-Bozer and Peng 2016). Acute and chronic pain influences neural network oscillations in different frequency bands in the medial prefrontal cortex (Fu et al. 2018). It has also been found that the occurrence of high-amplitude 6–9 Hz and 22–33 Hz oscillations in the thalamus is correlated to pain relief (Luo et al. 2020). Cortical theta amplitude is increased in rats with either acute or chronic pain (Leblanc et al. 2014).

Pain is a combination of multidimensional complex neuronal activities, and state-dependent network oscillations are thus a promising candidate for a neuronal signature of pain. Pain-dependent alterations of electrical activity have been described in multiple brain regions (Ploner, Sorg, and Gross 2017). Brain network oscillations (measured as rhythmic LFPs) are generated synchronously in discrete, yet functionally related areas, and the resulting functional networks are linked to specific behavioral, functional or vigilance conditions (Engel and Singer 2001; Buzsaki and Draguhn 2004; Uhlhaas and Singer 2006; Fries 2009; Buzsaki and Wang 2012; Singer 2018). Therefore, the activation of a distributed functional system like the pain matrix may be reflected in a specific pattern of neuronal network oscillations across the brain. Furthermore, network oscillations form higher-order patterns generating an enriched parameter space for potential functional signatures. For instance, slow frequency oscillations, like theta rhythms, can modulate high frequency oscillations such as gamma frequencies (Canolty et al. 2006). Such cross-frequency coupling (CFC) is associated with information processing during specific cognitive activities (Tort et al. 2010) and may well contribute to the signature of complex cognitive-emotional processing of pain. In disease studies, CFC has been indicated as a marker of Parkinson’s disease (de Hemptinne et al. 2013) and of animal models of Alzheimer’s disease (Zhang et al. 2016). Yet the role of CFC in pain processing is largely unknown.

1.4.2 Evoked potentials

Stimulus-evoked pain triggers not only behavioral nociceptive responses, but also immediate electrophysiological responses, called evoked potentials. Different modalities of stimuli result in different types of evoked potentials with specific patterns, normally containing several negative and positive peaks at defined time points or intervals (Karlin 1970). Based on the modality of the stimulus, they are called visually evoked potentials, auditory evoked potentials, somatosensory evoked potentials, laser-evoked potentials and so on. While conventional somatosensory evoked potentials result from tactile stimulation like touch or vibration, laser-evoked potentials reflect electrical correlates of pain processing (Chiappa and Ropper 1982; Treede, Lorenz, and Baumgartner 2003; Jones et al. 2016).

In human studies, laser-evoked potentials are well established for pain research, for example by applying intensive brief infrared laser beams onto a subject's skin (e.g. at the hand). This leads to sharp and acute pain, which can be reliably recorded (Bromm and Treede 1984; Plaghki and Mouraux 2003; Cruccu and Garcia-Larrea 2004; Ohara et al. 2004). Human laser-evoked potentials are normally recorded from EEG or ECoG, which has limitations in recording deep subcortical brain structures. Animal studies can overcome this problem and facilitate research on subcortical mechanisms of pain processing. However, laser-evoked potentials are rarely investigated in awake unrestrained rodents, partially due to the practical difficulty in precisely and reliably targeting and triggering stimulation in freely moving animals (Chaplan et al. 1994). An apparatus or method for convenient and reliable laser stimulation and recording of the resulting electrophysiological activity is highly desirable pain studies in rodents.

1.5 Aims of the study

Pain is a complex multidimensional process with both sensory and affective correlates. From acute nociceptive pain to chronic and severe neuropathic pain, a variety of rodent behavioral models are applied for mimicking pain processing in humans, and for analyzing the signature of stimulus-evoked and spontaneous pain. Amongst the structures participating in pain signaling are the ventral posterolateral thalamus, the anterior cingulate cortex, the somatosensory cortex, the insular cortex and the amygdala, which together comprise most parts of the so-called “pain matrix” or “pain network”. Thus, instead of focusing on single brain structures, it is promising to study multiregional activity and identify pain-specific patterns which, until now, have remained elusive. Electrophysiological measurements, such as local field potential recordings in freely moving mice can facilitate such systematic studies. Concerning stimulus-evoked nociception, laser-evoked potential recording is well established for evoked pain measurement in human studies. Despite of the advantages of rodent models for recording subcortical activity and studying pain-related mechanisms, laser-evoked potentials are rarely applied to rodents, due to practical difficulties. Hence, methods for stable and convenient evaluation of laser-evoked potential measurement in rodents are desirable. Therefore, I performed a systematic exploration of electrophysiological activity in freely moving mice during several types of pain, and I established a new device for measuring evoked pain responses in mice under defined conditions with minimal restrictions. In detail, I addressed the following tasks:

1. Investigate network activity in a wide range of brain structures in freely moving mice with and without acute pain, and analyze coordinated network oscillation patterns inner- and inter-regional.

2. Develop an apparatus to facilitate evoked potential recordings in freely moving mice, combined with simultaneous behavioral measurements.

3. Apply the custom made sensory testing apparatus to explore systematically the electrophysiological characteristics of evoked pain responses in both acute and inflammatory pain states.

2. Materials and methods

2.1 Ethics statement

The experiments were performed according to the guidelines of the European Science Foundation (2001), and have been approved by the Governmental Supervisory Panel on Animal Experiments of Baden Württemberg, Karlsruhe (G-115/14). Every effort was made for the use of a minimum number of animals in this study and to reduce the animal suffering.

2.2 Animal care and housing

C57BL/6N mice were purchased from Charles River Laboratories (Sulzfeld, Germany) at an age of 10-12 weeks. In the experiments of capsaicin-induced pain model (see below), sixteen animals were used (6 female, 10 male). In the experiments of laser/tactile stimulation-evoked pain (see below), nineteen male mice were used. Before surgery, the animals were housed in groups of two in a ventilated Scantainer (Scanbur BK, Denmark) on a normal 12/12-hour light/dark cycle (from 7 a.m. to 7 p.m. light was on), with free water and food supply. After surgery each mouse was housed separately to prevent damage of headstages, and was changed to inverted 12/12-hour light/dark cycle (from 7 a.m. to 7 p.m. light was off) to facilitate the following experiments. After completing the experiments the mice were sacrificed by an overdose of pentobarbital (i.p.) during brain perfusion (see below).

2.3 Electrode preparation

Electrodes for intracerebral field potential recordings (deep electrodes) were constructed from two insulated tungsten wires (diameter: 50 µm, California Fine Wire, USA) which were glued together and cut into approximately 2 cm length. Insulation was scratched off

from one end which was soldered to a copper pin (Farnell, Germany) and connected with the headstage.

Surface electrodes were prepared from stainless steel watch screws (diameter: 1mm, length: 3ms, DIN84, Wegertsender, Germany). Insulation of copper wire (diameter: 0.22 mm, 2 cm long, Conrad, Germany) was removed from both ends. One end was soldered to a gold-plated pin (Farnell, Germany) for assembly into the headstage and the other end was soldered to the stainless steel watch screw. The screw was then screwed into the skull during the surgery gently touching the surface of the brain.

2.4 Surgery for electrode implantation

Animals were anesthetized with 4% isoflurane (Baxter, Germany) together with medical oxygen (float rate: 1 L/minute). After ceasing of the righting reflex, buprenorphine (0.1 mg/kg bodyweight, 0.324 mg/ml buprenorphine hydrochloride solved in 18.5 ml sterile saline 0.9%, Temgesic, Irland) was subcutaneously injected for analgesia before and eight hours after surgery. During surgery, anesthetized animals were mounted into a stereotaxic frame (David Kopf Instruments, UK) under ongoing anesthesia with 1.0%–2.5% isoflurane. Body temperature was kept at 37-38°C by a heating pad (ATC-2000, World Precision Instruments, UK) and spontaneous breathing rate was checked regularly. After shaving the hair on the head the skull was exposed with a scalpel and the skin fixed with surgical thread (Vicryl V734E 4-0, Ethicon, Germany). Subsequently, holes were drilled at defined locations according to the coordinates from Paxinos and Franklin (Paxinos and Franklin 2019) using bregma as reference.

Regions	Coordinates (A/L/V)
OB ipsi	+4.5/-0.8/-1.4
ACC contra	+2/+0.35/-1.1
ACC ipsi	+2/-0.35/-1.1
S1 contra	-0.5/+1.4/-0.7
S1 ipsi	-0.5/-1.4/-0.7
Ins contra	-1.1/+3.7/-3.7
Ins ipsi	-1.1/-3.7/-3.7
VPL contra	-1.7/+1.7/-3.35
VPL ipsi	-1.7/-1.7/-3.35
PAC ipsi	-2.7/-2/epid
AMYG ipsi	-1.1/-2.3/-4.0

Table 2.1 Summary of the brain regions and their corresponding coordinates used for the experiments of capsaicin-induced pain.

In the experiments of capsaicin-induced pain, electrodes were implanted in five pain-related brain regions in the contralateral (c) and/or the ipsilateral (i) sides of the injected left hind paw: the primary somatosensory cortex (S1c, S1i), anterior cingulate cortex (ACCc, ACCi), ventral posterolateral thalamic nucleus (VPLc, VPLi), posterior insula (Insc, Insi) and central nucleus of the amygdala (AMYGi). In addition, electrodes were implanted in the olfactory bulb (OBi) and parietal cortex (PACi). Because of channel limitation of the INTAN amplifier, AMYG, OB, and PAC were only implanted in the left hemisphere (ipsilateral to injection side). The stereotaxic coordinates is shown in Table 2.1. The representative electrode positions are shown in Figure 3.1.1.

For experiments of laser/tactile stimulation-evoked pain, electrodes were implanted in six brain regions in the contralateral (c) and/or the ipsilateral (i) sides of the stimulated side (right hind paw), namely the primary somatosensory cortex (S1c, S1i), parietal cortex (PACc, PACi), ventral posterolateral thalamic nucleus (VPLc, VPLi), anterior cingulate cortex (ACCc, ACCi), ventral posterolateral thalamic nucleus (VPLc, VPLi), posterior insula (Insc, Insi) and central nucleus of the amygdala (AMYGc). Due to the channel restriction in our setup, AMYG was only implanted and recorded in the left hemisphere (contralateral to stimulation side). The stereotaxic coordinates is shown in Table 2.2. The representative electrode positions are shown in Figure 3.2.5.

Regions	Coordinates (A/L/V)
ACCc	+1.98/-0.35/-1.7
ACCi	+1.98/+0.35/-1.7
S1c	-1.06/-1.4/-0.7
S1i	-1.06/+1.4/-0.7
Insc	-1.06/-3.7/-3.5
Insi	-1.06/+3.7/-3.5
VPLc	-1.7/-1.8/-3.7
VPLi	-1.7/+1.8/-3.7
PACc	-2.06/-1.5/-0.5
PACi	-2.06/-1.5/epid
AMYGc	-1.06/-2.2/-4.7

Table 2.2 Summary of the brain regions and their corresponding coordinates used for the experiments of laser/tactile stimulation evoked pain.

Grounding (GND) and reference electrodes (REF) were screwed to the surface of the cerebellum (Figure 3.1.1 and 3.2.2). Electrodes were fixed with the flowable composite (Filtek Supreme XTE, 3M, USA) and with dental cement (Paladur, Heraeus GmbH, Germany). All contact pins were inserted into a dummy female connector for assembly into a headstage and later kept for protection. After surgery, the animals were placed into the home cage and the environment was maintained at 28°C until the animals woke up. Immediately after waking the animals were transferred to the housing scantainer for one week of recovery.

2.5 Local field potential recordings

In general, local field potentials (LFPs) were recorded in pain-related brain structures (see details in Chapter 2.4) in freely moving mice. LFPs were amplified (RHA2116, Intan Technologies), filtered (1-500 Hz, including the accelerometer signals), digitized (at a rate of 2.5 kHz), and stored in a computer for offline analysis using custom-written MATLAB (The MathWorks) functions. In total, there were 16 input channels, including a custom-added 3-D-accelerometer connected to three of them. Representative raw LFP traces are shown in Figure 3.1.2.

2.6 Capsaicin-induced pain model

After electrode implantation, mice were kept in their own home cages for recovery for one week, with an inverted circadian light/dark rhythm. After the following habituation recordings, LFPs were recorded in the home cage condition. During the recordings, saline (Sal) was injected into the left hind paw. The next day, the same recordings were repeated again with injection of 5% capsaicin (Caps, 10 µl) in the same mouse, to induce acute pain responses. The capsaicin solution was prepared by solving 200 mg capsaicin powder into a mixture solution of 2 ml ethanol and 38 ml iso-tonic NaCl solution (Figure 3.1.1).

2.7 Custom made apparatus for sensory testing

Laser-evoked potentials have been commonly used in human pain study, while in animal study there is a lack of reliable and convenient method for laser-evoked potential measurement. To facilitate the recording of laser-evoked potentials in mice, I designed and constructed a new apparatus, with supports from Lee Embray (electronics) and Jürgen Schmitt (mechanics).

The measurement device was based on a custom made stainless steel scaffold carrying a round metal plate as a basis for the laser stimulator (MRC Systems GmbH, Germany). The stimulator head was able to be effortlessly and quietly moved to the target position of the mouse hind paw. Focal distance of the laser stimulator was 30 mm. The beam of 4 mm diameter was focused to 50 µm diameter by a lens in the focal plane. The duration of laser pulses could be varied from 1 to 100 ms. The laser stimulator head was easily removable and could be replaced by a custom made tactile stimulator with the same dimension (see below for details). The position of the stimulator head was manipulated by moving a connected control stick. The position of the stimulator could be adjusted and fixed by using a screw to clamp it in the control stick assembly. A bottom camera was mounted close to the laser stimulator head to allow monitoring the position of the stimulation from underneath, such that the laser beam or mechanical device could be precisely positioned to the targeted mouse hind paw.

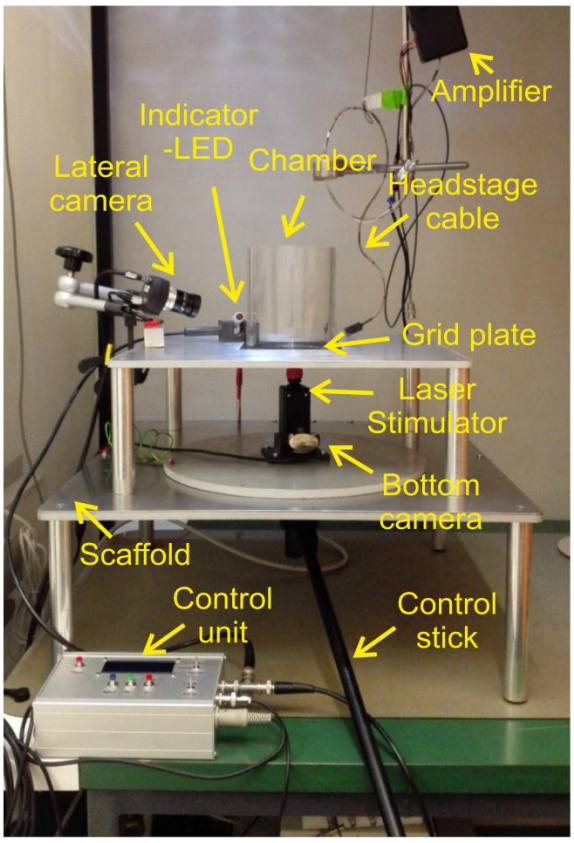

Figure 2.7.1 An overview photo of the custom built apparatus with annotations of the main compartments.

A 3D printed (Formlabs Form2, USA) circular grid plate (10cm in diameter) was mounted in a 10 cm hole above the plate for stimulation devices, carrying a transparent tempered glass chamber. The mouse will be placed inside the chamber during experiments. The space inside the chamber was large enough to allow free moving of a mouse, while small enough to keep its paws within convenient reach for the laser or tactile stimulator heads. Cables from the headstage reach the amplifier board (Intan Technologies, USA) above the chamber. A HD-camera (iDS, Germany) was fixed beside the chamber to record the behavior of the mouse. Video images (14 fps, display resolution 1280 x 1024) were fed into uEye Cockpit software (iDS, Germany) on a connected computer. The camera also recorded a red indicator-LED light on the top of the mouse platform showing when the laser stimulation was triggered. Signals for laser stimulation and indicator-LED light were synchronized with local field potential signals by using a custom made control unit (see details below). Records of evoked potentials and videos were presented and saved on a

connected computer for further analysis (Figure 3.2.1 A and B). The setup was built with supports from Lee Embray and Jürgen Schmitt.

A control unit was originally designed to contain the following functions (Figure 2.7.2):

1. To trigger the laser/tactile stimulator either manually or automatically.

2. To flash the red LED indicator (in view of the lateral camera) synchronously with the triggering.

3. To control the pre/post-recording of the lateral camera recordings to reduce the amount of video recorded to only relevant sections thus to save hard disc memory and to simplify post data analysis.

4. To control all of the above either manually or with random timing. A minimum and a maximum time could be set and the trigger fell randomly within these times. In practice of the experiments in this project, the random triggering and control function were not utilized and triggers were made using the manual trigger switch on the control unit.

Figure 2.7.2 A close view of the control unit.

The design was based on a microprocessor from MicroChip and programmed in C using MPLAB X IDE and was battery powered to reduce any possible introduction of extra

noise from an external power supply. All parameters were capable to be adjusted using the simple two line LCD display and three menu buttons.

The two trigger outputs were able to be adjusted to output a trigger pulse of duration 1-250 ms. Trigger 1 (TRIG 1) was set to 1 ms and was used to trigger the laser stimulator, which only required a short pulse and laser-on duration was set on the laser driver itself. Trigger 2 (TRIG 2) was set to 100 ms and was used to drive the red indicator-LED in view of the lateral camera. 100 ms was sufficient time to show in videos when the laser was triggered. Trigger 2 was also fed to the electrophysiology recording system allowing the video to be synchronized with the data recorded from the mouse by aligning the trigger signal to the LED-on period in the video.

As for the automatic trigger function, the pre- and post-record times (pre-record maximum of 16 seconds, post-record maximum of 240 seconds) were set to 3 and 30 seconds accordingly. A Safe/Armed switch was required to eliminate accidental triggering of the system (accidental manual trigger button pressing) creating possible dangers for the mouse and operator as well as recording unwanted data. The polarity switch was added in case other equipment was to be used that may require an inverted trigger pulse rather than a positive trigger pulse.

The control unit was able to drive the experiment automatically with the exception of aiming the stimulator on the mouse paw although it was decided to manually trigger the system rather than use the random automatic trigger facility. All recorded data and video was recorded on a PC for later offline analysis (Figure 3.2.1).

Mechanical (tactile) stimulator

A mechanical tactile stimulator was custom-made to be interchangeable with the laser stimulator head, it was therefore built with the exact same dimensions as the laser module. A needle with blunt tip can be easily mounted to the top of the stimulator to convey tactile stimulation (Figure 2.7.3).

A 12 V solenoid (Conrad Electronics) was used to create the movable stimulator, and this was mounted between two Plexiglas halves creating the body of the stimulator with the connections to the solenoid terminated with a BNC mounted on the bottom of the body.

The solenoid was rated at 12 V but due to the very short time the coil would be energized and the long periods of time between uses. To obtain a suitable stimulus, we used an extra power supply unit (PSU) to provide TTL trigger pulses with higher voltage.

Tests were performed to measure the time taken between the TTL trigger pulse and the physical stimulation of the paw, which was carried out using a piezo sensor positioned in place of the paw. The piezo sensor was connected to the first channel of an oscilloscope (Textronix TDS2024), while the TTL trigger pulse was connected to a second oscilloscope channel. It was then possible to measure the duration between the two for various voltage settings across the solenoid. Increasing the voltage up to 27 V created the optimal stimulus and reduced the operating time while improving time variations to a negligible amount, at 27 V the time between TTL pulse and physical stimulation was measured at a constant 24 ms, this time of delay was used to synchronize all recorded video and data for tactile stimulation.

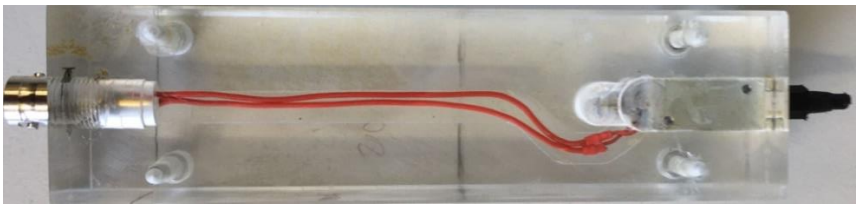

Figure 2.7.3 A close view of the tactile stimulator head.

2.8 Evoked potential recordings

One week after electrode implantation, mice were placed in the custom made apparatus described in Chapter 2.7. Habituation recordings were conducted for one hour a day and for 2-3 days dependent on the animals' performance. After habituation, LFPs were recorded in freely moving mice placed in the custom built device. During the recordings, mechanical (tactile) and laser stimuli were administrated for evoked potentials. During the trials, a cardboard partition was put between the apparatus and the experimenter to prevent visual contacts to the experimenter.

In naïve mice

Nineteen male mice were used for evoked potential recordings. We tried to use a minimum number of stimulations to reduce the suffering of the animals. Stimulations were applied when the animal was awake and resting such that the paw could be targeted. First, tactile stimulations were administrated 3-6 times onto the right hind paw of the mouse. Afterwards, the tactile stimulator was replaced by the laser stimulator. Laser stimulations were also applied onto the right hind paw for 3-6 times. The laser pulse durations used were 3ms (2.3mJ), 5ms (5mJ) and 10ms (11.7mJ), respectively. The interval between two stimulations was at least 30 seconds to prevent damage to the mouse paw or adaptation of the mouse to the stimulation. After every experiment, the chamber, the grid plate and the stimulators and the scaffold of the custom made device were cleaned up with ethanol to eliminate smells of the animal to avoid influencing the following recordings.

In CFA-induced inflammatory pain

In the evoked potential recordings in naïve mice, nineteen mice were used to conduct both mechanical (tactile) and laser stimulation. Afterwards, complete Freund's adjuvant (CFA) was applied to induce inflammatory pain. In order to induce inflammatory pain, ten of the nineteen mice were subsequently injected with 20 μL undiluted complete Freund's Adjuvant (CFA, Sigma-Aldrich, Munich, Germany) into the intraplantar surface of the right hind under isoflurane anesthesia. Eight mice were injected with 0.9% saline (Sal) as control group. Both mechanical and laser stimulations were performed during the LFP recordings as the same way as in trials in naïve mice, respectively on day 2 and day 4 after CFA/Sal injection.

2.9 Behavioral measurements of pain

Electronic von Frey hair test

An electronic von Frey hair test device (Bioseb, France) was used to evaluate hyperalgesia in both capsaicin-induced acute pain and in CFA-induced inflammatory pain.

Each mouse was placed in an acrylic glass chamber with a metal mesh base for 30 minutes to adapt to the environment. Von Frey hair was then carefully placed beneath the plantar surface of the hind paw with gradually increasing force to touch the paw until its

withdrawal. The paw withdrawal threshold was recorded automatically by the electronic system. The test was repeated three times for each hind paw alternating between the two sides.

In capsaicin-induced acute pain, electronic von Frey hair tests were done before and after (2 minutes and 1 hour after) saline and capsaicin injection, respectively. In CFA-induced inflammatory pain, von Frey hair tests were applied before (day 0) and on day 2 as well as on day 4 after CFA and saline injection, respectively. The mean of the three repeats were calculated for further analysis (see details in Chapter 2.11).

Pain-related behaviors by laser and mechanical stimulation

In the experiments of evoked pain responses by laser or mechanical stimulation, the pain-related behaviors were recorded by the lateral camera. From the videos, the percentage and the latency of right hind paw withdrawal were evaluated. Several spontaneous pain-related behaviors following the stimulation were measured, including guarding, freezing and flinching (adapted from (Luger et al. 2002; Deuis, Dvorakova, and Vetter 2017). Besides, a pain score summarized the occurrence of each pain-related behavior and can provide an integrated dimension of pain rating (See details in Chapter 2.11.2).

2.10 Histology

After completion of all the experiments of each animal, the animal was anesthetized by intraperitoneal injection of an overdose of pentobarbital (100mg/kg). Then the mouse was applied trans-cardiac perfusion with Phosphate-Buffered Saline (PBS) and subsequently 4% paraformaldehyde (PFA). The brain was carefully taken out and stored in 4% PFA at 4°C for at least two days. Afterwards, the brain was coronally cut into 50 µm thick slices, using a Vibratom (Leica VT 1200S). Slices were stained with Cresyl Violet (Nissl staining) and checked by light microscopy to verify the electrode position.

2.11 Data analysis

This chapter summarizes analysis methods in aspects of both electrophysiology and behaviors in pain processing.

2.11.1 Movement and respiration rate

In capsaicin-induced pain, two-minute time windows in different conditions (BL, Sal, Caps, Caps 1h) were selected for analysis. To make sure that the effects were from pain but not from confounding effect of movement or respiration, I did the analysis as follows:

Movement

Accelerometry integral was used for assessing the animal's movement. It was measured by three orthogonally mounted accelerometers on the headstage. Comparisons were done between the control and pain conditions. Gravity-induced signals were eliminated by the high-pass filter (1Hz). Data was analyzed by dividing the integral signals of each of the three accelerometer channel by the epoch length of two seconds and then calculating the mean values of all three accelerometer channels over all epochs.

Respiration rate

Respiration rate was computed from the number of inspiratory or expiratory cycles per second recorded from respiration-related oscillations in the olfactory bulb in LFP recordings (Jessberger et al. 2016).

2.11.2 Pain ratings

Capsaicin-induced pain

Electronic von Frey hair was performed to assess the pain ratings. The withdrawal latency of the left hind paw of tested mouse was recorded. The averaged paw withdraw latency of each animal from the first two minutes directly after the respective injection (Sal, Caps) were compared to that of two minutes record under baseline (BL) conditions one hour before saline injection. Besides, the recordings of two minutes after one hour capsaicin injection (Caps (1h)) were calculated to assess if effects were reversible or long-lasting within the expected time. Data were presented as mean values with SEM.

Evoked pain by laser or mechanical stimuli

For the experiments of acute laser/mechanical stimulation, pain ratings were conducted by assessing pain-related behaviors in video recordings by the lateral camera in the custom

made apparatus. The period of thirty seconds after the stimulation was used for analysis. The indicator-LED flashed red light of 100ms simultaneously with the time of the stimulation trigger, which was used as the synchronization signal of the behavior and the LFP recording (Figure 3.2.1 and 3.2.2). In experiments of tactile stimulation, a 24 ms delay was observed from the trigger to the blunt tip of the tactile stimulator physically reaching the mouse hind paw because of mechanical movement of the stimulator needle (see detail in Chapter 2.7). This delay of 24 ms was gauged and applied in the data analysis.

Percentage and latency of right hind paw withdrawal towards the stimulation were measured according to the videos. In addition, stimulation-induced pain-like behaviors, including guarding, freezing and flinching were evaluated (Luger et al. 2002; Deuis, Dvorakova, and Vetter 2017). Guarding time was defined as the time of keeping lifting right hind paw or putting less weight on the paw when the mouse was moving or resting. Freezing time referred to the time of restraining every movement apart from those which was necessary for respiration. Flinching times meant the number of times of fast shaking of the hind paw. To summarize and integrate all the measured behaviors, a pain score was introduced (modified from (Abdus-Saboor et al. 2019). The pain score summed up the appearance of all measured behaviors. For instance, a mouse with two of the three behaviors obtained a score of 2 for the specific trial. In each experiment, each behavioral response of each animal was averaged from the 3-6 stimulations, respectively. Data were shown as individual and mean values with SEM.

CFA-induced inflammatory pain

For the pain rating of CFA/saline injection, electronic von Frey hair test was conducted. Before (day 0) and after (day 2, day 4) injection, the test was done on both hind paw of the mouse and was repeated three times on each paw. In each day of test, the mean withdrawal latency of each paw of three measurements of each mouse was calculated separately. Data were presented as mean with SEM.

2.11.3 Local field potentials

The data of local field potentials (LFPs) were analyzed with built-in and custom-written MATLAB (MathWorks, USA) routines. Raw data was inspected visually and periods with artifacts were excluded from further analysis. See raw LFP traces in Figure 3.1.2. Network oscillations in multiple brain regions were analyzed in the aspects of power spectral density, cross-frequency coupling and interregional coherence.

Power spectral density (PSD)

PSD is a measurement of a signal's power in the frequency domain transformed from the time domain by Fourier transformation. In this study, it was calculated with the pwelch function (MATLAB, Signal Processing Toolbox) with 4 seconds Hamming window and 50% overlap. Frequency bands were divided into six ranges: 1-4 Hz, 4-12 Hz, 12-30 Hz, 30-80 Hz, 80-120 Hz and 120-160 Hz. Band power for each frequency range was the sum of all PSD values of the respective band. Power was normalized based on the following formula:

$$normalized\ Power = \frac{Power_{post\ injection} - Power_{baseline}}{Power_{post\ injection} + Power_{baseline}}$$

Cross-frequency coupling

Cross-frequency coupling (CFC) is the association of neural oscillations in multiple frequency bands. In this study, I used the phase-amplitude coupling, which represents how strong the amplitude of high gamma frequencies is modulated by the phase of slow rhythms, such as theta or respiration-related rhythms.

To assess the intensity of phase-amplitude coupling, the Kullback-Liebler based modulation index (MI) was used as described by Tort et al. (Tort et al. 2010). The MI value assesses two frequency ranges of interest: a slower phase-modulating frequency (fp) and a faster amplitude-modulating frequency (fa). The phase of the slower frequency was divided into bins of eighteen 20 degree intervals, for each of which the respective amplitude envelope value of the faster frequency was calculated. The CFC was absent when the mean of the faster frequency amplitude was uniformly distributed, while strong in a diverged distribution. That is, the divergence of this distribution from the uniform

distribution indicated how strong the amplitude of the faster frequency was modulated by the phase of the slower frequency, resulting in a MI value between 0 and 1. The comodulation map was plotted by calculating the MI of each frequency band pair and presenting the results in a two-dimensional pseudocolored figure. One dimension represented the phase-modulating frequency bands and the other the amplitude-modulating frequency bands. Warm color in the comodulation plot indicated that the phase of fp modulated the amplitude of fa.

In this study, slower frequency of 1-15 Hz and faster frequency of 20-200 Hz was computed in the states of before, 2 minutes and 1 hour after injection of saline/capsaicin, respectively. The mean amplitude of the faster frequency in each phase bin was normalized to the summation of amplitude though the whole cycle by the same formula as the normalization of PSD values.

Coherence

The interregional coherence analysis can be for evaluating the relationship between two brain regions. Power transfer between two regions was estimated in coherence analysis.

In the study of capsaicin-induced pain, magnitude-squared coherence was computed using the mscohere.m function (MATLAB Signal Processing Toolbox). A two-second time window was analyzed with 50% overlap for each of the six frequency bands (1-4 Hz, 4-12 Hz, 12-30 Hz, 30-80 Hz, 80-120 Hz and 120-160 Hz) and each condition (Sal, Caps, Caps 1h), respectively. Eleven brain regions were involved in the analysis, contributing to an 11 × 11 matrix in each condition and each frequency band. The group averages of the interregional coherences for all frequency bands were computed and then normalized to baseline according to the same formula as the PSD values above. The normalized coherence between each two brain regions was shown in one block of a color map, with warmer color indicating stronger interregional coherence.

2.11.4 Evoked potentials

In the study of evoked pain responses, evoked potentials by mechanical and laser stimulation were analyzed from the LFP recordings, by custom-written routines in MATLAB (Math Works, USA). Raw traces of evoked potentials of each animal were

averaged (from 3-6 stimulations), respectively. The raw traces showed a typical and reproducible pattern of positive and negative peaks following sensory stimulation. Among the peaks, the first positive peak was too small and too variable to be used for systematic analysis. The amplitudes of the subsequent peaks (N1, P2 and N2) were calculated from baseline. Based on this, we computed the vertex peak-to-peak amplitude (P2-N1). Data was shown as individual values and mean values with standard error of the mean (SEM).

2.12 Statistics

Data were calculated and presented as mean values (sometimes with individual values) ± standard error of the mean (SEM), if not stated differently. Normality of the datasets was tested by Anderson-Darling test. In the study of capsaicin-induced pain, data were compared with t-test, followed by Benjamini and Hochberg multiple comparisons test, if not stated differently. In the study of evoked pain responses, for column analyses, two-tailed paired t-test or repeated measurement of one-way ANOVA with Tukey's multiple comparisons was applied for normally distributed datasets. Wilcoxon matched-pairs signed rank test or Friedman test with Dunn's multiple comparisons test was used for non-Gaussian distributed data. For group analyses, two-way repeated measurement ANOVA was calculated with Bonferroni's multiple comparisons test. The significance was shown on the figures with asterisks or hashtag (*$p<0.05$, **$p<0.01$, ***$p<0.001$, ****$p<0.0001$; ###$p<0.001$, ####$p<0.0001$).

In addition, in the study of capsaicin-induced pain, a multivariate regression analysis was adopted to identify potential differences when several parameters were integrated. Data were fitted to multivariate logistic regression models to detect the parameters making a difference in the differentiating saline from capsaicin injection. Among 6 frequency bands from 11 brain regions, there were 11 parameters for CFC, 66 parameters for PSD (11*6), and 330 parameters for coherence (55 combinations of interregional coherence among 6 frequency bands). And from 16 mice, each of which were applied both saline and capsaicin injection, 32 observations were obtained. By applying multiple imputation (Li, Stuart, and Allison 2015) in the light of a predictive mean matching approach (Rubin and Schenker 1986), missing values of the parameters out of malfunction of electrode were imputed and added to the parameter set. In total, there were 7.95% missing values for

PSD and CFC analysis as well as 14.20% for coherence analysis, as a result of the exclusion of 14 channels, most of which were from ipsilateral S1 of three mice.

A variable selection was done because there were a lot more parameters than observations in the dataset. By selecting the variables, noise in the data was reduced, resulting in a smaller possibility of conclusions driven by chance. Besides, this selection allowed for discovery of suitable variables which best fitted to distinguish capsaicin from saline injection. For these purpose, the elastic net (Zou and Hastie 2005; Friedman, Hastie, and Tibshirani 2010) is an appropriate model for variable selection when parameter were more than observations (p>n). In a normal logistic regression, the expectation of the outcome variable Y given the covariates X is calculated as:

$$E(Y|X) = \frac{1}{1 + \exp(-\mathrm{X}^{\mathrm{T}}\beta)}$$

While in elastic net the formula was restrained by:

$$\alpha\left|\left|\beta\right|\right|_1 + (1 - \alpha)\left|\left|\beta\right|\right|_2^2 \leq t$$

This constraint led to a sparser vector β and thus less variables selected in the elastic net model.

By applying grid search and 8-fold cross-validation, the parameters t and α were selected. Firstly, the dataset was randomly divided into 8 folds of equal size. Then, for every combination of t and α from the predefined grid, each fold was test once and the remaining 7 folds were trained to predict the missing one by elastic net. This resulted in 8 predictions, the mean accuracy of which was compared as the metric to assess which combination of t and α gave rise to the best prediction. Finally, the parameters were selected to be included into the model with β of a non-zero value.

The selected variables (PSD, CFC, and coherence) in each analysis were fitted to a logistic regression classification model. The outcome variate was the type of injection (saline or capsaicin) and the selected variables were considered as covariates. To appraise the classification models, receiver operating characteristics (ROC) is usually performed. In our study, the respective sensitivities and specificities were computed for every possible threshold of classification between capsaicin and saline injection. The sensitivity was

plotted as ordinate and the specificity abscissae. The area under curve (AUC) indicates the performance of the classification, resulting in a range of 0.5 -1 (1 represents a perfect classification while 0.5 referred to a chance level of classification). The AUC values and the prediction accuracy were calculated with 95% confidence intervals (CIs) and plotted on the ROC-curves. The confidence intervals were calculated according to the methods by Wilson (Chiang 1966). Wilcoxon-Mann-Whitney U-test (DeLong, DeLong, and Clarke-Pearson 1988) was performed to test whether the AUC of capsaicin and saline groups were significantly differed from chance (AUC = 0.5). For the purpose of refraining overfitting and of presenting a realistic estimate of the ROC-curves, they were brought about by 8-fold cross-validation. As a result, beta values were calculated as a mean of all the cross-validations. All p-values from the classification were corrected by Benjamini and Hochberg multiple comparisons test. Univariate significant tests were done in MATLAB (MathWorks, USA) and further computations were performed in R (R Core Team 2018).

3. Results

In this study, I did systematic analysis of electrophysiological features across brain regions in freely moving mice in different pain conditions. In capsaicin-induced acute pain, neuronal network oscillations were analyzed from local field potential recordings. Then, to facilitate the study of laser-evoked potentials in mice, a new apparatus was developed and evaluated. Last, by using the custom built apparatus, I studied the pain-related evoked potential features in multiple brain regions in both naïve mice and in mice with inflammatory pain.

3.1 Neuronal network oscillations of freely-moving mice in capsaicin-induced pain

In order to find a network-level correlate of acute, prolonged pain we recorded field potentials from various relevant brain regions. The targeted brain regions for recordings and analysis were anterior cingulate cortex (ACC), insular cortex (Ins), primary somatosensory cortex (S1), ventral posterolateral thalamic nucleus (VPL), central nucleus of the amygdala (AMYG), olfactory bulb (OB) and the parietal cortex (PAC). AMYG, OB and PAC were only recoded in the ipsilateral side of the capsaicin/saline injection (left hind paw), due to the restricted number of recording channels (Figure 3.1.1 A). The electrode positions were verified by Nissl staining (Figure 3.1.1 B, C and D). One week after the electrode implantation, habituation recordings of local field potentials (LFPs) were performed in the home cage of freely moving mice. Another week later, trials of LFP recordings were conducted during which saline was injected into the mouse hind paw, followed by capsaicin injection on the second day under the same conditions (Figure 3.1.1 A). The experiments and data analysis in this part of study were done together with Simon Ponsel.

For analysis of LFPs, periods of two minutes of recordings from the respective brain structures were chosen during four conditions: 1, baseline activity before any manipulation

(BL); 2, immediately after injection of saline (Sal); 3, immediately after injection of capsaicin (Caps); 4, one hour post injection of capsaicin (Caps 1h) (Figure 3.1.1 A).

Representative examples of raw LFP signals from the analyzed brain regions during the four conditions are shown in Figure 3.1.2. In addition to recordings of standard patterns of network activity, conditions were suited to include the respiration-entrained rhythm (RR) that overlaps with theta oscillations (Nguyen Chi et al. 2016) and encompasses frequencies up to ~8 Hz in the present study. RR is most pronounced in OB but, interestingly, was also clearly visible in ACC, Ins and VPL (Figure 3.1.2).

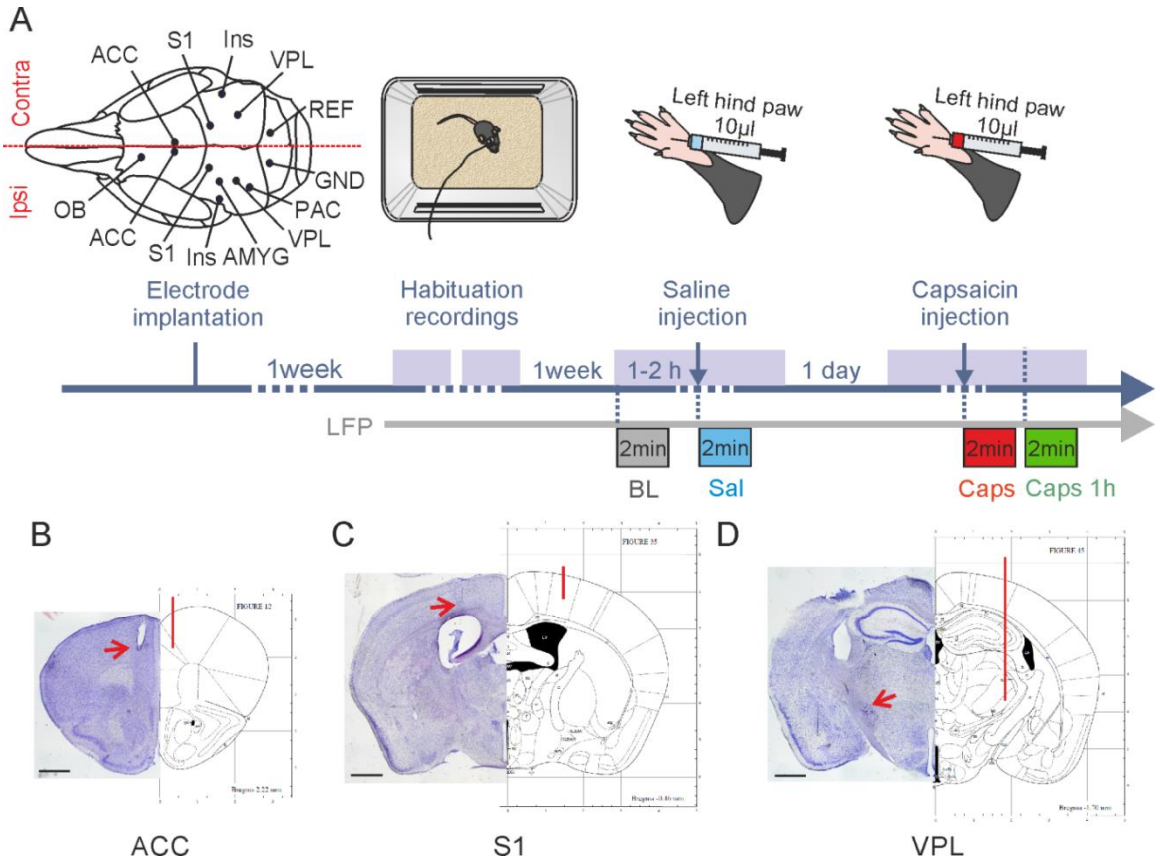

Figure 3.1.1 **Schematic drawing of experimental time course and electrode position**

A, Experimental design of the study. The left scheme shows the brain regions with chronically implanted electrodes ipsi- and/or contralateral to injection side: ACC: anterior cingulate cortex; S1: primary somatosensory cortex; Ins: insular cortex; VPL: ventral posterior-lateral thalamic nucleus; AMYG: central nucleus of amygdala; PAC: parietal cortex; OB: olfactory bulb. Two screws were implanted manually above the cerebellum as ground (GND) and reference (REF) electrodes, respectively. One week after surgery, habituation recordings were done (see middle scheme): first, local field potential (LFP) recordings in the animal's home cage for one hour, followed by a four hours recording on the following day. One week after habituation, trials with saline/capsaicin injection were performed in the home cage (right scheme): 10 µl saline (Sal) was injected into the left hind paw during ongoing LFP recordings. On the second day of recording, Capsaicin (Caps; 10 µl, 5mg/ml) was administrated into the same paw during the recording. Recordings for analysis contained two minutes (2 min) of baseline activity (BL, grey), two minutes after saline injection (Sal, blue), two minutes after capsaicin injection (Caps, red) and two minutes at one hour after capsaicin injection (Caps 1h, green). B - D, verification of electrode positions by Nissl staining. Left side of panels: representative coronal slices showing the location of implanted electrodes in ACC (B), S1 (C) and VPL (D). The lesioned positons of the electrodes are marked with red arrows. Scale bar: 1mm. Right side of panels: stereotaxic position of the electrodes indicated by red lines in a schematic illustration (Paxinos and Franklin, 2004).

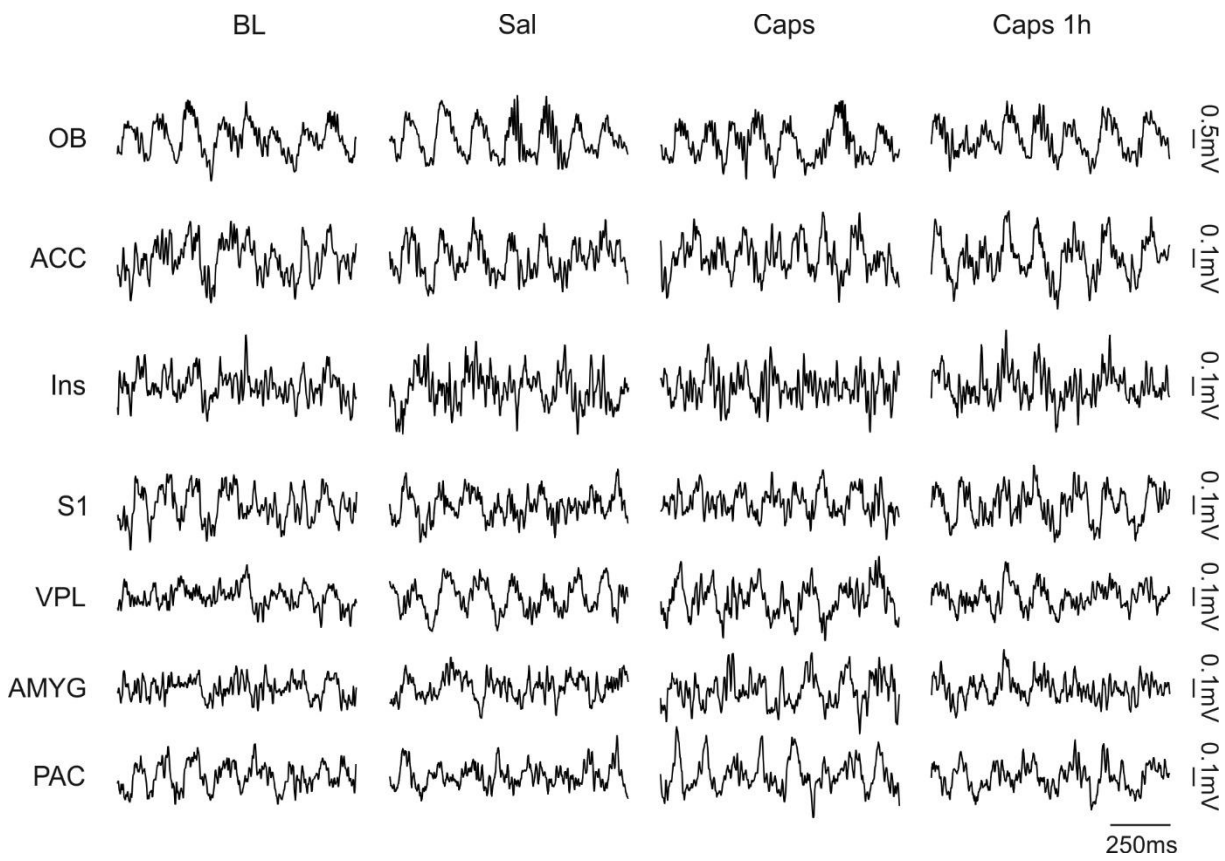

Figure 3.1.2 Raw local field potential (LFP) traces of recorded brain structures and experimental conditions.

Recorded brain regions from top to bottom: OB: olfactory bulb; ACC: anterior cingulate cortex; Ins: Insular cortex; S1: primary somatosensory cortex; VPL: ventral posterior-lateral thalamic nucleus; AMYG: central nucleus of amygdala; PAC: parietal cortex. LFP traces were taken from the hemisphere contralateral to the injection side with exception of OB, AMYG and PAC which were recorded only ipsilaterally. Analyzed conditions from left to right: baseline recording (BL); immediately after Sal injection (Sal); immediately after capsaicin injection (Caps); one hour after Caps injection (Caps 1h). Note that slow frequency oscillations (< 8 Hz) in most of the brain regions are coherent with oscillations in OB.

3.1.1 Behavioral tests: pain, respiration rate and movement

To rule out the confounding effect of respiration and movement, we analyzed averaged respiration rates (Figure 3.1.3 A) movement activity (Figure 3.1.3 B) under the four analyzed conditions. Respiration was monitored by oscillations in olfactory bulb (OB) and movements were measured as the integral of the three accelerometer signals. Respiration rates differed between the four conditions (one-way ANOVA test; $F(3,45) = 4.065$; $p<0.05$; $n=16$). Multiple comparisons revealed a significant reduction of respiration rates between baseline (BL, 8.5 Hz) and capsaicin (Caps, 7.5 Hz) (Tukey's multiple comparisons test, $F(3,45) = 4.065$, $p<0.05$, $n=16$). However, no significant difference was detected in any other pairwise comparison, especially not between Caps and Sal (the control group). As for movement activity, there was no significant change in the integrated motor activity between the four conditions (one-way ANOVA test; $F(3,45) = 0.2427$; $p>0.5$; $n=16$;Figure 3.1.3 B).

Visual inspection during the experiments revealed that mice frequently licked the left hind paw during the first two minutes after injection of capsaicin, indicating ongoing pain. In contrast, no hind paw licking was observed after saline injection. As a quantitative measure, pain sensation was validated with the electronic von Frey hair test in six animals. Similar to the traditional von Frey hair, the electronic von Frey hair test evaluates mechanical hyperalgesia by measuring the threshold of paw withdrawal following mechanical stimulation. An advantage of the electronic von Frey hair is that less repeats are needed, thus leading to less habituation and stress for the animal. Averaged paw withdrawal latencies showed a significant difference between the control group (Sal) and the capsaicin group (Caps) (two-way ANOVA; $F(1,15) = 40,71$; $p<0.0001$; $n=6$; Figure 3.1.3 C). Mean withdrawal threshold decreased significantly immediately (2 min) and one hour (1 h) after capsaicin injection (Caps) compared to saline injection (Sal) (Bonferroni's multiple comparison test, $p<0.001$ at 2min and $p<0.01$ at 1h; $n=6$). This result suggests clear signs of tonic pain following capsaicin injection, with hyperalgesia persisting at least until one hour after the nociceptive cue.

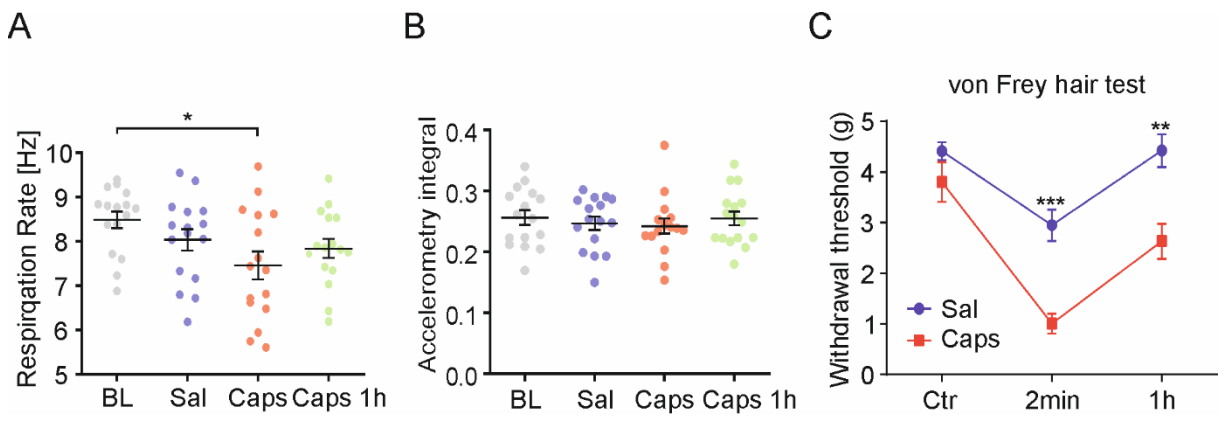

Figure 3.1.3 Quantitative measurements of respiration rate, movements and mechanical withdrawal threshold.

A, Averaged Respiration rates of the four analyzed conditions: baseline (BL), the first two minutes after saline (Sal) or capsaicin (Caps) injections as well as one hour after capsaicin injection (Caps 1h). A significant decrease of respiration rate was found between BL and Caps (from mean values of 8.5 Hz to 7.5 Hz). Note that there was no difference between Caps and the control group (Sal). Data are shown as mean values with SEM. Significance was tested with one-way ANOVA with Tukey's multiple comparisons test, $F(3,45) = 4.065$; *$p<0.05$; $n=16$]. B, Mean movement activity levels based on integration of accelerometer signals. There was no difference between the four conditions. Data are shown as mean values with SEM. One-way ANOVA; $F(3,45) = 0.2427$; $p>0.5$; $n=16$. C, Von Frey hair test revealed increased pain sensation of two minutes and one hour after capsaicin injection than saline injection. Data are shown as mean values with SEM. Significance was tested with two-way repeated-measures ANOVA with Bonferroni's multiple comparisons test ($n=6$; *** $p <0.001$ at 2 min after Caps; ** $p<0.01$ at one hour after Caps).

3.1.2 Power spectrum density and cross-frequency coupling in acute pain

Next, the frequency content of network oscillations was measured for all frequency bands in all measured brain regions during two-minute periods in the four analyzing conditions. For this, power spectral density (PSD) was computed and normalized based on the formula shown in Methods. The ipsilateral ACC showed decreased band power in the 80-120 Hz band before multiple comparison corrections (Figure 3.1.4 C). However, no power changes were detected in the first two minutes of acute pain (Caps) compared to saline (Sal) injection, after multiple comparison correction.

Next, cross-frequency coupling (CFC) was analyzed. This higher-ordered feature indicates that the amplitude of a high-frequency oscillation is rhythmically modulated by the phase of an underlying low-frequency oscillation. In our recordings, we were specifically interested in coupling between the respiration-related rhythm, RR or theta oscillations and different frequency bands of gamma oscillations. For quantitative analysis we calculated the modulation index (MI) which indicates the strength of CFC between low-frequency phase (1 - 15 Hz) and high-frequency amplitude (20 - 200 Hz). Without correction for multiple testing, cross-frequency coupling (CFC) between 1-12 Hz and 80-120 Hz increased in four regions (ACCc, ACCi, S1i and PACi). Figure 3.1.4 A shows an example of co-modulation plots after saline and immediately as well as one hour after capsaicin injection in ACCi. The warm color spot suggests an increased MI in ipsilateral ACC after capsaicin injection compared to saline injection. For a summary of normalized MI values in ACCi see Figure 3.1.4 B. At the same time, band power of slow waves (1-12 Hz) did not change and gamma band power rather decreased (80-120 Hz) in Caps compared to Sal (Figure 3.1.4 C and D), underlying that the observed increase in phase-amplitude coupling was not due to increase in band power. However, after correcting for multiple testing, these parameters were not significantly changed any more.

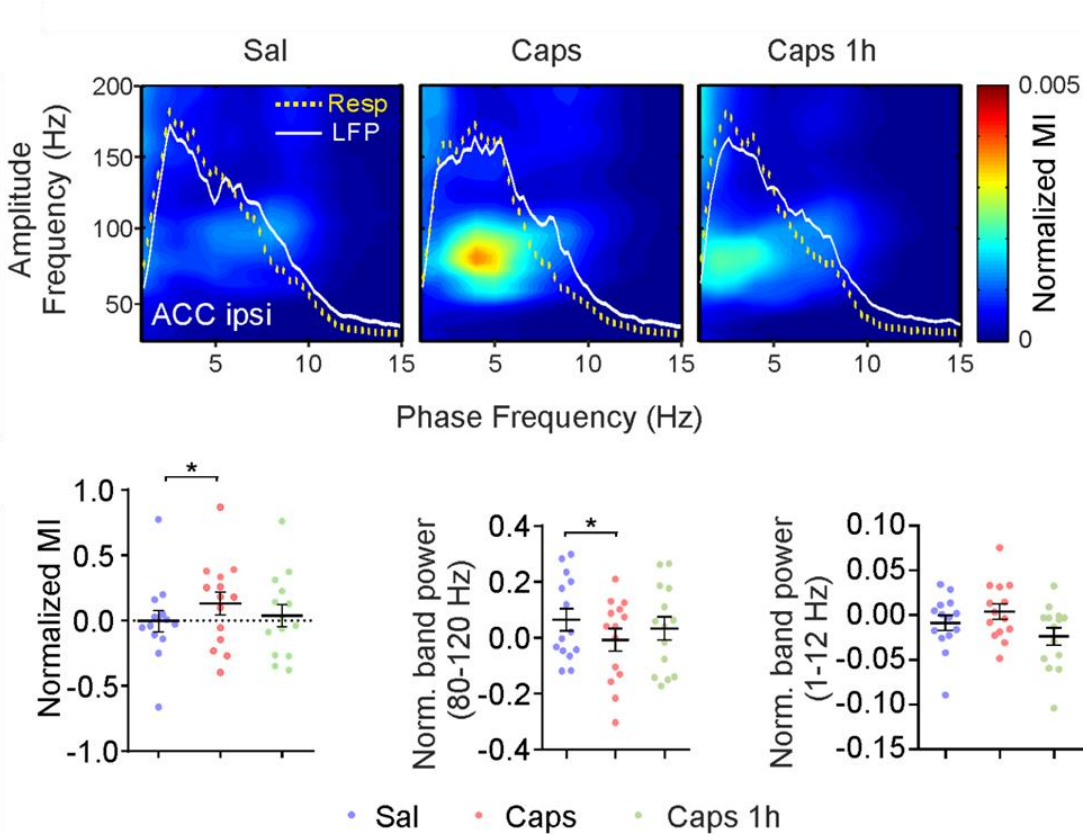

Figure 3.1.4 Cross-frequency coupling in ipsilateral anterior cingulate cortex in capsaicin-induced pain.

A, Cross-frequency coupling (CFC) in ipsilateral anterior cingulate cortex (ACCi) immediately after saline (Sal) or capsaicin (Caps) injection as well as one hour after Capsaicin (Caps 1h). Averaged heat maps (n=14) are shown. Ordinates: Oscillation frequencies of 20 - 200 Hz; Abscissae: Phase frequencies of 1 - 15 Hz. Color reflects the strength of the modulation index (MI) of CFC (Tort et al., 2010). Superimposed white solid lines indicate the power spectral density (PSD) of LFPs in ACCi in the respective recording conditions, while yellow dashed lines refer to the LFP in OB, corresponding to respiration rate (Yanovsky et al., 2014). B, Mean modulation index (MI) between phases of low frequencies (1 - 12 Hz) and amplitudes of gamma (80-120) as shown in A. MI values were normalized to baseline before averaging. The mean MI values significantly increased in Caps compared to Sal before multiple corrections. C, Averaged gamma (80-120 Hz) band power in ACCi corresponding to A decreased between Sal and Caps before multiple corrections. D, Averaged band power of low frequencies (1-12 Hz) did not alter between Sal and Caps. In B, C and D, individual and mean values with SEM are shown; paired t-test; *p<0.05, **p<0.01; n=14. While after Benjamini and Hochberg multiple corrections, none of the parameters remained significantly changed.

3.1.3 Interregional coherence in capsaicin-induced pain

A broadly distributed network is involved in pain processing. Therefore, interregional coherence of rhythmic activity was analyzed from our LFP recordings, including in multiple brain areas and frequency bands under the different conditions. Interregional coherence was calculated between all pairs of the eleven recorded regions and for six frequency bands (1-4 Hz, 4-12 Hz, 12-30 Hz, 30-80 Hz, 80-120 Hz and 120-160 Hz) immediately after saline (Sal) and capsaicin (Caps) injection, as well as one hour after capsaicin injection (Caps 1h).

A variety of significant changes in interregional coherence were found between Sal and Caps conditions. Before multiple corrections, differences were mostly found for frequencies up to 30 Hz, with highest abundance at 4 – 12 Hz. Color-coded heat maps in Figure 3.1.5 A show coherence coefficients for Sal (first row) and Caps (second and third row) in three frequency ranges: 1-4 Hz (left column), 4-12 Hz (middle column) and 12-30 Hz (right column). Warm colors indicate higher interregional coherence between two respective regions. Significant differences were observed between Caps and Sal (Figure 3.1.5 B), as well as Caps 1h and Sal ($p < 0.05$, presented in Figure 3.5.1 C with topographic relationships).

Specifically, compared to Sal condition, interregional coherence of 4-12 Hz was significantly elevated under Caps conditions between OBi and VPLc / VPLi; between ACCi and ACCc / S1i / VPLc / VPLi; between ACCc and Insi / AMYGi / VPLc / VPLi; between S1c and Insi / AMYGi / VPLc / VPLi; as well as between S1i and Insi / AMYGi. In the frequency range from 12-30 Hz, coherence increased between PACi and OBi / VPLi; and between S1c and Insc (Figure 3.1.5 B). In sum, coherence of oscillations significantly increased in Caps conditions compared to Sal, except for an isolated decrease between S1c and Insc. In all three higher frequency ranges (30-80 Hz, 80-120 Hz and 120-160 Hz), only few changes in interregional coherence were discovered. Coherence increased in Caps compared to Sal in the 30-80 Hz range between OBi and AMYGi / VPLi and in the 120-160 Hz range between OBi and Insi (data not shown). None of the apparent pairwise changes in interregional coherence, however, were still significant after correction by multiple testing.

One hour after capsaicin injection, several apparent pairwise changes of coherence were present compared to saline injection (Sal; all with $p < 0.05$; Figure 3.1.5 C). In the 1-4 Hz frequency band, reduction of interregional coherence was found between AMYGi and ACCc / PACi; between OBi and PACi; between S1i and ACCc. On the other hand, coherence increased between S1i and Insi. In the 4-12 Hz band an increase in coherence between ACCc and VPLi was the only alteration. In the 12-30 Hz frequency band, increased coherence was found between multiple brain regions: between OBi and Insi / VPLi / AMYGi / PACi; between Insi and VPLi / VPLc / AMYGi / PACi; between AMYGi and VPLi / PACi; and between S1c and VPLc. A similar pattern was observed in the 30-80 Hz band with elevated coherence between OBi and Insi / VPLi / PACi; between Insi and AMYGi / S1i / PACi; between VPLi and AMYGi / S1i; between S1c and ACCc / AMYGi. In the 80-120 Hz band, coherence showed increases between ACCc and AMYGi. In the 120-160 HZ band, increased coherence was detected between OBi and Insi; and between ACCc and PACi / VPLc / AMYGi (data not shown). Again, these apparent changes didn't remain significant after correction for multiple comparisons.

To sum up, interregional coherence of oscillations between multiple brain regions seemed to increase under capsaicin-induced tonic pain without multiple corrections, most remarkably in the frequency range of 4-12 Hz. This increase of coherence seemed to largely recover one hour after capsaicin injection, except that the increases of coherence in the frequency ranges of 12-30 Hz and 30-80 Hz remains one hour after capsaicin injection, mainly involving OBi and other ipsilateral structures. Due to the large number of pairwise combinations, however, none of the apparent differences reached significance after correcting for multiple comparisons. This, the strength of simple pairwise comparisons is limited for such high-dimensional data.

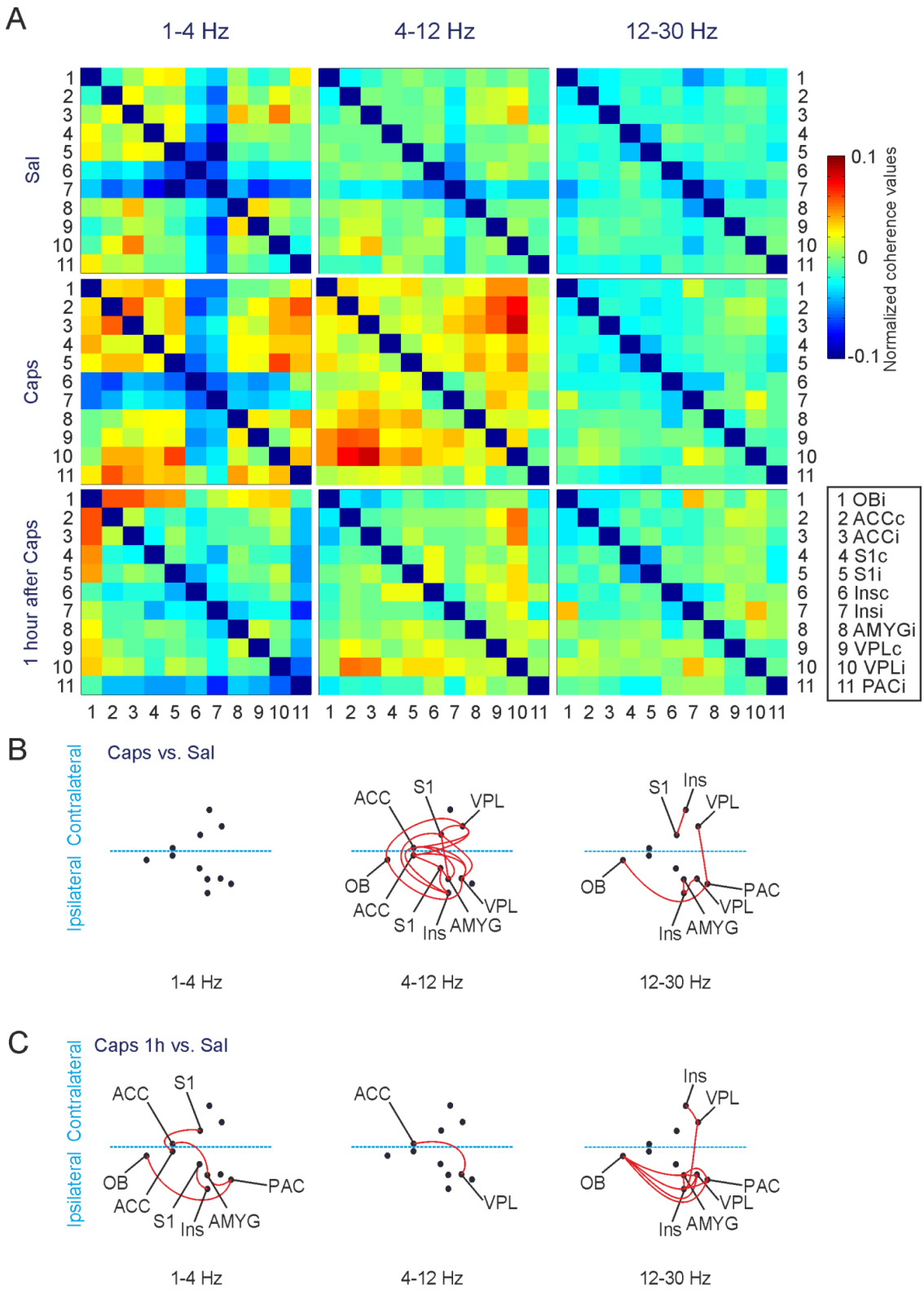

Figure 3.1.5 Coherence between multiple brain regions mainly from frequencies.

A, Color coded maps of interregional coherence between the eleven analyzed brain structures: 1: ipsilateral olfactory bulb (OBi); 2, 3: contralateral and ipsilateral anterior cingulate cortex (ACCc, ACCi); 4, 5: contralateral and ipsilateral primary somatosensory cortex (S1c, S1i); 6, 7:

contralateral and ipsilateral insular cortex (Insc, Insi); 8: ipsilateral central amygdala (AMYGi); 9, 10: contralateral and ipsilateral ventral posterolateral thalamic nucleus (VPLc, VPLi); 11: ipsilateral parietal cortex (PACi). The columns from left to right show coherence for frequencies of 1 - 4 Hz, 4 - 12 Hz and 12 - 30 Hz, respectively. The first row illustrates changes of coherences after saline injection normalized to baseline (Sal), the second row the changes after capsaicin injection normalized to baseline (Caps) and the third row the difference of one hour after Capsaicin injection normalized to baseline (Caps 1h). B and C, Schematic summary of significant differences ($p<0.05$) of interregional coherence for the above mentioned three frequency bands in A. B: Comparison between Caps and Sal; C: Caps 1h compared to Sal. The black dots indicate the individual electrode positions on the mouse skull and the red lines shows the significant changes between the connected brain regions.

3.1.4 Classification analysis for pain sensation

The pairwise comparison of coherences showed that multiple differences in individual parameters do not easily lead to a statistically valid signature of different states. We therefore tried to describe capsaicin-induced changes as differences in complex patterns. For this, we applied classification analysis to abstract features of the respective patterns and searched for a clear for differentiation between capsaicin injection-induced pain from saline injection. This part of data analysis was supported by Maximilian Pilz.

In order to discover a specific pattern for the pain state, a logistic regression model was selected for classification. Firstly, elastic net analysis (Zou and Hastie 2005) was used as a variable reduction method, by which the most influential parameters for classifying Caps versus Sal states were defined independent of the significance of individual pairwise comparisons (see details in Methods). The results of classification by logistic regression were then presented with receiver operating characteristic (ROC) curves (Figure 3.1.6). All p-values were corrected with the method by Benjamini and Hochberg for multiple comparisons testing.

Fourteen values were selected out of sixty-six potential variables from power (PSD) analysis by elastic net analysis and subsequent logistic regression (Figure 3.1.6 A). Based on these selected variables, the area under the curve (AUC) in the receiver operating characteristic (ROC) curves was 0.650 (95% CI [0.477, 0.791]) which was not significantly different from 0.5 (chance level). With the same method, seven variables were selected out of eleven CFC variables (Figure 3.1.6 B). Despite of a higher AUC of 0.711 (95% CI [0.538, 0.838]), the variables of CFC again did not show a significant difference in classification between saline and capsaicin injection. On the other hand, from the 330 variables of coherence, nine selected variables resulted in a good classification with an AUC of 0.785 (95% CI [0.617, 0.893]), which was better than chance (Figure 3.1.6 C). The selected variables were: S1i-VPLi (4-12 Hz, β: 80.1), OBi-ACCc (4-12 Hz, β: 114.3), OBi-VPLc (4-12 Hz, β: 124.4), OBi-VPLi (4-12 Hz, β: 191.5), OBi-VPLi (12-30 Hz, β: 46.9), OBi-PACi (12-30 Hz, β: 62.7), S1c-Insc (12-30 Hz, β: 195.0), OBi-Insi (30-80 Hz, β: 15.4), Insi-PACi (30-80 Hz, β: 138.8).

Having three different types of data (PSD, CFC and coherence) it was interesting to look whether an integrated classification could be obtained. Using the same analysis method, nine variables were selected, leading to a good classification with an AUC of 0.926 (95% CI [0.783, 0.977]). In other words, these nine variables allowed for a reliable classification between capsaicin and saline injection conditions. The selected variables were: coherence of S1i-VPLi (4-12 Hz, β: 66.4), OBi-ACCc (4-12 Hz, β: 121.1), OBi-VPLc (4-12 Hz, β: 144.5), OBi-VPLi (4-12 Hz, β: 184.4), OBi-VPLi (12-30 Hz, β: 0.4), OBi-PACi (12-30 Hz, β: 51.1), S1c-Insc (12-30 Hz, β: 160.3), Insi-PACi (30-80 Hz, β: 99.1) and PSD of AMYGi (120-160 Hz, β: 35.1). Among these variables, CFC didn't contribute to the final selection (Figure 3.1.6 D).

Clinical EEG studies in humans are usually restricted to frequencies up to 30 Hz. We therefore tried to reach a reliable classification after selecting only variables with a frequency below 30 Hz from PSD and coherence values (Figure 3.1.6 E). Five variables were selected from a total of 198, resulting in an AUC of 0.738 (95% CI [0.567, 0.859]), which still allowed a significant classification of pain sensation. The selected variables were: coherence between S1i-VPLi (4-12 Hz, β: 9), OBi-VPLc (4-12 Hz, β: 2.0), OBi-VPLi (4-12 Hz, β: 9.6), OBi-VPLi (12-30 Hz, β: 12.0), as well as PSD of S1c (12-30 Hz, β: 4.9).

Classification analysis was also performed between saline injection and the state at one hour after capsaicin injection, to test if there was a recovery of the pain-induced alterations. In this situation, no significant classification with results better than chance was found other than for CFC, which reached an AUC of 0.719 (95% CI [0.546, 0.844]) when using selected regions: ACCi, S1i, VPLc, VPLi, Insc, Insi and PACi (data not shown).

In addition to the classification based on electrophysiological features (PSD, CFC and coherence), non-specific effects of gender, respiration rate and movement ('clinical' parameters) were also analyzed. These parameters were constant within the whole classification process and were not used as variables. Classification alone with gender, respiration rate and movement only reached an AUC of 0.566 (95% CI [0.397, 0.722]), which was not significantly different from chance. Furthermore, including the three parameters into the integrated classification (combining PSD, CFC and coherence, see above) did not improve the result of this classification. On the contrary, the AUC was

reduced from 0.926 to 0.801. To test for gender effects, we performed a Chi square test for gender and injection type (saline or capsaicin), which did not provide any significant classification. A DeLong test was performed to compare the ROC curves statistically, resulting in a significant change between ‘clinical’ and. all parameters ($p<0.05$). This result revealed a better classification by using all the electrophysiological parameters than selecting the clinical parameters (Figure 3.1.6 F). One hour after capsaicin injection, no significant change in AUC was found compared to saline injection.

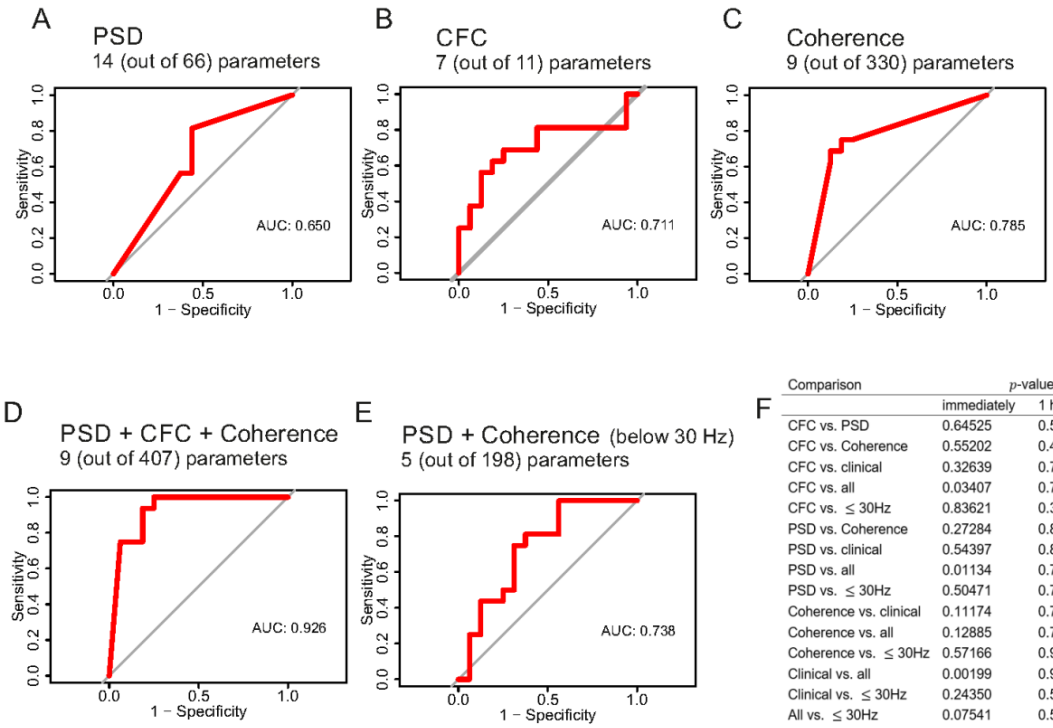

F

Comparison	*p*-value	
	immediately	1 hour after
CFC vs. PSD	0.64525	0.54218
CFC vs. Coherence	0.55202	0.48804
CFC vs. clinical	0.32639	0.73349
CFC vs. all	0.03407	0.76494
CFC vs. ≤ 30Hz	0.83621	0.37967
PSD vs. Coherence	0.27284	0.88588
PSD vs. clinical	0.54397	0.81454
PSD vs. all	0.01134	0.79374
PSD vs. ≤ 30Hz	0.50471	0.76125
Coherence vs. clinical	0.11174	0.74310
Coherence vs. all	0.12885	0.70549
Coherence vs. ≤ 30Hz	0.57166	0.90182
Clinical vs. all	0.00199	0.97802
Clinical vs. ≤ 30Hz	0.24350	0.55830
All vs. ≤ 30Hz	0.07541	0.58443

Figure 3.1.6 Classification of pain sensation by logistic regression with variable selection by elastic net model.

Logistic regression was adopted as the classifier for pain sensation, after a pre-selection of variables by elastic net model. The performance of the classification is presented by receiver operating characteristic (ROC) curves. Results were evaluated by computing the area under the curve (AUC). A, Fourteen variables were selected from 66 variables of PSD, resulting in a classification (Caps vs. Sal) with an AUC of 0.650. B, Classification of pain sensation by using 7 variables from CFC reached an AUC of 0.711. C, Classification of pain sensation by using 9 out of 360 variables from interregional coherence obtained an AUC of 0.785. D, The integrated classification of pain by using 9 out of 407 variables from PSD, CFC and Coherence reached a significant difference with an AUC of 0.926. E, Classification using only variables of PSD and coherence from frequency bands below 30 Hz, with an AUC of 0.738 by selecting 3 out of 198 variables. F, DeLong test used for comparisons of the classification performance of each ROC curve immediately and one hour after capsaicin injection (Caps vs. Caps 1h). P values show significant differences between both situations after applying the Benjamini and Hochberg multiple comparisons test.

3.1.5 Summary of this part of study

In this part of study, we reported capsaicin-induced changes of electrophysiological signals at the network level in a wide range of brain regions in the mouse. Several changes of electrical activity were found following injection of capsaicin as compared to saline: Cross-frequency coupling between low (1-12 Hz) and high (80-120 Hz) frequency oscillations was increased in several brain regions, as was the power within a sub-band of gamma (80-120) in ipsilateral ACC. In addition, interregional coherence between different brain areas was increased, mainly in the theta frequency range (4-12 Hz). However, due to the large number of parameters being compared, none of these changes was significant after controlling for multiple testing. To overcome this problem, a variable selection was performed with an elastic net model (Zou and Hastie 2005). With as few as ten selected variables a classification of pain versus non-pain with an AUC of 0.926 could be achieved. When analysis was confined to frequencies below 30 Hz, the elastic net approach still found a significant set of five parameters, resulting in an AUC of 0.738.

3.2 Development and assessment of a new apparatus for evoked sensory testing

3.2.1 Development of a new apparatus for sensory testing

The simultaneous acquisition of precisely timed electrophysiological and behavioral evoked responses in freely moving mice would be very useful in pain research as well as in other fields of sensory physiology. In this part of the thesis, I constructed an apparatus for this purpose, focusing on laser-induced heat pain and local mechanical stimulation with a fast reacting actuator. The apparatus combined sensory stimulation with data recording of both electrophysiology and behavior (Figure 3.2.1). The design of electronic circuits and the construction of the apparatus were supported by Lee Embray (electronics) and Jürgen Schmitt (mechanics).

The scaffold of the sensory stimulation system contains two layers. The upper layer holds a grid plate supporting a transparent chamber where the mouse stays during the experiment. The lower layer supports the laser stimulator, where the laser beam can be manually triggered to target the mouse hind paw through the grid plate. A control stick controls the position of the stimulator, making it possible to target the mouse paw at any position within the grid. A bottom camera close to the stimulator allows controlling the correct position of the stimulator by presenting the paw of the animal on a PC screen. A lateral camera records the behavior of the mouse, with an indicator-LED showing the precise timing of laser stimulation. Local field potentials (LFPs) including laser-evoked potentials can be recorded during the whole process of experiment. The electrophysiological signals as well as the laser stimulation are synchronized through a trigger signal from a custom-made control unit. Both the evoked potentials and videos of behaviors are presented and stored in a connected PC (Figure 3.2.1 A).

Besides the laser stimulation, the apparatus is also designed to be compatible to mechanical stimulations, for example tactile stimulation with a small rod. For this, a tactile stimulator with exactly the same size as the laser beam was built. It was controlled by a tactile stimulator driver and a separate power supply unit (PSU) to provide enough energy for stimulation. The tactile stimulator shared the same control system as the laser control

unit. All components and their connections are shown in Figure 3.2.1 B. In addition, Figure 3.2.2 shows the design of the control unit, and Figure 3.2.3 the tactile stimulator.

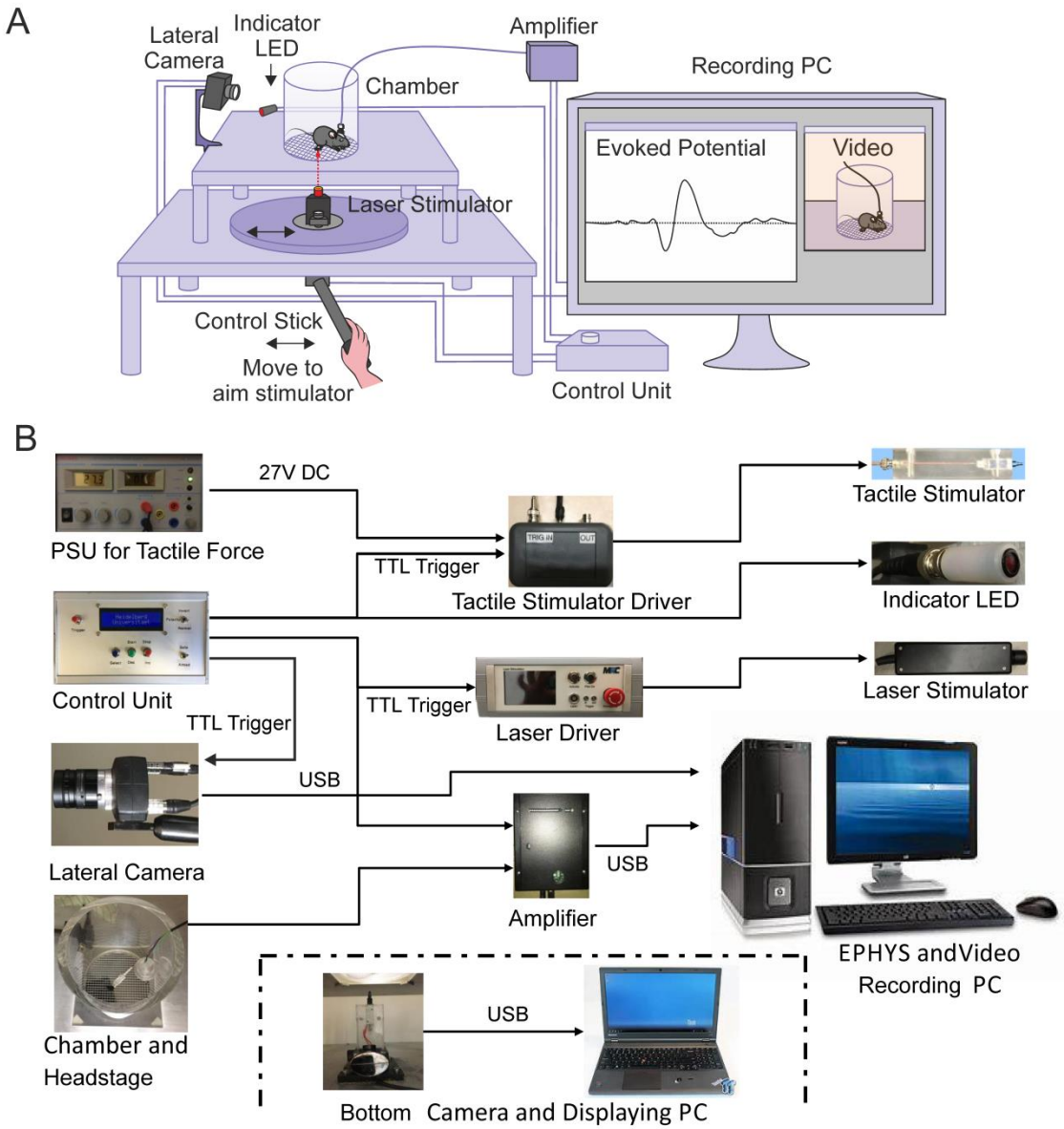

Figure 3.2.1 Illustration of the custom built apparatus for sensory testing.

A, Schematic showing the structure and connections of the custom built apparatus. B, General connectivity of the complete setup with photos of each compartment. Power supplies and controls are shown on the left, interfaces in the center part and stimulators and data acquisition system on the right. The camera and laptop at the bottom are separated from the rest of the setup and are only used for targeting the stimulator on the mouse paw. Figure 3.2.1 B was provided by Lee Embray.

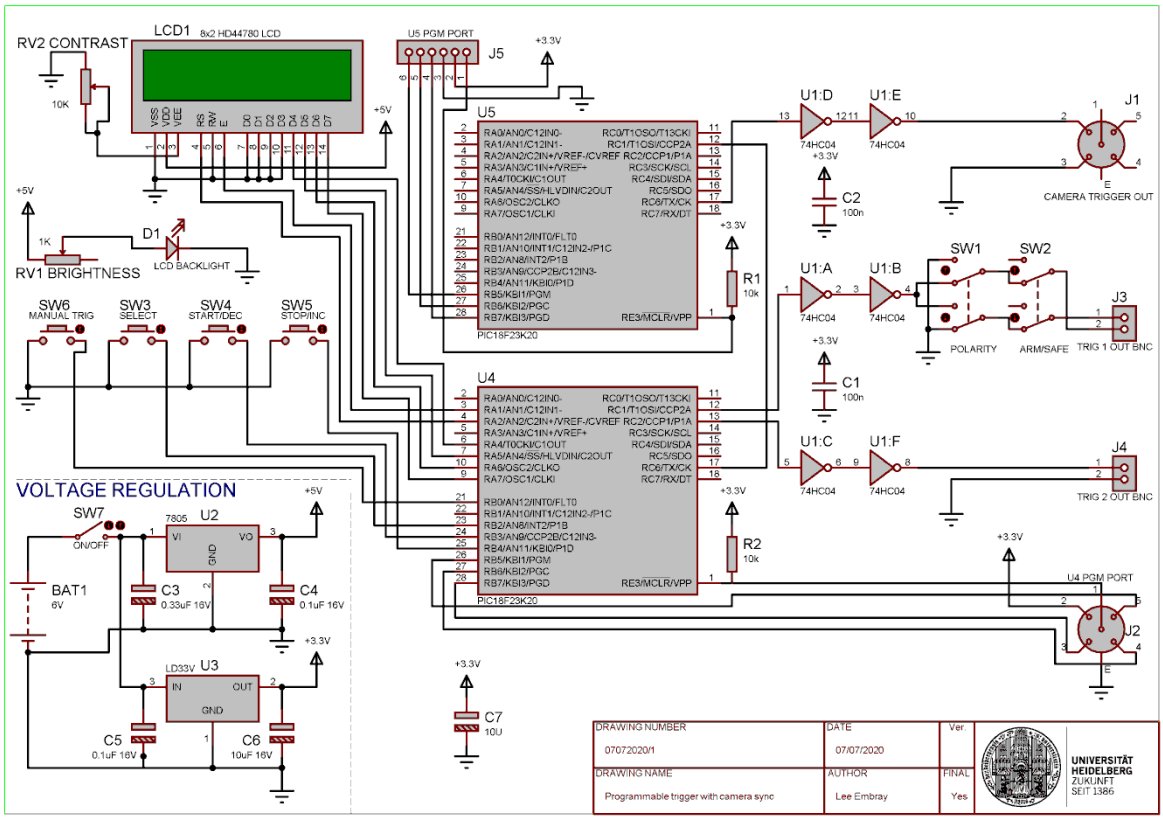

Figure 3.2.2 The electronic schematic of the control unit.

The second dedicated microprocessor (U5) solely responsible for accurately triggering the frame recordings of the camera. All other features are handled by the first microprocessor (U4). This figure was provided by Lee Embray.

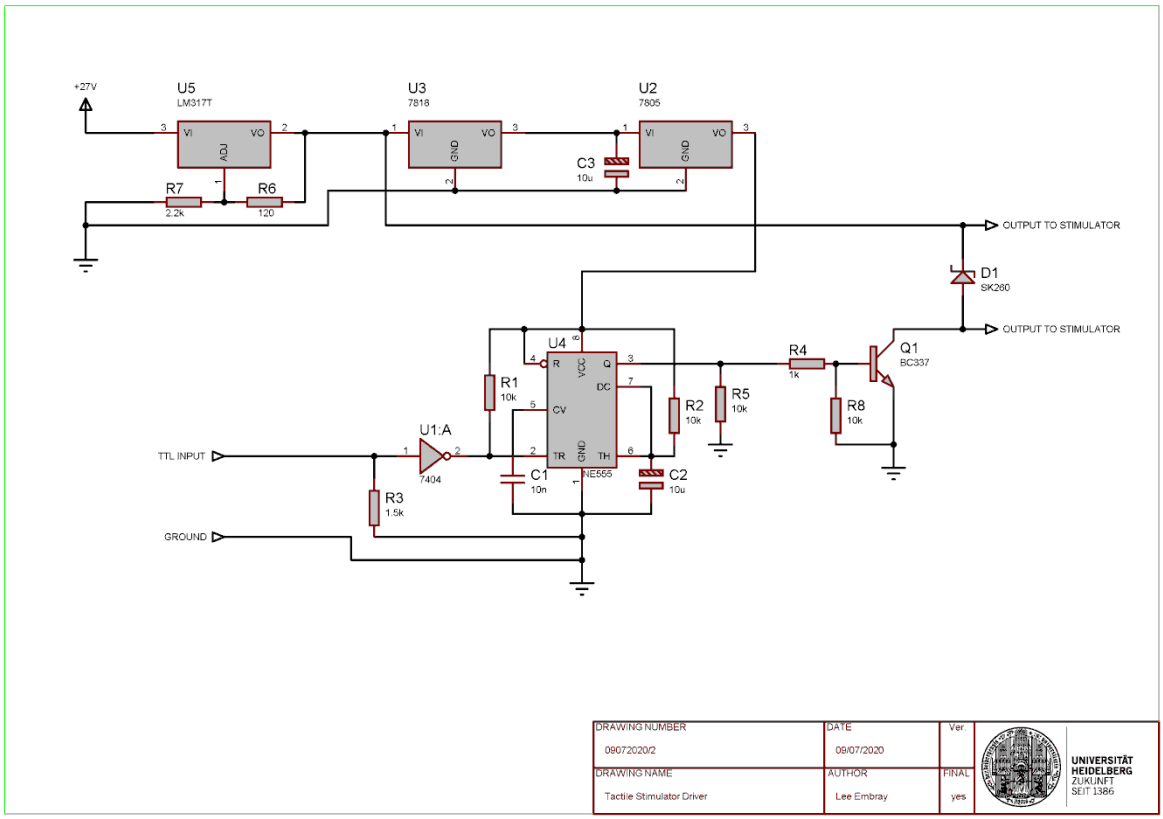

Figure 3.2.3 The electronic schematic of the tactile stimulator.

The 27V is reduced to 5v to power the NE555 chip which is responsible for the duration of the pulse sent to the actuator. U5 regulates the output voltage to 24V when the input voltage is equal or more than 27V, using an input voltage of less than 27V reduces the force applied to the actuator and increases the actuation time. This figure was provided by Lee Embray.

3.2.2 Assessment of the custom built apparatus

The custom built apparatus was tested in freely moving mice which had been previously implanted with electrodes in six brain regions including the primary somatosensory cortex (S1), parietal cortex (PACc, PACi), ventral posterolateral thalamic nucleus (VPLc, VPLi), anterior cingulate cortex (ACCc, ACCi), ventral posterolateral thalamic nucleus (VPLc, VPLi), posterior insula (Insc, Insi) and central nucleus of the amygdala (AMYGc), either in one or both hemisphere (Figure 3.2.4). The positions of the electrodes were validated by Nissl staining of coronal brain slices (Figure 3.2.5).

Recordings of local field potentials and behavioral responses towards stimuli started after recovery from surgery and a subsequent period of habituation to the experimental environment (Figure 3.2.4 A). The laser/tactile stimulation was triggered through the grid plate, by guidance of a bottom camera to aim the laser beam towards the hind paw of the freely moving mouse (Figure 3.2.4 B and C). A lateral camera recorded the behavior of the animal during the stimulation (from the mouse was immobile to 30 seconds post-stimulation). A red indicator-LED was activated simultaneously with the stimulation trigger to indicate the time of sensory cues. The LED light was directed towards the camera, facilitating its observation and excluding that it provided an additional cue for the mouse (Figure 3.2.4 D and E).

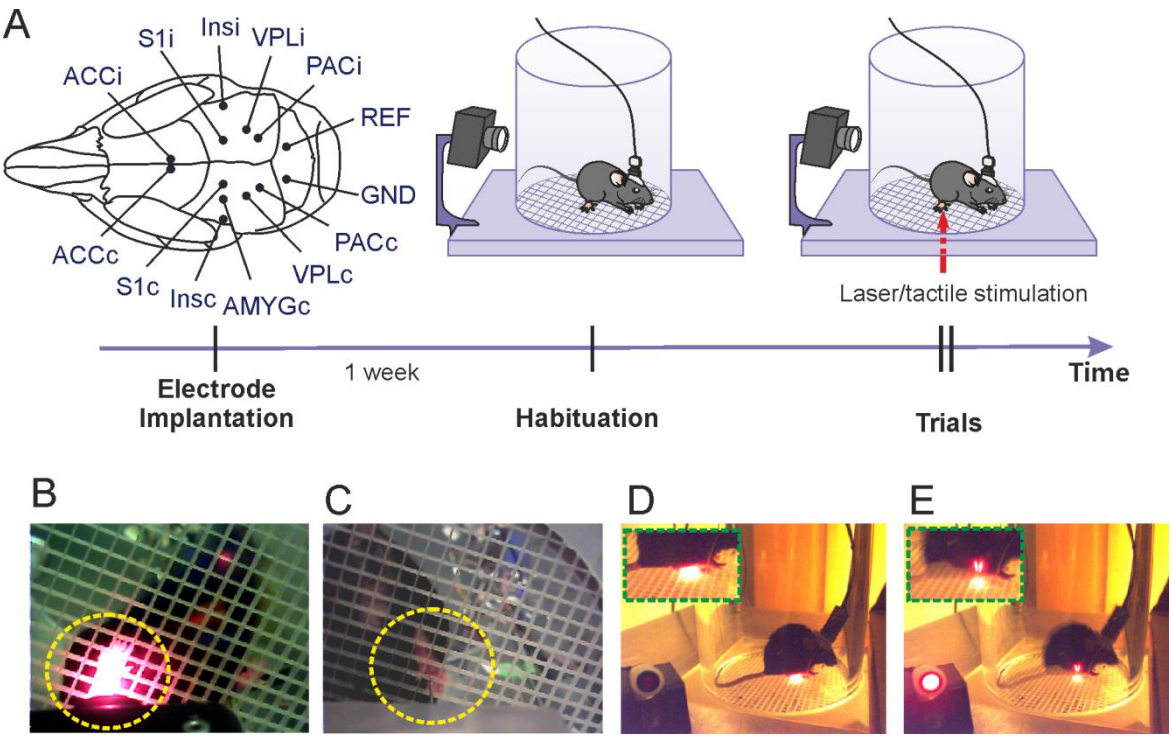

Figure 3.2.4 Experimental procedure for the assessment of the custom made apparatus.

A, Schematic illustration of the experimental procedure. One week following electrode implantation several habituation trials were performed. Afterwards, recording trials with laser/tactile stimulations were conducted. The view from the bottom camera shows the mouse right hind paw targeted by the laser (B) and by the tactile stimulator (C). D,E the view of the lateral camera shows the posture and behavior of the mouse. Panel D shows a resting situation, panel E shows paw withdrawal following laser stimulation.

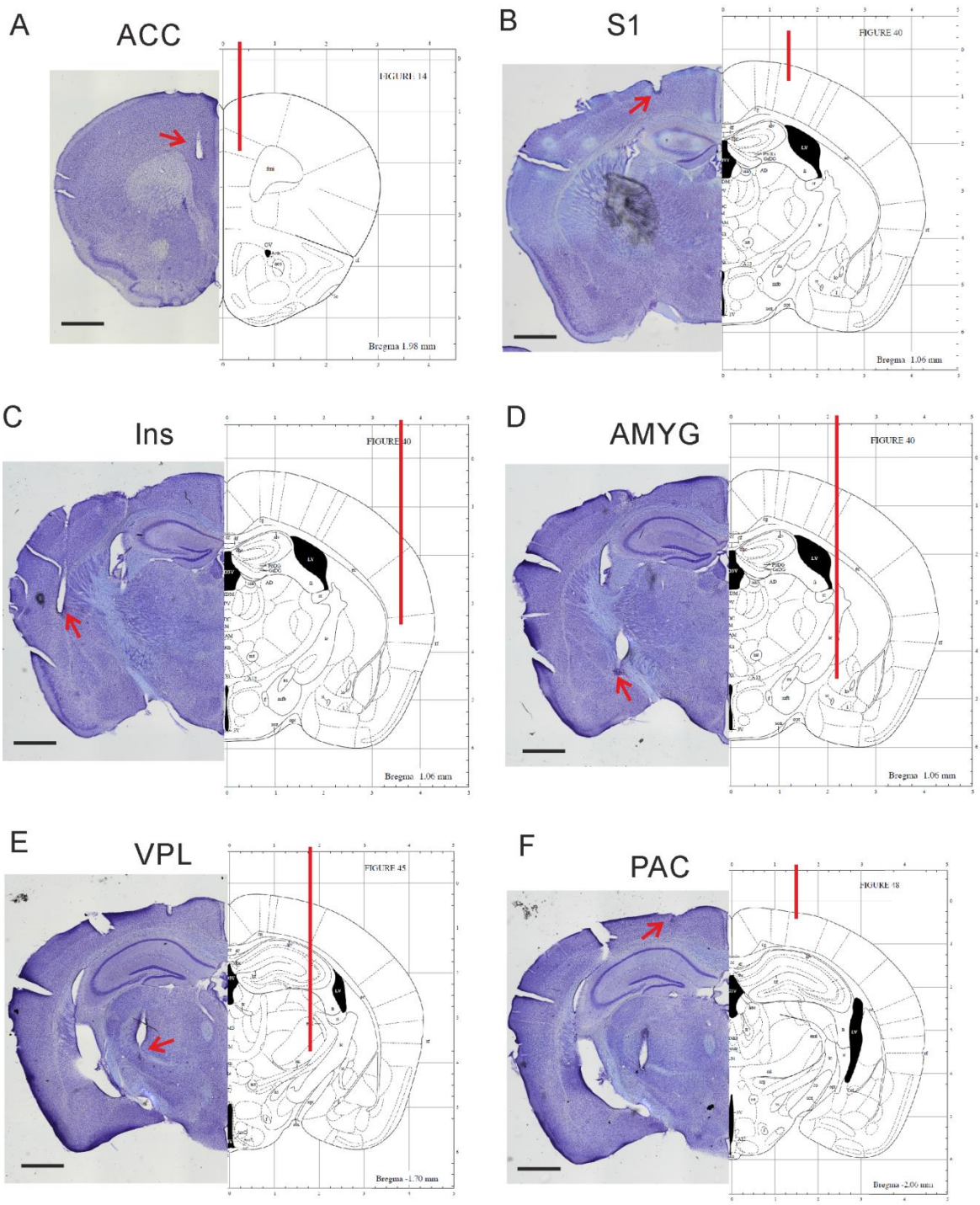

Figure 3.2.5 Verification of the electrode position by Nissl staining.

A-F, On the left side of each figure, representative coronal slices with Nissl staining show the implanting positions of electrodes in ACC (A), S1 (B), Ins (C), AMYG (D), VPL (E) and PAC (F), respectively. Red arrows indicate the lesioned position of the respective electrodes. The right side of each figure shows a scheme of the targeted brain regions with the electrode position marked by red lines (Paxinos and Franklin, 2004).

To assess the functions of the custom-made apparatus, laser stimuli of different durations (3ms, 5ms and 10ms) were applied to induce different stimulus intensities (Figure 3.2.6). To find the right range of durations, stimuli were firstly tested for painfulness at human fingers. In mice, these stimulus pulses led to 100 % right hind paw withdrawal, indicating pain or at least an adverse sensation (data not shown). The latency of hind paw withdrawal decreased significantly from 5 ms to 10 ms of laser stimulations, indicating different intensities of the sensation (Figure 3.2.6 D). Following paw withdrawal, several behavioral features indicating pain were recorded and analyzed. Mice returned their hind paw to the grid in a guarding manner, holding the paw aloft, or reduced ground contact to the heel or toes of the paw while resting or moving, which was referred to as guarding time (Figure 3.2.6 A). Freezing behavior was also observed, which was defined by no visible movements except for respiration (Figure 3.2.6 B). In some trials, mice showed several fast paw shakes, called flinching (Figure 3.2.6 C). All these behaviors served as a behavioral measure of pain sensitivity. For quantification, time of guarding and freezing, as well as times of flinching within 30 seconds post laser stimulation were measured.

Averaged behavioral features of each animal are shown in Figure 3.2.6 E, F and G. The hind paw guarding time significantly increased after 10 ms laser stimulation compared to 3 ms or 5 ms (Figure 3.2.6 E). Differences in freezing and flinching, despite of an apparently graded response to laser stimulation of different durations, did not reach statistical significance (Figure 3.2.6 F and G). As the total measuring time (30s) was relatively short, there was a relatively big variation of the behaviors. To summarize the pain-related behavioral features more accurately, the integrative effect of pain sensitivity was measured by calculating a simplified pain score. The pain score summed up the occurrence of guarding, freezing or flinching of each animal in each trial. For example, a mouse displaying two of the three behavioral features obtained a pain score of two in the respective trial. There was a significant increase of pain score at 10 ms laser stimulation compared to 3 ms, suggesting increased pain sensitivity (Figure 3.2.6 H).

To conclude, the apparatus was capable to induce graded pain sensation by laser stimuli and to record the pain-related behavioral features of freely moving mice.

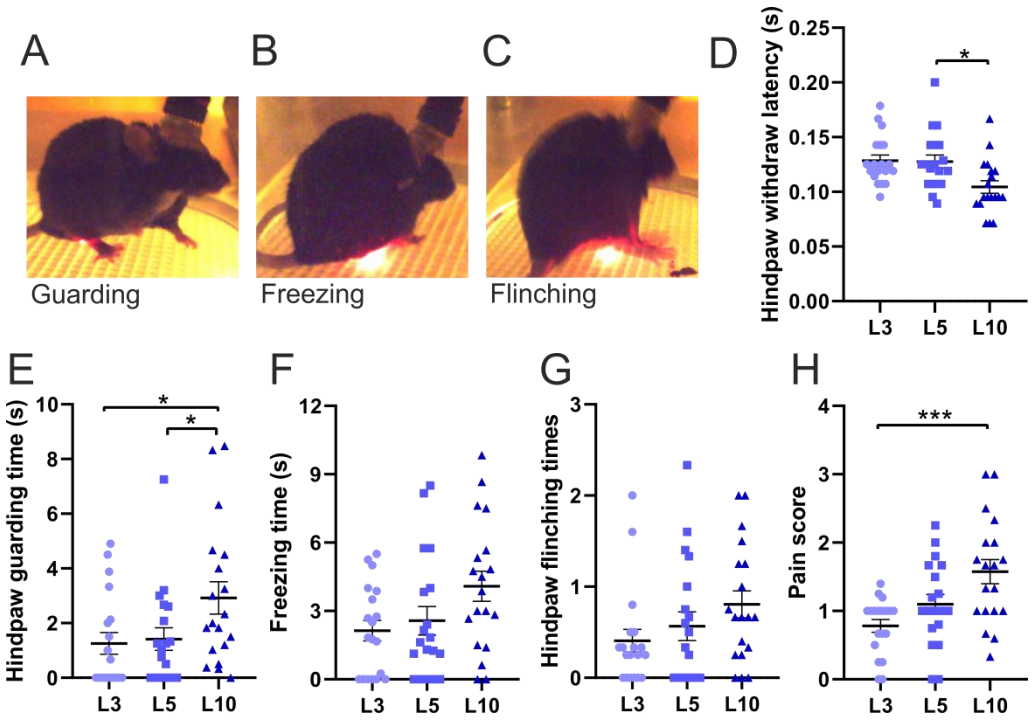

Figure 3.2.6 Behavioral features in response to laser stimulation of different intensities.

A-C, Examples of the guarding (A), freezing (B) and flinching (C) behaviors following laser stimulation by video records. D, Hind paw withdrawal latency towards laser stimulation of 3 ms (L3), 5 ms (L5) and 10 ms (L10). E-G, Quantification of pain-related behaviors as guarding time (E), freezing time (F) and flinching times (G). H, Pain score calculated from the total occurrence of guarding time, freezing time and flinching times. From D-H, averaged data of individual mice are presented with SEM. Friedman test with Dunn's multiple comparisons test for D, F, G and H; repeated measures of one-way ANOVA with Tukey's multiple comparisons test for E; n=19; *p<0.05, ***p<0.001.

In parallel to behavioral recordings, laser-evoked local field potentials were recorded from multiple brain regions including contralateral (left brain hemisphere) primary somatosensory cortex (S1c), which is pain-related brain structure widely investigated in both human and animal study (Figure 3.2.7). Evoked potentials of each animal were averaged for laser durations of 3 ms, 5 ms and 10 ms, respectively (Figure 3.2.7 A). For quantification of this signal, amplitudes of the first negative peak (N1), the second positive peak (P2) and the second negative peak (N2) were computed from baseline (Figure 3.2.7 B, C and D). A potential first positive peak was excluded from evoked potential analysis since it was unreliable and highly variant (see details in Methods). In human studies,

vertex amplitude is usually measured as the highest peak-to-peak amplitude. I therefore calculated the vertex amplitude of P2-N1 in mice (Figure 3.2.7 E). Consistent with the behavioral responses, a significant increase of the averaged N1 and P2-N1 amplitude was observed for increasing laser stimulation duration from 3ms to 10ms (Figure 3.2.7 B and E). Amplitudes of P2 and N2 amplitudes did not change with increasing laser duration, despite of a tendency of increase (Figure 3.2.7 C and D). No significant changes with laser pulse duration were observed in peak latencies of N1, P2 and N2 (data not shown).

To sum up, electrophysiological measurements yielded consistent, comparable and graded responses to an acute painful laser stimulus.

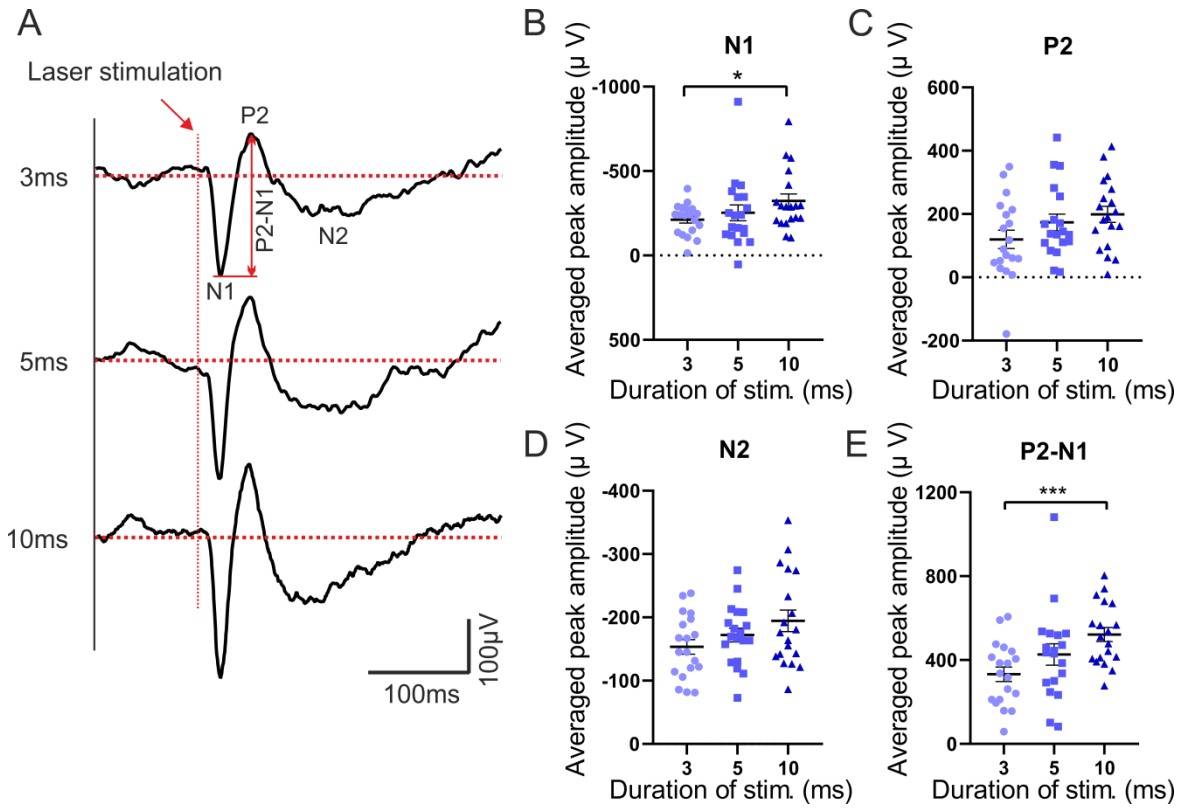

Figure 3.2.7 Features of laser stimulation-evoked potentials of different durations.

A, Mean laser-evoked potentials in S1 contralateral to the stimulation side. Data from all animals undergoing laser durations (3ms, 5ms and 10ms) on the right hind paw. The red arrow indicates the arrival time of the stimulation pulse. The dashed red horizontal lines refer to the baseline. The first negative peak (N1), the second positive peak (P2), the second negative peak (N2) and the vertex peak P2-N1 are indicated in the figure. B-E, Averaged peak amplitudes of N1 (B), P2 (C), N2 (D) and P2-N1 (E). For B-E, averaged data of individual mice are shown with SEM. Friedman test with Dunn's multiple comparisons test, n=19, *p<0.05, ***p<0.001.

In addition to laser stimulation, the custom built device is suited to convey mechanical (tactile) stimulation, too. A mechanical stimulator was constructed with a blunt needle tip to convey tactile stimulation. The tactile stimulator has exactly the same size as the laser stimulator, facilitating the integration into the apparatus, as well as switching between tactile and laser stimulation (Figure 3.2.8).

Next, I measured the evoked responses following mechanical (tactile) stimuli of the right hind paw which served as non-pain control stimuli for our pain studies. Evoked potentials were measured and averaged by the same method as applied for laser stimulation (Figure 3.2.8 A). Reliable N1, P2 and N2 responses in contralateral S1 were observed with a mean delay of 24 ms between the trigger time (Trigger) and the cue to the mouse hind paw (Tactile stimulation). Only 68% of trials resulted in hind paw withdrawal which was significantly less than reactions to laser stimulation (100%; Figure 3.2.8 B). Compared to 10 ms laser stimulation, the tactile stimulation resulted in significantly lower values in all measured behavioral features including hind paw withdrawal latency (Figure 2.7.1 C), guarding time (Figure 3.2.8 D), freezing time (Figure 3.2.8 E) and flinching times (Figure 3.2.8 F). Consistently, the integrative pain score of tactile stimulation was much lower than that of laser stimulation (Figure 3.2.8 G).

Taken together, the custom-made apparatus was able to measure responses to mechanical stimuli, with a good differentiation between mechanical and laser stimulation.

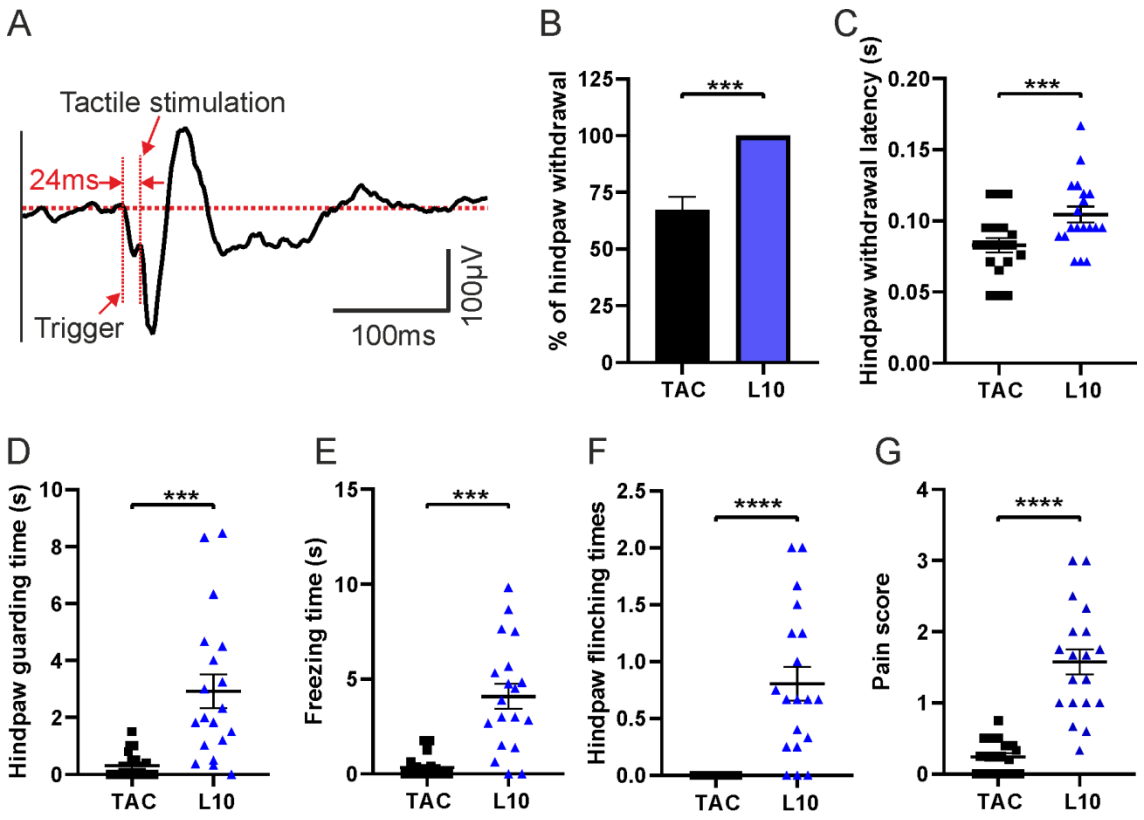

Figure 3.2.8 Evoked potentials and behavioral responses following mechanical tactile stimulation.

A, Averaged evoked potential after tactile stimuli recorded in S1 contralateral to the stimulation side. Due to the mechanical trigger, there is a delay of 24ms from the trigger to touch because of the mechanical delay in activation of the actuator. And the noise of the trigger also led to a sound-evoked component before the stimulation reaching the paw. B, Mechanical tactile stimulation (TAC) led to lower percentage of paw withdrawal compared to 10ms laser stimulation (L10). C-F, Significantly lower values for tactile stimulation (TAC) compared to 10ms (L10) laser stimulation in hind paw withdrawal latency (C), guarding time (D), freezing time (E) and flinching times (F). G, Pain score calculated from frequency of occurrence of guarding time, freezing time and flinching times. For B-G, averaged data are shown with SEM. Wilcoxon matched-pairs signed rank test for B,C,E,F and G; two-tailed paired t-test for D, n=19, ***p<0.001, ****p<0.0001.

3.2.3 Summary of this part of study

In this part of study, we developed a new apparatus for evoked responses of freely moving mice during sensory testing. The custom built apparatus allowed electrophysiological recordings of laser-evoked potentials as well as pain-related behaviors of the animal. Graded pain responses of both evoked potentials and behavioral features were reliably acquired by laser stimulations of different durations. Besides, the apparatus was also suited for mechanical tactile stimulation which elicited significantly lower levels of pain-related behaviors and can serve as a non-painful control.

3.3 Electrophysiology of evoked pain responses: naïve and in inflammatory pain

As described in the last chapter, a custom built apparatus was developed and assessed for pain/tactile sensory testing. Electrophysiological data from contralateral (to stimulation side) primary somatosensory cortex (S1c) was presented above as an example for the functional assessment of the apparatus. For a more complete picture, the apparatus was used to measure evoked potentials from multiple structures on both brain hemispheres: the contralateral and ipsilateral primary somatosensory cortex (S1c, S1i), parietal cortex (PACc, PACi), ventral posterolateral thalamic nucleus (VPLc, VPLi), anterior cingulate cortex (ACCc, ACCi), ventral posterolateral thalamic nucleus (VPLc, VPLi), posterior insula (Insc, Insi) and central nucleus of the amygdala (AMYGc). In this chapter, I report the respective evoked potentials following laser and tactile stimulation in these brain regions in both naïve mice and mice with inflammatory pain.

3.3.1 Laser-evoked potentials in multiple brain regions of naïve mice

To create a graded pain responses, laser stimuli of different durations (3 ms, 5 ms and 10 ms) were applied to the right hind paw of freely moving mice. The laser-evoked potentials were averaged from the mean potentials of all trials of each animal in one experiment. As the most prominent early component, vertex amplitude is widely used in evoked potential analysis. In this part of study, I present the vertex amplitude of P2-N1, which integrates the amplitude changes of N1 and P2. Additionally, N2 peak amplitude was measured as the late component of the evoked potentials (Figure 3.3.1 and Figure 3.3.2). Peak latencies were analyzed respectively for N1, P2 and N2.

On the contralateral side to stimulation, the vertex amplitude of P2-N1 increased significantly after 10 ms laser stimulation compared to 3 ms. This was seen in multiple brain regions including S1, PAC, VPL, ACC and Ins, but not in AMYG (Figure 3.3.1 A). Thus, we found a graded increase of response sensitivity following rising laser intensities, compatible with increasing induction of pain. Moreover, multiple brain regions were involved in these apparently pain-related evoked responses. On the ipsilateral side to the stimulation, a significant increase of P2-N1 between 3 ms and 10 ms laser stimuli was

detected in PAC, VPL and ACC, yet not in S1 and Ins (Figure 3.3.2 A). Due to the limited number of recording channels, ipsilateral AMYG could not be recorded. On the other hand, the peak amplitude of N2 did not significantly change across the recorded regions (Figure 3.3.1B and Figure 3.3.2 B). Peak latency did not differ between different durations of laser stimuli. As an example, peak latencies of N1, P2 and N2 of both contralateral and ipsilateral S1 following laser stimulation are presented in Figure 3.3.3.

Taken together, multiple brain regions including S1, PAC, VPL, ACC and Ins were involved in processing of the acute pain sensation following laser stimulation. The vertex amplitude of P2-N1 increased with increasing laser stimulation intensity in multiple brain regions, both contralaterally and ipsilaterally. As shown in Figure 3.2.6, pain rating was also higher as the laser intensity increased. Thus, P2-N1, the vertex amplitude of the evoked potential, may serve as an electrophysiological marker of the acute pain level by laser stimulation in freely moving mice.

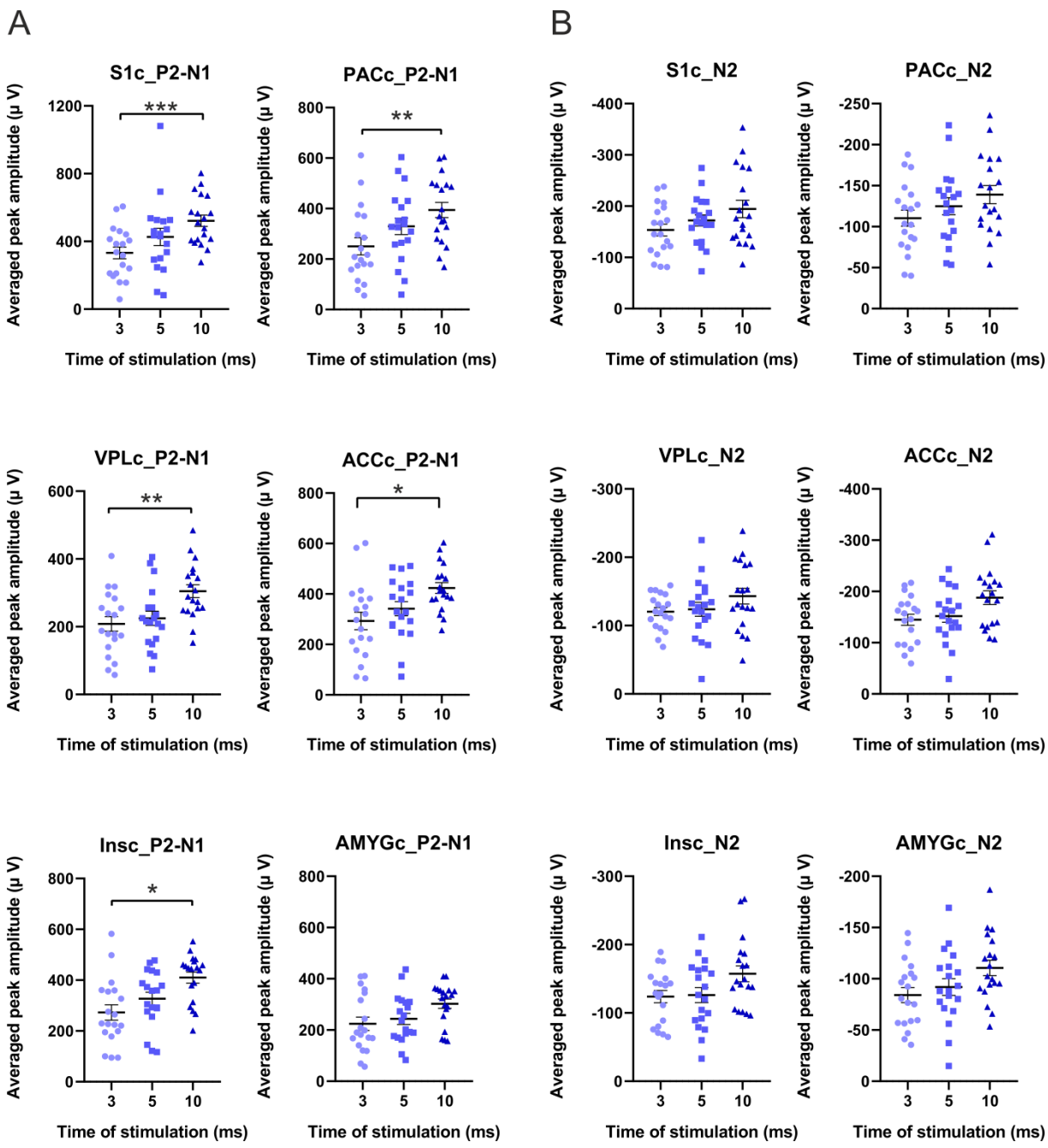

Figure 3.3.1 Peak amplitudes of laser-evoked potentials in multiple brain regions contralateral to stimulation side.

A, Vertex amplitudes (P2-N1) of recorded brain structures contralateral to stimulation side, following laser stimulation of 3 ms, 5 ms and 10 ms. B, Amplitudes of the second negative peak (N2) under the same conditions as in A. Averaged date of individual mice are shown with SEM. Friedman test with Dunn's multiple comparisons test, n=19, *p<0.05, **p<0.01, ***p<0.001.

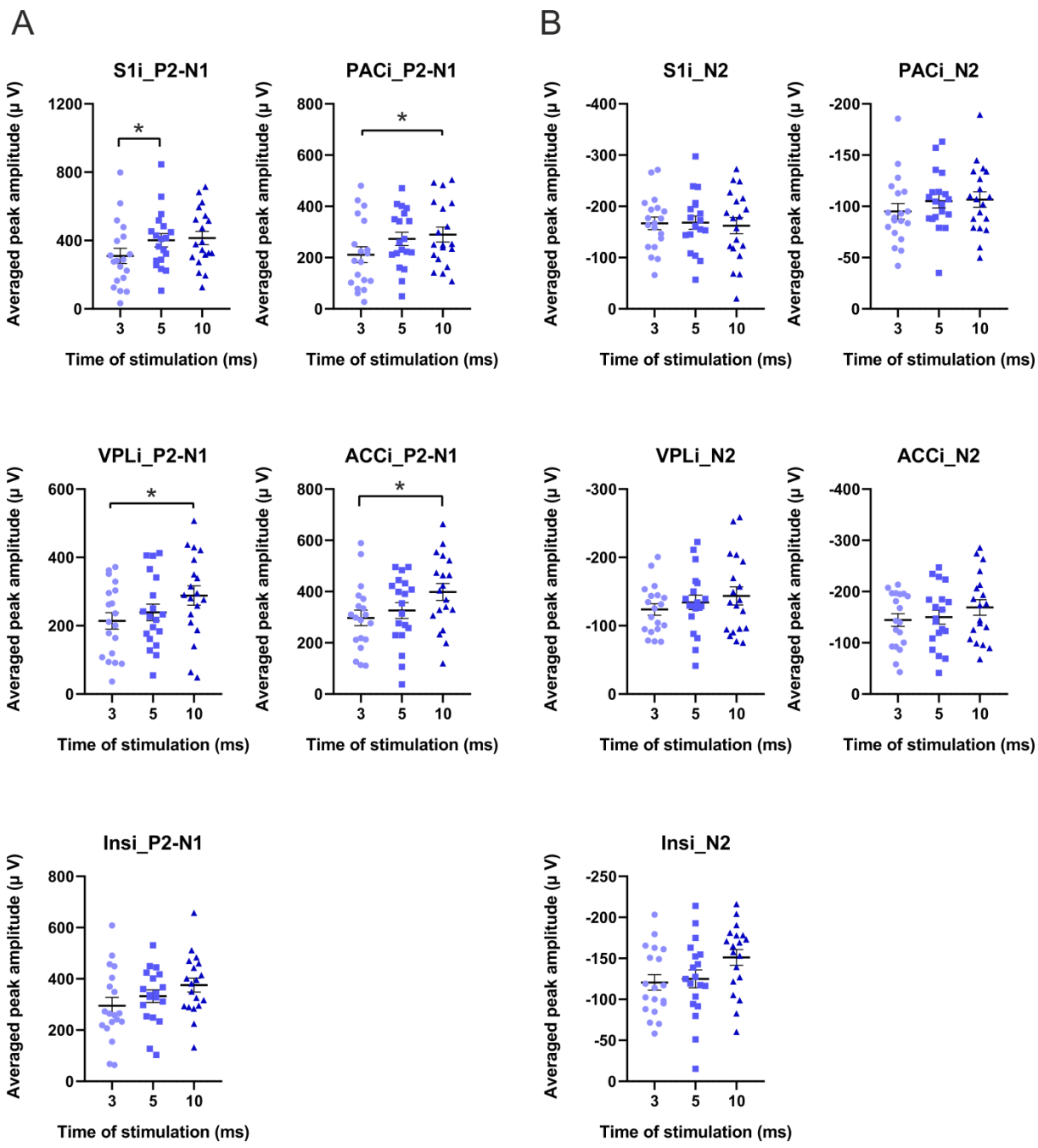

Figure 3.3.2 Peak amplitudes of laser-evoked potentials in multiple brain regions ipsilateral to stimulation side.

A, Vertex amplitudes (P2-N1) of recorded brain structures ipsilateral to stimulation side, following laser stimulation of 3 ms, 5 ms and 10 ms. B, Amplitudes of the second negative peak (N2) under the same conditions as in A. Averaged date of individual mice are shown with SEM. Friedman test with Dunn's multiple comparisons test, n=19, *p<0.05.

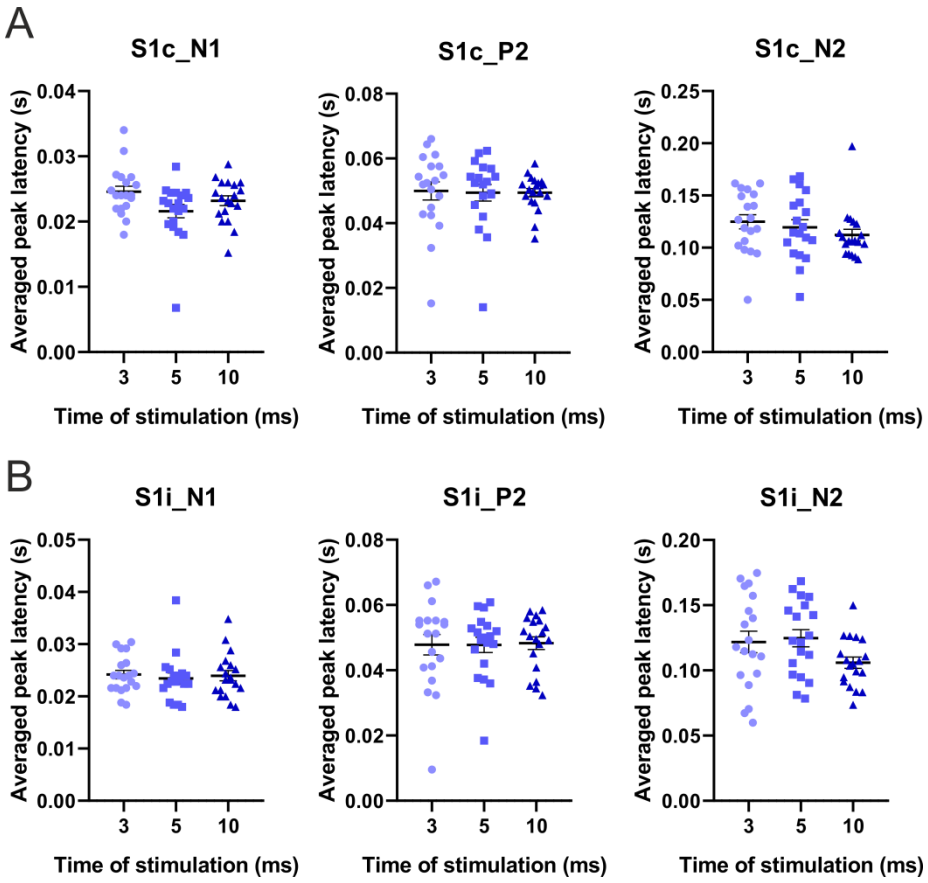

Figure 3.3.3 The peak latencies in contralateral and ipsilateral primary somatosensory cortex.

A, Peak latencies of N1, P2 and N2 in S1 contralateral to stimulation side following 3 ms, 5 ms and 10 ms laser stimulation, respectively. B, Peak latencies of N1, P2 and N2 in S1 ipsilateral to stimulation side under same conditions as in A. Averaged date of individual mice are shown with SEM. No significant differences were observed between conditions. Friedman test with Dunn's multiple comparisons test, n=19.

3.3.2 Hyperalgesia in CFA-induced inflammatory pain

Following validation of the approach in healthy, naive mice, we wanted to apply the new apparatus to study a prolonged, clinically relevant form of pain. For this, we recorded electrophysiological responses to painful stimuli in mice with inflammatory pain. Injection of complete Freund's adjuvant (CFA) is well established in inducing inflammatory pain and is routinely used for this purpose in animal experiments. Intraplantar injection of CFA results in peripheral tissue injury and hypersensitivity to tactile stimulation (Maiaru et al. 2018). CFA (undiluted, 20 µL) was injected under the plantar surface of the right hind paw. Paw withdrawal threshold at baseline (day 0), day 2 and day 4 after CFA injection was measured by the electronic von Frey hair test on both paws, contralateral and ipsilateral to the injection (see details in Methods). As a control, saline (Sal) was injected followed by the von Frey test (n=8; Figure 3.3.4).

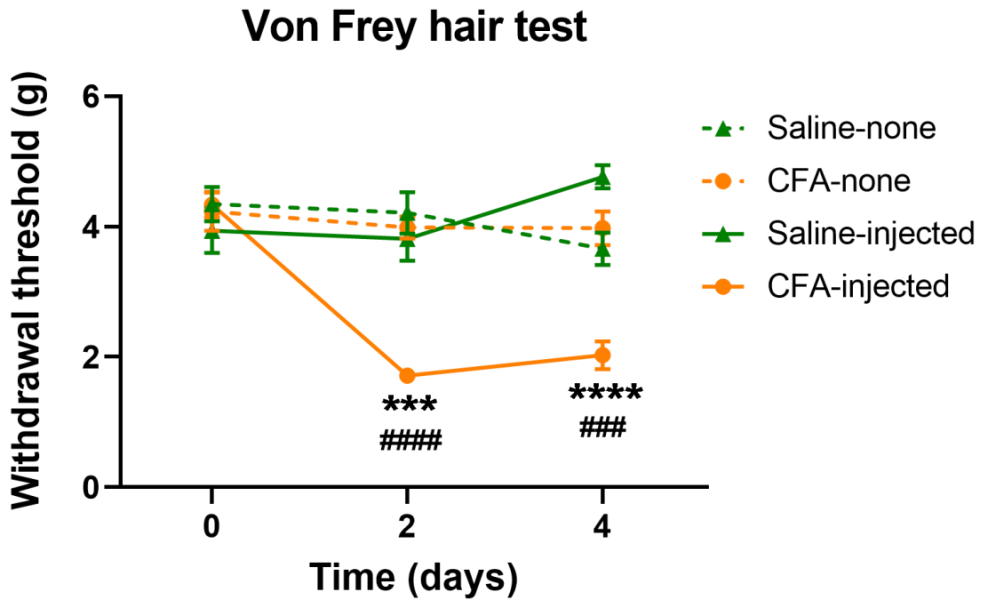

Figure 3.3.4 Von Frey hair test for the validation of hyperalgesia post CFA injection.

The withdrawal threshold (g) of both hind paws was measured at baseline (0), day 2 and day 4 after CFA injections in the right hind paw. Saline controls were measured in the same way as CFA-injected animals. CFA-injected and CFA-none: injected and not-injected paw of mice in CFA injection group; Saline-injected and Saline-none: injected and not-injected paw of mice in saline injection group. Data are presented as mean with SEM. Repeated measurement of two-way ANOVA with Bonferroni's multiple comparisons test; CFA-injected vs. saline-injected: ***p<0.001

(day 2), ****p<0.0001 (day 4); CFA-injected vs. CFA-none (contralateral paw of CFA-injected mice): ####p<0.0001 (day 2), ###p<0.001 (day 4). N=8 for both saline and CFA injection groups.

As shown in Figure 3.3.4, the withdrawal threshold of both injected and not-injected paws in both CFA (CFA-injected, CFA-none) and saline injection (Saline-injected, Saline-none) groups are shown, respectively. The baseline withdrawal threshold (day 0) of both paws with either CFA or saline injection did not differ. However, on day 2 and day 4, the withdrawal threshold of the right hind paw (CFA-injected, orange solid line) decreased significantly from that of the saline-injected group (green solid line). Likewise, the withdrawal threshold of the CFA-injected paw was significantly lower than that of the left paw without injection (CFA-none, orange dashed line).

To conclude, our injection of CFA successfully created inflammatory pain in the right hind paw of mice, with a remarkable hyperalgesia on day 2 and day 4 after CFA injection.

3.3.3 Laser-evoked potentials in multiple brain regions in inflammatory pain

To evaluate laser-evoked potentials of freely moving mice in inflammatory pain, laser stimulations of 10 ms were performed before (d0) as well as two days (d2) and four days (d4) after CFA injection. Saline injection (Sal) was conducted in a separate group of mice which served as controls. Representative mean evoked potentials in contralateral S1 are shown in Figure 3.3.5. The vertex amplitude of P2-N1, as well as N2 (as a late component of the evoked potential) was selected for amplitude analysis.

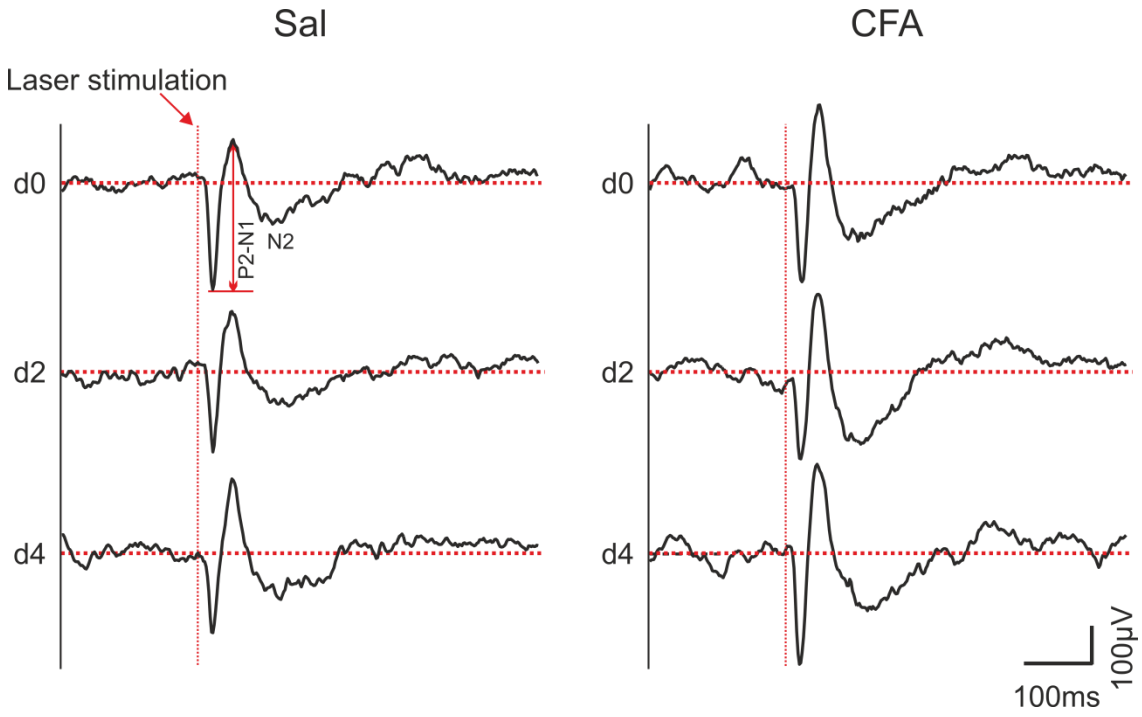

Figure 3.3.5 Averaged evoked potentials following laser stimulation in contralateral S1of mice with inflammatory pain.

Left and right sides show averaged evoked potentials after 10 ms laser stimulation following saline and CFA injection, respectively. From top to bottom, the evoked potentials of baseline (d0), day 2 (d2) and day 4 (d4) after injection are shown. The red horizontal dashed lines represented the baseline for amplitude analysis, and the red vertical lines indicate the timing of laser stimulation. The vertex amplitude of P2-N1 and the second negative peak (N2) are marked. N=8 for saline group and n=10 for CFA injection group.

The peak amplitudes including P2-N1 and N2 were are presented for all recorded brain regions contralateral to 10 ms laser stimulation in Figure 3.3.6. The vertex amplitude P2-N1 did not change significantly between healthy mice (Sal) and mice with inflammatory pain (CFA), different from what was observed in evoked potentials of healthy mice (Figure 3.3.6 A). On the other hand, in several brain regions including S1, PAC, VPL, ACC and AMYG, the N2 peak amplitude significantly increased on day 2 after CFA injection compared to controls (Figure 3.3.6 B). This time matches with the presence of the acute inflammatory process. In sum, N2 peak amplitude, but not the vertex amplitude of P2-N1 increased significantly in multiple brain regions contralateral to laser stimulation in the acute inflammatory pain.

Similarly, in the ipsilateral hemisphere to laser stimulation, no significant difference of P2-N1 amplitude was detected between CFA and Sal groups (Figure 3.3.7 A). Again, significant increases of N2 peak amplitude were found in ipsilateral S1 and VPL on day 2 after CFA injection (Figure 3.3.7 B). These results suggest that the brain structures ipsilateral to noxious stimulation are also involved in pain processing, although effects were not as widely distributed as in the contralateral side. Again, N2, rather than P2-N1, increased towards the laser-evoked noxious response in inflammatory pain, indicating an electrophysiological pattern different from that of laser-evoked pain in naïve mice.

Interestingly, the peak latency of N2 in contralateral S1 decreased significantly on day 2 after CFA injection compared to Sal, indicating faster processing of stimuli in inflammatory pain (Figure 3.3.8 A). The peak latency of N1 in contralateral AMYG significantly decreased on day 4 after CFA injection, although with no significant changes in peak amplitude (Figure 3.3.8 B). On the contrary, the ipsilateral N2 peak latency of ACC was enhanced on day 4 after CFA injection, despite no significant changes in peak amplitude (Figure 3.3.8 C). Taken together, although there were significant changes in peak latency of certain brain regions in inflammatory pain, the effects were too divergent to reach a solid conclusion.

To sum up, in both hemispheres, contralateral and ipsilateral to laser stimulation, N2 peak amplitude of laser-evoked potentials, but not P2-N1 vertex amplitude, significantly increased in multiple brain regions during inflammatory pain, suggesting changes in electrophysiological patterns compared to naïve mice.

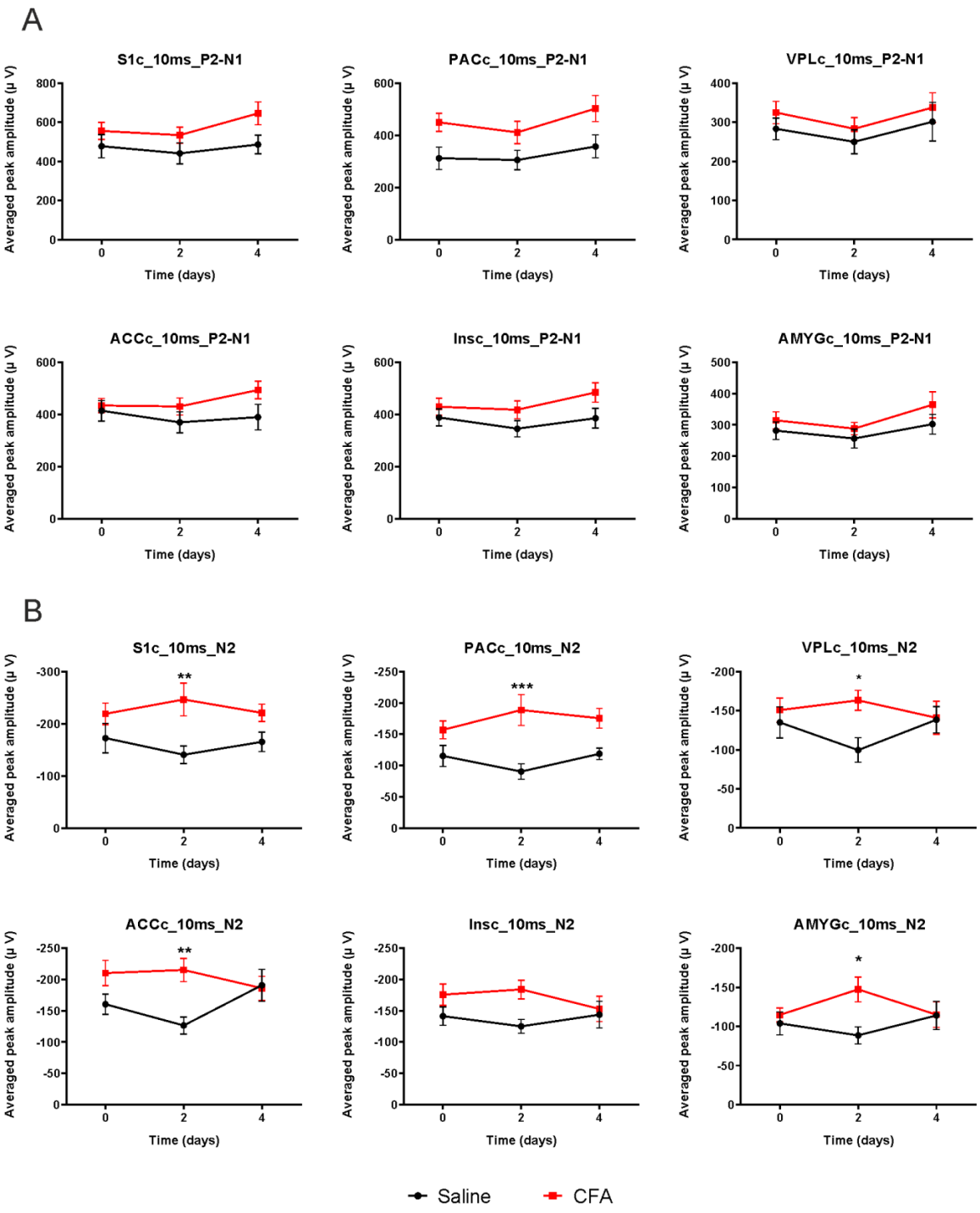

Figure 3.3.6 Peak amplitudes of laser-evoked potentials in multiple contralateral brain structures in inflammatory pain.

A-B, Mean peak amplitudes P2-N1(A) and N2 (B) of 10 ms laser-evoked potentials in all recorded contralateral brain regions on day 0, 2, 4 after CFA and saline injection. Black marker: Saline injection; red marker: CFA injection. Data are presented as mean with SEM. Repeated measurement of two-way ANOVA with Bonferroni's multiple comparisons test; CFA vs. Saline: *p<0.05, **p<0.01, ***p<0.001. N=8 for saline group and n=10 for CFA injection group.

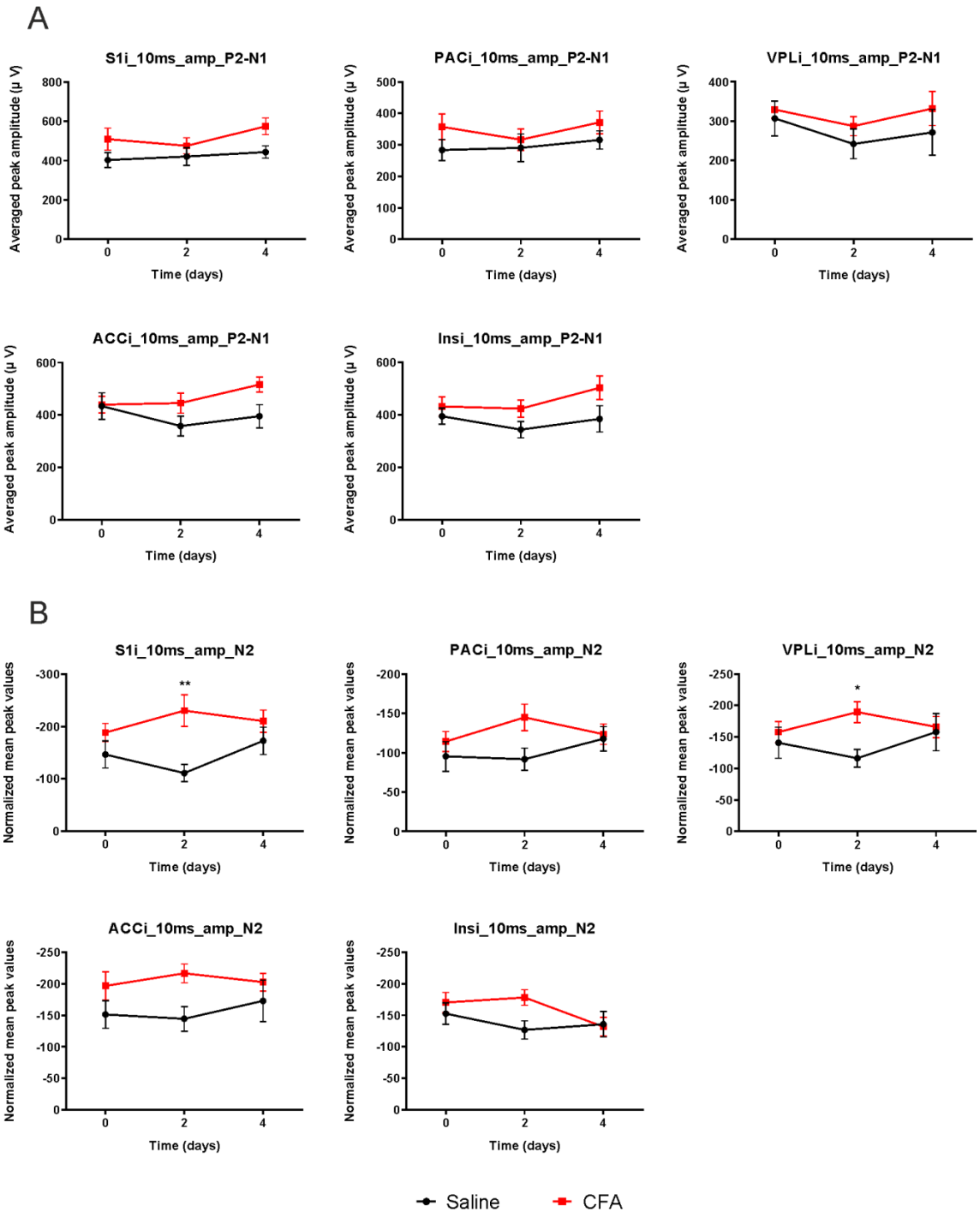

Figure 3.3.7 Peak amplitudes of laser-evoked potentials in multiple ipsilateral brain structures in inflammatory pain.

A-B, Mean peak amplitudes of P2-N1(A) and N2 (B) of 10 ms laser-evoked potentials in all recorded ipsilateral brain regions on day 0, 2, 4 after CFA and saline injection. Black marker: Saline injection; red marker: CFA injection. Data are presented as mean with SEM. Repeated measurement of two-way ANOVA with Bonferroni's multiple comparisons test; CFA vs. Saline: *p<0.05, **p<0.01. N=8 for saline group and n=10 for CFA injection group.

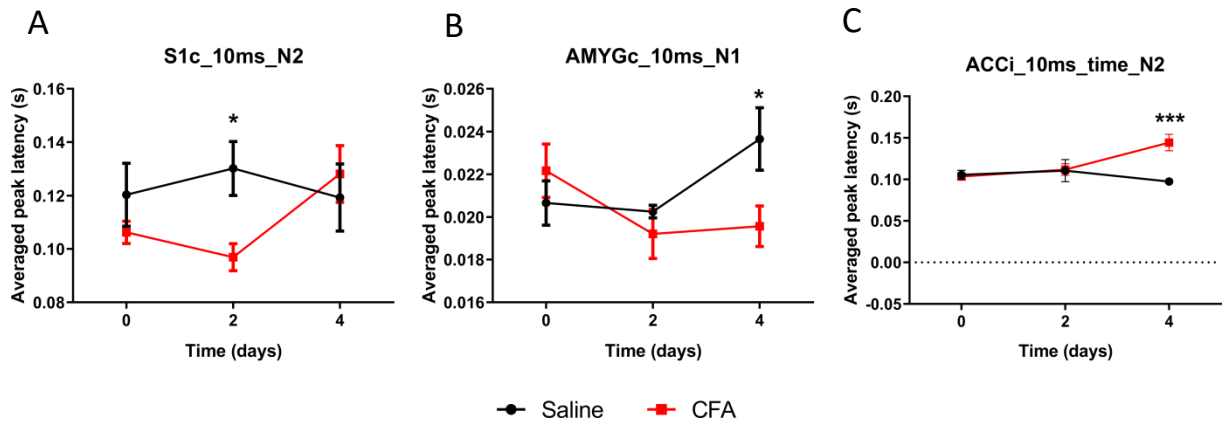

Figure 3.3.8 Peak latency of laser-evoked potentials in brain regions with significant changes during inflammatory pain.

A-C, Significantly changed peak latencies of evoked potentials by 10 ms laser stimulation in S1c (A), AMYGc (B) and ACCi (C). Data are presented as mean with SEM. Repeated measurement of two-way ANOVA with Bonferroni's multiple comparisons test; CFA vs. Saline: *p<0.05, ***p<0.001. N=8 for Saline group and n=10 for CFA injection group.

3.3.4 Evoked-potentials by mechanical stimulation in inflammatory pain

In addition to laser stimulation, mechanical (tactile) stimulation was also applied to evaluate the pain responses in CFA-induced inflammatory pain. Similar to the laser stimuli, tactile stimulation was conducted before (d0) as well as two days (d2) and four days (d4) after CFA/saline injection by using the custom built tactile stimulator. As a representative example, mean evoked potentials following tactile stimulation during inflammatory pain in contralateral S1 are shown (Figure 3.3.9). Similar to laser-evoked potentials, the vertex amplitude of P2-N1, as well as N2 as the late component of the tactile evoked potentials was used for amplitude analysis.

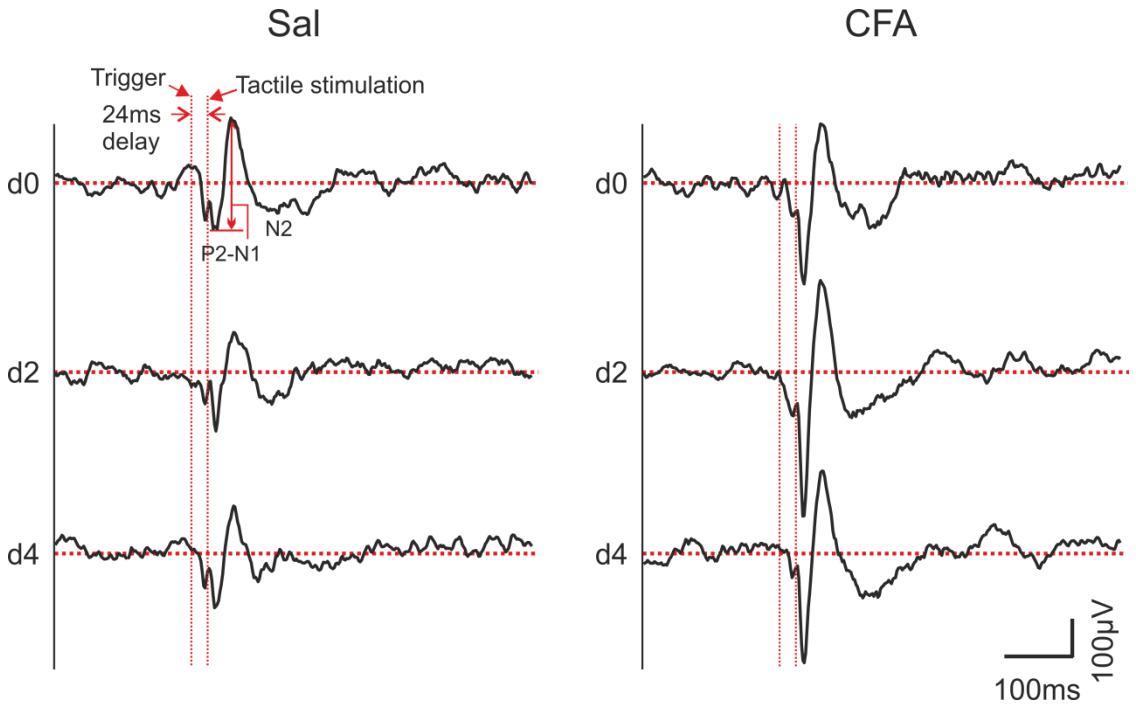

Figure 3.3.9 Averaged evoked potentials following tactile stimulation in contralateral S1of mice with inflammatory pain.

Left and right panels show averaged evoked potentials following mechanical (tactile) stimulation after saline and CFA injection, respectively. From top to bottom, evoked potentials of baseline (d0), day 2 (d2) and day 4 (d4) after injection are shown. Red horizontal dashed lines represent the baseline for amplitude analysis, and red vertical lines indicate the timing of laser stimulation. The vertex amplitude of P2-N1 and the second negative peak (N2) are marked. There was a delay of 24 ms from the trigger of stimulation to physical touching the paw. N=8 for Saline group and n=10 for CFA injection group.

The peak amplitudes including P2-N1 and N2 were analyzed and are presented for all recorded brain structures contralateral to tactile stimulation in Figure 3.3.10. Compared to saline injection, the vertex amplitude of P2-N1 was significantly higher in contralateral S1 and PAC on day 2 after CFA injection (Figure 3.3.10 A). No significant changes were observed in other contralateral brain regions. The peak amplitude of N2 also did not show any significant change across all recorded regions (Figure 3.3.10 B). These responses reflected a clearly different electrophysiological pattern from that of laser-evoked potentials in inflammatory pain.

In the ipsilateral hemisphere, no significant change in responses to tactile stimulation of either P2-N1 or N2 was detected in all recorded brain regions (Figure 3.3.11 A and B).

While the peak amplitude did not change, the peak latency of N1 had significantly lower values on day 4 after CFA injection than in the saline group in contralateral S1c, PACc, ACCc (Figure 3.3.12 A), and VPLi (Figure 3.3.12 B).

To summarize, the tactile stimulation resulted in higher P2-N1 peak amplitudes exclusively in contralateral S1 and PAC, but not in any other recorded region. N2 was not significantly changed across all analyzed regions. These results suggest a different electrophysiological pattern following mechanical tactile stimulation in inflammatory pain compared to laser-evoked potentials.

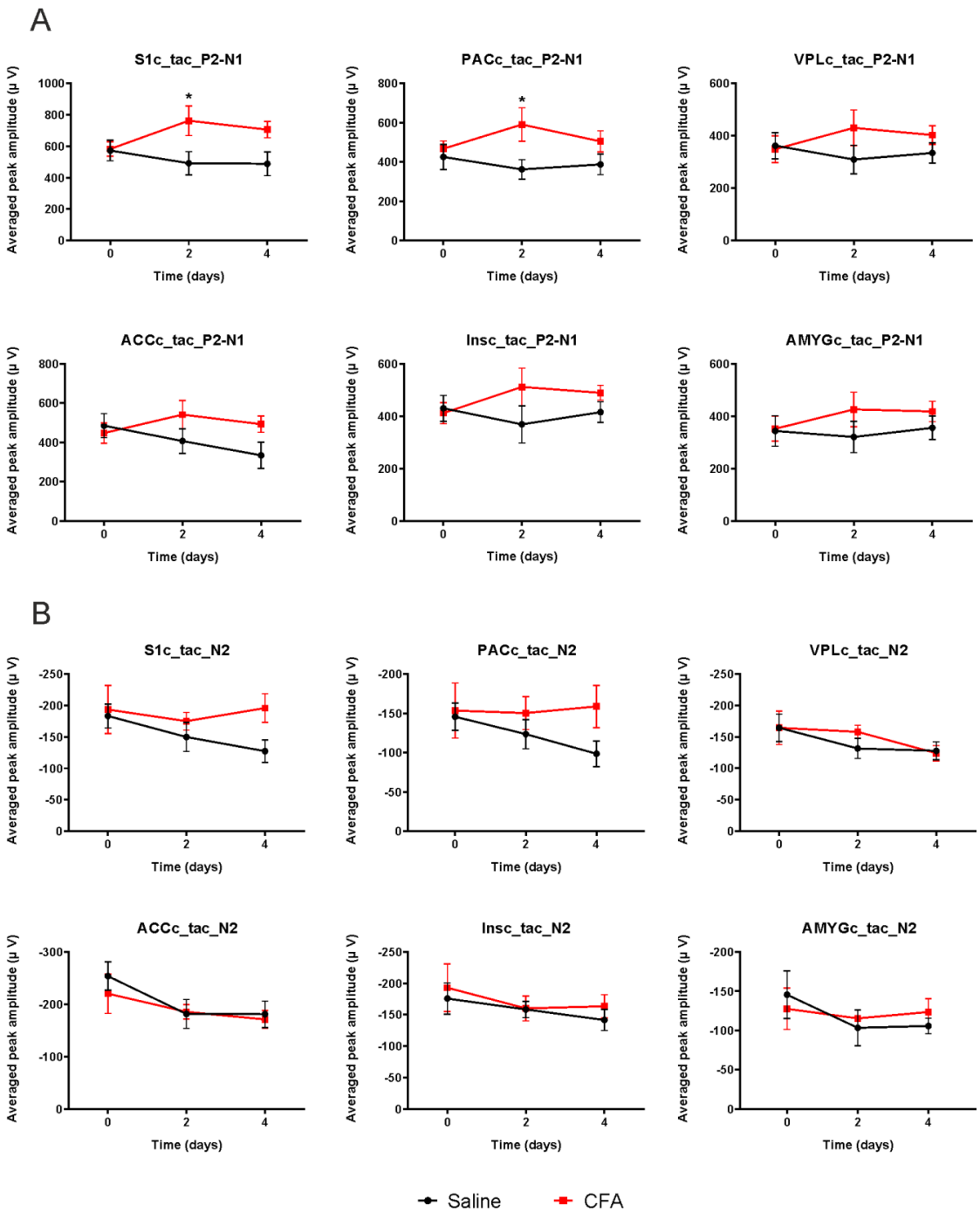

Figure 3.3.10 Peak amplitudes of tactile stimulation evoked potentials in multiple brain regions contralateral to stimulation side.

A-B, Mean peak amplitudes of P2-N1 (A) and N2 (B) of tactile stimulation-evoked potentials in all recorded ipsilateral brain regions on day 0, 2, 4 after CFA and saline injection. Black marker: Saline injection; red marker: CFA injection. Data are presented as mean with SEM. Repeated measurement of two-way ANOVA with Bonferroni's multiple comparisons test; CFA vs. Saline: *p<0.05. N=8 for saline group and n=10 for CFA injection group.

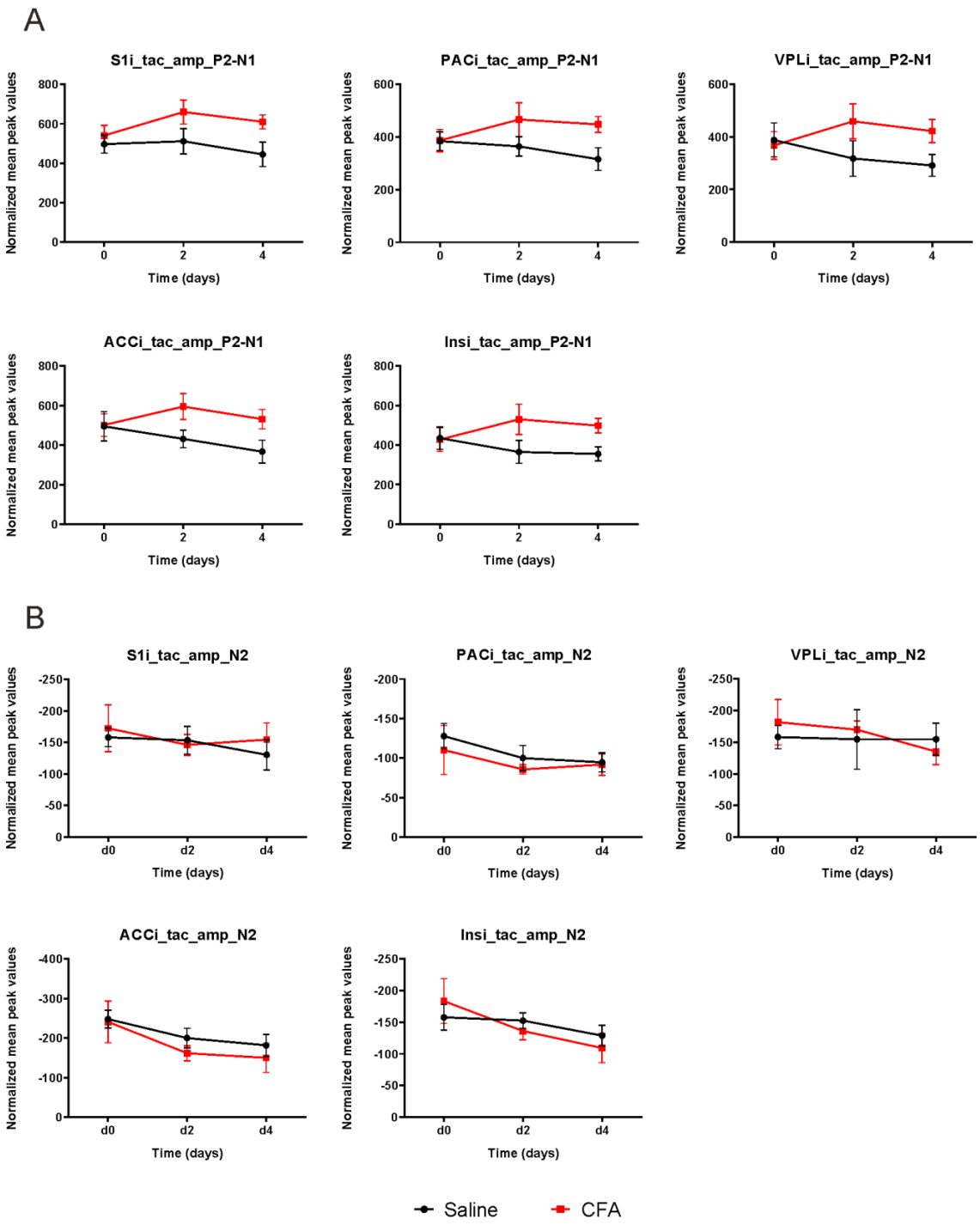

Figure 3.3.11 Peak amplitudes of tactile stimulation evoked potentials in multiple brain regions ipsilateral to stimulation side.

A-B, Mean peak amplitudes of P2-N1 (A) and N2 (B) of tactile stimulation-evoked potentials in all recorded ipsilateral brain regions on day 0, 2, 4 after CFA and saline injection. Black marker: Saline injection; red marker: CFA injection. Data are presented as mean with SEM. Repeated measurement of two-way ANOVA with Bonferroni's multiple comparisons test; no significance was observed. N=8 for Saline group and n=10 for CFA injection group.

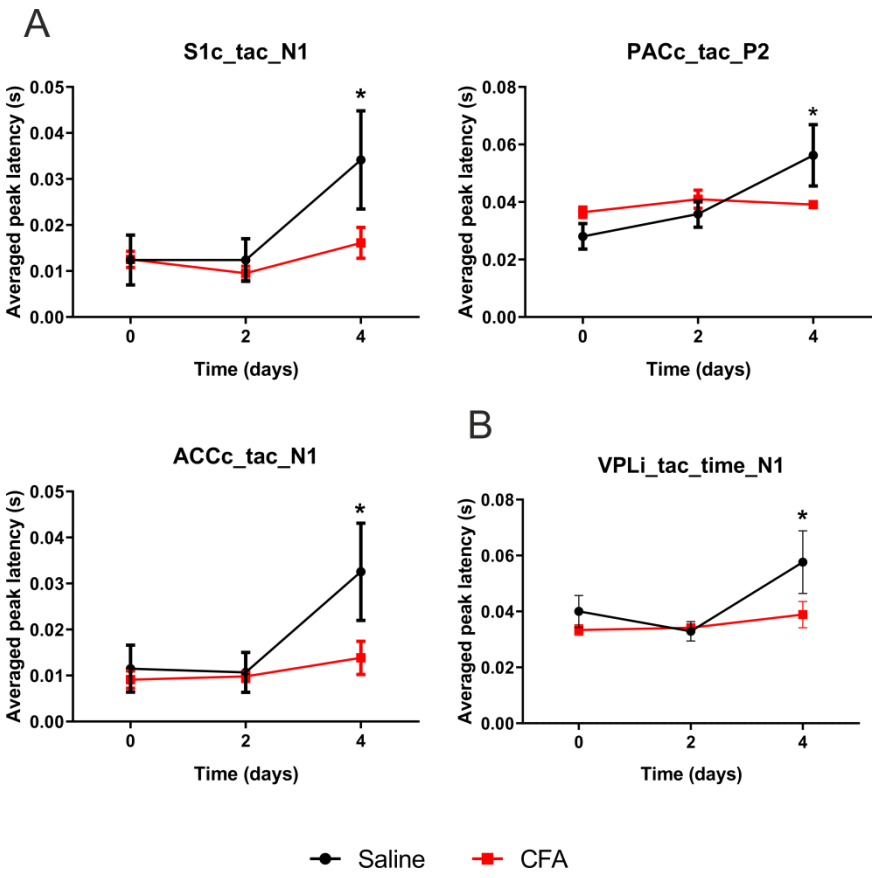

Figure 3.3.12 Significant peak latency changes in several brain regions following tactile stimulation in inflammatory pain.

A, Significantly changed peak latency of evoked potentials in the ACC contralateral to tactile stimulation. B, Significantly changed peak latencies of evoked potentials In VPL ipsilateral to tactile stimulation. Data are presented as mean with SEM. Repeated measurement of two-way ANOVA with Bonferroni's multiple comparisons test; CFA vs. Saline: *p<0.05. N=8 for Saline group and n=10 for CFA injection group.

3.3.5 Summary of this part of study

Responses to laser stimulation resulted in characteristic evoked potentials in multiple brain regions including S1, PAC, VPL, ACC and Ins. The vertex amplitude of P2-N1 in both contralateral and ipsilateral hemisphere increased significantly as the laser intensity was elevated, whereas N2 peak values did not change. This result indicates that the vertex amplitude of P2-N1 may serve as a potential marker for acute laser-evoked pain in naïve freely moving mice.

In an inflammatory pain model induced by CFA injection, N2 peak amplitude, instead of P2-N1 vertex amplitude, had significantly higher amplitudes during inflammatory pain. This finding reveals a different electrophysiological response pattern compared to acute laser-evoked potentials in naïve mice. In addition, more contralateral regions than ipsilateral ones were involved in the specific changes following inflammatory pain.

Different from laser-evoked potentials in inflammatory pain, tactile stimulation-evoked potentials only resulted in higher P2-N1 peak amplitudes in contralateral S1 and PAC after CFA injection than after saline injection. No significant changes of N2 amplitude were detected across all recorded regions.

4. Discussion

This study focuses on systematically exploring electrophysiological features across brain regions in freely moving mice. In capsaicin-induced acute pain, I found alterations of distributed network oscillations in multiple brain structures. A new apparatus was successfully developed for the study of laser-evoked potentials in mice. By using the custom made device, I found the specific patterns respectively in laser- and mechanical (tactile) - evoked potentials, in both naïve mice and in mice with inflammatory pain.

4.1 Alterations of network oscillations during capsaicin-induced pain

In the study of capsaicin-induced pain, changes of electrophysiological signals were found at the network level in multiple brain regions in freely moving mice. In pair-wise comparisons with the saline-injected control group, capsaicin injections led to increases of cross-frequency coupling between low (1-12 Hz) and high (80-120 Hz) frequency oscillations in several brain regions, as well as a power decrease of a sub-band of gamma (80-120) in ipsilateral ACC. Besides, interregional coherence was enhanced between different brain structures, most prominently in the theta frequency range (4-12 Hz). However, none of these alterations stayed significant after correction for multiple comparisons, which had to be applied to compensate for the large number of parameters. In order to deal with this problem and to derive relevant parameters in capsaicin-induced pain processing, a variable selection by the elastic net model (Zou and Hastie 2005) was performed. A classification of capsaicin versus saline injection was achieved with an AUC of 0.926, indicating a high sensitivity and specificity of a parameter set of as few as ten variables. Furthermore, even when the parameter selection was restrained to frequencies below 30 Hz, the classification still worked with an AUC of 0.738, using five selected parameters. These results suggest that there are indeed specific distributed neuronal network oscillations during capsaicin-induced pain in freely moving mice. While the present study is restricted to mice in a specific experimental paradigm, similar approaches may be helpful to detect electrophysiological classifiers of pain in human routine EEG.

Previous reports from rats and humans found an increase of power in theta frequency as well as other frequency ranges during acute pain (Leblanc et al. 2014; LeBlanc et al. 2016; Nickel et al. 2017). In our study, such an increased power was not observed in capsaicin-induced pain compared to saline control. This is possibly due to differences in species (rats versus mice), methods of pain model (laser-evoked pain versus capsaicin) and further sources of variability in the experimental conditions.

Due to the lack of clear power alterations in pain responses, I sought for higher-order network properties such as cross-frequency coupling and interregional coherence. Within these parameters, a capsaicin injection-specific modulation of cross-frequency coupling was detected: gamma oscillations in the 80 - 120 Hz band were more strongly modulated by slow oscillations of 1 – 12 Hz in the ipsilateral and contralateral anterior cingulate cortex (ACC), ipsilateral somatosensory cortex (S1i) and ipsilateral parietal cortex (PACi). In the low frequency range (1 -12 Hz), several kinds of network activities overlap with each other, including theta oscillations, respiration-related network oscillations (RR) and sleep-related slow waves (Yanovsky et al. 2014; Tort, Brankack, and Draguhn 2018). Sleep-related slow oscillations are excluded in our data since I recorded exclusively from waking mice. However, as previously described (Yanovsky et al. 2014) and as shown in this study, theta oscillations and respiration-related activities (RR) occurred simultaneously with overlapping frequencies. Interestingly, the altered coupling of gamma frequency of 80-120 Hz to slow frequency bands was reported to be selectively modulated by RR, but not theta oscillations in waking mice (Zhong et al. 2017). Hence, I suggest that the modulation of CFC in capsaicin-induced pain is related to altered respiration.

It is still under discussion whether slow oscillations in the rodent brain are generated by neuronal processes at the very location of measurement, or transferred passively across considerable distances from other brain structures simply by biophysical means (Kajikawa and Schroeder 2011). Unfortunately the distinction between the two mechanisms is not possible with the monopolar electrodes used in our study. Based on previous studies in our lab, I assume that the observed slow oscillations (especially RR) are generated at the sites of measurement, accompanied by clear neurophysiological mechanisms. With respect to respiration-related oscillations (RR) our lab has recently reported the following features: First, RR goes along with current sinks and sources in the mouse hippocampus (Yanovsky et al. 2014); second, RR selectively engages a specific gamma sub-band in cross-

frequency coupling (Zhong et al. 2017); third, RR is involved in the rhythmic entrainment of unit discharges such as neuronal spikes in hippocampus, parietal cortex and prefrontal cortex (Yanovsky et al. 2014; Nguyen et al. 2016; Zhong et al. 2017; Tort et al. 2018). Similar findings were also reported for theta oscillations, although there are indeed indications for volume-conducted theta oscillations from hippocampus to adjacent cortical areas (Sirota et al. 2003). According to these data, the wide-ranging slow rhythmic network activity observed in this study is at least not exclusively a result of volume conduction, and has direct effects on neuronal discharges in at least some of the studied regions.

In addition, this study suggests the anterior cingulate cortex (ACC) to be an important brain structure in acute pain processing, in line with previous studies (Hutchison et al. 1999; Lieberman and Eisenberger 2015; Bliss et al. 2016). Cross-frequency coupling was found to be enhanced in both the contralateral and ipsilateral ACC. Most somatosensory signals are crossing sides in the spinal cord and represent the contralateral side of body. Thus, our finding of bilateral changes may points towards a higher-order process in the anterior cingulum, consistent with its known role in attention and emotional processing of pain (Rainville et al. 1997; Shackman et al. 2011). This is supported by observations that both ipsilateral and contralateral painful stimuli can evoke responses in the cingulum (Hutchison et al. 1999). Interestingly, it was demonstrated that neuropathic pain leads to metabolic alterations primarily in ipsilateral cingulate cortex (Shen et al. 2019).

Coherence is considered to be involved in communication and integrated information processing between distant brain structures (Fries 2015). In this study, changes of interregional coherence were found in both hemispheres and were more pronounced between ipsilateral regions, underlying integrated perception of capsaicin-induced pain. Interestingly, enhancement of coherence was mostly restrained to frequency bands below 30 Hz. This indicates that slow oscillations play an important role in coordination of long-range network activity (Reinhart and Nguyen 2019). The finding may facilitate the search for clinically usable diagnostic parameters in case of human studies, where EEG recordings are mostly restricted to frequencies below 30 Hz. Indeed, previous human studies indicate specific changes like reduced oscillations in the alpha band under acute pain (Nir et al. 2012; Shao et al. 2012; Li et al. 2016). Such changes, however, may reflect mixed effects of multiple mental processes including vigilance, shifts in attention or fear.

On the other hand, pain-related alterations in the gamma frequency bands have been suggested to be more specific (Peng et al. 2014; Schulz et al. 2015; Li et al. 2016). Similarly, higher order features of neuronal network activity, such as CFC and coherence, reflect complex dynamic interactions in the pain matrix and probably contribute to a more specific pain signature (Kucyi and Davis 2015).

An elastic net model (Zou and Hastie 2005) was applied to derive a signature from the combined signals and to overcome the above mentioned multiple comparisons problem at the same time. The elastic net model is an approach for variable reduction and selection of relevant parameters, which is necessary for avoiding overfitting of a limited data set. From the logistic regression classifier following parameter selection, informative sets of five to nine parameters were revealed, leading to a distinction between capsaicin-induced pain and control group with AUC values up to > 0.9. Interestingly, the selected parameters predominantly consisted of coherence data, except for a PSD parameter of ipsilateral AMYG in the 120 – 160 Hz domain. This is again a hint that interregional coherence features are of special importance for network activity in acute pain. Furthermore, even the mere use of frequencies below 30 Hz resulted in a reasonable classification with an AUC of 0.738, opening chances for the use of similar approaches in human EEG recordings with limited band width.

In our present experiments, however, it is hard to prove that the electrophysiological alterations were exclusively caused by pain. Actually it remains a challenge to distinguish genuine electrophysiological markers of pain from saliency (Legrain et al. 2011). In addition, pain itself is a complex process including a large variety of behavioral and mental responses, rather than a mere sensation. In support of the occurrence of prolonged pain in our experimental animals, we demonstrated that capsaicin induced clear hyperalgesia to mechanical stimulation (von Frey hair) together with paw licking behavior. No paw licking was observed after saline injection. Consistent with these behavioral characteristics, the clearest discrimination between capsaicin and saline injection by electrophysiological classifiers was found at early times after the injection, rather than one hour later. At this later time, the respective electrophysiological parameters of power, CFC and coherence were normalized to baseline values which had been recorded before any injection. This suggests specific, transient network alterations in response to capsaicin but not to saline. To sum up, the observed network alterations in the early phase after

capsaicin injection are very likely induced by pain, rather than by unspecific factors following the injection.

To sum up, I found electrophysiological changes mainly in interregional coherence, implying that pain processing involves distributed, co-active networks within the pain matrix. It is promising to study specific signatures of acute pain by means of electrophysiological measures of brain oscillations in freely moving mice. Further studies are still needed to reveal the underlying mechanisms and the differential role of the different altered parameters for pain processing (Mouraux and Iannetti 2018). Nonetheless, a combination of network parameters - mostly higher-order phenomena - is able to classify the state of capsaicin-induced pain versus saline control. These findings can be beneficial for further studies on neurophysiological signatures of pain at the network level.

4.2 Custom made apparatus for evoked sensory test of freely moving mice

In order to facilitate studies of evoked sensory responses in freely moving mice, a device consisting of both stimulation and recording systems was designed and built. The custom made apparatus can provide laser (painful) and tactile stimulation in freely behaving mice with simultaneous recording of evoked potentials and behavioral responses. To make it easy and reliable for analysis, the trigger signal of the stimulus, the evoked potential recordings and the behavioral responses are precisely synchronized by the apparatus and presented in the LFP recording program and the accompanying video. As shown in Chapter 3.2.2, pain-specific behavior and evoked potential features both showed significant increases at 10 ms laser stimulation compared to 3 ms. This result indicates a good differentiation and graded responses of pain reactions upon laser stimulation. Furthermore, the apparatus is capable to perform mechanical (tactile) stimulation, which also evoked reliable field potential responses in the recordings. Behavioral features following tactile stimulation demonstrated significantly lower levels of pain rating compared to laser stimulation, again indicating a good discrimination between evoked responses to painful and non-painful stimuli. Taken together, the custom built apparatus can provide reproducible measurements of both laser and tactile stimulation, with a good differentiation between them.

As an important electrophysiological signal, evoked potentials have been widely studied in basic and clinical contexts (Chiappa and Ropper 1982; Karlin 1970; Norcia et al. 2015). Laser-evoked potentials have been broadly used for thermal pain studies in humans (Treede, Lorenz, and Baumgartner 2003; Jones et al. 2016). For instance, it has been well established and verified that brief painful infrared lasers can act as a nociceptive stimulus in humans (Bromm and Treede 1984; Plaghki and Mouraux 2003). For human EEG or ECoG routines, laser-evoked potentials can be reliably recorded as electrophysiological pain responses (Bromm and Treede 1991; Cruccu and Garcia-Larrea 2004; Ohara et al. 2004). Despite of the convenience and reliability, there are some deficiencies of evoked potential studies in humans. One prominent drawback is that most human studies are not able to record evoked potentials from deep subcortical brain structures. In this case, animal studies can contribute important data, allowing recording of local field potentials with less limitations. For example, ECoG was used for studying of laser-evoked potentials in freely moving rats (Peng et al. 2018). Yet the application of laser-evoked potential studies in animals is much less frequent than in humans. This is partially due to the practical difficulty in precisely and reliably triggering laser stimulation in awake and unrestraint mice (Chaplan et al. 1994). Human subjects can well understand and follow the instruction of the experimenter, while this is unrealistic when it comes to study using mice. In a pain study, mice can move a lot during experiments, adding to the difficulty in targeting the stimulator on the small size of the mouse paw. While movement restrictions can facilitate precise laser stimulation, they may impose extra mental and physical burdens on the mice, and may lead to unreal experimental readouts caused by these stressors. They may also hurt the mice.

Our custom made device carries a small chamber (10 cm diameter), which allows free movement of a mouse, though within a limited space. The relatively small size of the chamber decreases the difficulty in targeting the stimulator on the mouse paw. Besides, a cardboard partition placed between the animal and the experimenter can prevent visual contact, thus reducing the stress of the mouse and avoiding the experimenter’s presence as an extra cue for the mouse. Instead of EEG or ECoG, field potential recordings by depth electrodes were performed, making it possible to collect evoked potential data from both cortical and subcortical regions.

In addition to evoked potential recordings, the custom built device is capable to simultaneously record behavioral responses towards stimulation. Several animal models for heat-evoked pain tests are widely used, including the hot plate test, Hargreaves test, thermal probe test and so on (Deuis, Dvorakova, and Vetter 2017). The hot plat test is designed for measurement of global pain evoked movements, rather than specific paw withdrawal due to localize pain sources (Eddy and Leimbach 1953). In contrast, the Hargreaves test does allow behavioral measurements of unrestrained rodents following heat cues specifically targeted to the mouse hind paw (Hargreaves et al. 1988; Yeomans and Proudfit 1994). However, the Hargreaves test is commonly used in pure behavioral tests without simultaneous electrophysiological recordings. In addition, when it comes to the measurement of electrophysiological characteristics, the paw withdrawal latency in Hargreaves test is relatively long (seconds), leading to inaccuracy in comparing behavior with evoked potential data which have a delay of a few tens of milliseconds and a very high time resolution (milliseconds). Our custom made device solves the time scale problem by applying laser pulses with high intensity and short duration (3ms, 5ms and 10ms). This kind of stimulation is strong enough to evoke pain responses in rather short time, making it precise enough for a direct correlation of evoked potentials with behavioral data. As a further advantage, the intense laser stimulus with short-lasting pulses is similar to stimuli used in human studies (Greffrath, Baumgartner, and Treede 2007), resulting in a better comparison between animal and human research.

Following hind paw withdrawal, a set of pain-evoked behaviors can give hints to lasting pain, such as guarding, flinching and freezing (Luger et al. 2002; Tappe-Theodor and Kuner 2014; Pitzer, Kuner, and Tappe-Theodor 2016). Real-time video recordings of the animal during the experiment are ideal for measurement and documentation of such responses (Abdus-Saboor et al. 2019). Within the custom built apparatus, a HD-camera is installed laterally to the recording chamber and can record the evoked behavioral responses of mice in each trial, respectively. The videos recorded by the lateral camera also contain an indicator -LED marking the laser pulse and making it possible to accurately measure the paw withdraw latency at millisecond resolution, consistent with the timing of evoked potentials.

Apart from laser stimulation, the custom built apparatus supports mechanical (tactile) stimulation. As a method for hyperalgesia and allodynia towards mechanical stimulation,

the von Frey hair test is well established and widely used (Pitzer, Kuner, and Tappe-Theodor 2016). However, measurements with von Frey hairs are highly dependent on the experimenter's skills in targeting the von Frey hair on the mouse hind paw and increasing force gradually (Yoburn et al. 1984). Besides, like the Hargreaves test, it takes relatively long time until paw withdrawal (seconds range). This would be a drawback when comparing the tactile stimulation data to evoked potentials. A custom made tactile stimulator was thus developed to solve the problem. By manipulation of a power supply unit (PSU), the intensity of tactile stimulation can be adjusted. Stimuli with a power above 27 V supplied a powerful and stable tactile stimulation with an interval of 24 ms between triggering the stimulator and physically touching the paw. This 24 ms delay is inevitable due to the mechanical design, but it can be substracted as a constant delay. It is, therefore, still possible to analyze the behavioral and the electrophysiological data within the millisecond time. A blunt tip needle on the stimulator ensures tactile but not painful stimulation. The tactile stimulator was constructed in the same size as the laser stimulator, allowing flexible exchange between both devices. Both the tactile and laser stimulator share the same trigger control system operated by the custom made control unit. Hence, by simply directing the stimulator onto the mouse hind paw and then pressing the trigger button on the control unit, painful or tactile stimuli can be easily and reliably conveyed. This design largely reduces the operation difficulties and increases the precision of stimulation.

In the experiments for assessment and validation of the custom built apparatus, evoked potentials as well as the evoked behavioral features by laser or tactile stimulation were recorded. The results reveal reliable and precise measurement of both evoked potentials and behavioral paradigms by the respective stimulation. When comparing the pain-related evoked behaviors, the pain score of tactile stimulation was much lower than that of laser stimulation, indicating a good discrimination between pain and non-pain responses by the custom made device. Taken together, our custom built apparatus is well suited for reliable, precise and simultaneous measurement of electrophysiological and behavioral data following both heat pain stimuli and mechanical stimulation.

In sum, an apparatus was developed with functions combining evoked potential recordings as well as behavioral measurements in freely moving mice. Heat (laser) pain stimulation and mechanical tactile stimulation can be flexibly performed with a good differentiation

between each other. In fact, other kinds of contact stimulation are also potentially applicable in this apparatus, if they have the same size to fit into the apparatus. Beyond the study of acute pain responses, it is also feasible to apply this apparatus to investigations of evoked pain responses in more complex pain models like chronic or inflammatory pain, or for comparing wildtype versus knockout mice. The custom made apparatus may be a versatile tool to study processing of painful and non-painful somatosensory responses in freely moving mice.

4.3 Electrophysiological features of stimulation-evoked pain

By using the custom built apparatus, electrophysiological characteristics evoked by laser and tactile stimulation were recorded in unrestrained waking mice, both in naïve mice and in mice with inflammatory pain.

In naïve mice, there are intensity-dependent changes of laser-evoked potentials across multiple brain structures including S1, PAC, VPL, ACC and Ins. The vertex amplitude of P2-N1 significantly increased in both contralateral and ipsilateral hemisphere as the stimulation intensity increased, while N2 peak amplitude did not change. No changes of peak latency were observed in healthy mice. Next, inflammatory pain was induced by injection of complete Freund's adjuvant (CFA). The electronic von Frey hair test verified hyperalgesia two days and four days after CFA injection, compared to saline control. Interestingly, I found specific alterations of laser-evoked responses in this situation: in mice with inflammatory pain, peak amplitude of N2, rather than that of P2-N1, had significantly higher values following laser stimulation in several brain regions including S1, PAC, VPL, ACC and AMYG. In addition, mechanical (tactile) stimulation was also performed during inflammatory pain, showing allodynia during the von Frey hair test. Before injection, the stimulation was tactile despite of the obvious evoked potentials, whereas the tactile stimulation could be painful due to hypersensitivity in inflammatory pain. Different from laser-evoked potentials, the mechanical stimulation led to higher P2-N1 peak amplitudes only in contralateral S1 and PAC, while N2 amplitude did not differ across all recorded brain structures. In addition, I found significant changes of peak latency in several brain regions following either laser or mechanical stimulation during inflammatory pain, yet the effects were too divergent to reach a solid conclusion.

This small study shows that multiple brain regions take part in the processing of pain evoked potentials both in healthy mice and in mice with inflammatory pain. S1 exhibits significant changes in pain evoked potentials, no matter whether mice are healthy suffer from inflammation. This painspecific alteration can be evoked by laser or – in mice with inflammation - by mechanical stimuli. As a hub for processing somatic sensations, S1 is well documented in dealing with pain information (Bushnell et al. 1999; Gross et al. 2007; Dowman, Rissacher, and Schuckers 2008; Zhang et al. 2012; Uhelski, Davis, and Fuchs 2012). Our study again verifies this important role of S1 in pain processing. Interestingly, potentials in parietal cortex (PAC) showed significant differences between all experimental conditions. PAC receives convergent information from all sensory modalities and has projections to several brain areas. It is thus engaged in a large set perceptive and cognitive operations including attention, memory, decision making, spatial representations, motor control and others (Howard et al. 2016; Scheffzuk et al. 2011; Sestieri, Shulman, and Corbetta 2017; Hadjidimitrakis et al. 2019). Evidence from human studies established PAC as an area involved in the conscious appreciation of pain, probably through orientation and attention towards noxious stimuli (Duncan and Albanese 2003). Our results in mice are in line with this implication and suggest that PAC plays an important part in evoked pain processing in both healthy and inflammation states and by both laser and mechanical stimuli. Increased vertex amplitudes of laser-evoked potentials were observed also in ACC and VPL, both in healthy and inflammation states. ACC is known to mediate sensory components of perception. It is, for example, activated during uncertain expectation of painful stimulation, a condition leading to enhanced transient brain responses in humans (Lenz et al. 1998; Sawamoto et al. 2000). As a hub of ascending sensory signals from the spinal cord, VPL projects to multiple brain regions including S1 and Ins (Treede et al. 2000). Of note, in our study changes in Ins were only found in laser-evoked potentials in naïve mice but not in mice with inflammatory pain, while VPL showed significant changes in both groups. This indicates that during inflammatory pain, pain signals may project to Ins without passing through VPL. Although AMYG has been reported to be involved in the affective dimension of pain, like pain expectancy (Schneider et al. 2001; Bornhovd et al. 2002), it is only found changed in laser-evoked potentials in inflammation state but not in naive mice in this study. Increasing evidence suggests that chronic pain and acute pain have different processing mechanisms in AMYG, which has also emerged as a key brain structure for emotional

responses like learned fear, anxiety and depression (Neugebauer 2015). Thus our observation in AMYG could be a result from affective process, like learned fear, during inflammatory pain that lasts for several days. Nevertheless, mechanical stimulation evoked potentials in inflammation shows no change except for in S1 and PAC. This result suggest that different types of stimuli may evoke pain by different mechanisms.

Interestingly, different amplitude changes were observed in evoked potentials by different stimuli (laser/ mechanical) and in different states (naive/ with inflammatory pain), respectively. Laser stimulation in naive mice evoked vertex amplitude changes (P2-N1) but no alteration of the late component (N2) in both cortical and subcortical areas. However, under inflammatory pain, N2 showed significant higher peak amplitudes in multiple brain structures while P2-N1 amplitude did not change. This finding is difficult to interpret with the limited data available. However, intense infrared laser stimulation can simultaneously activate Aδ- and C-fiber receptors in the skin (Bromm and Treede 1984) which might offer a potential explanation of the findings. Due to the different conduction velocity of these two fiber types (Aδ: 3∼30 m/s; C: 0.5∼2 m/s), laser stimulation typically evokes a first pricking pain related to Aδ fibers and a subsequent burning pain related to C fibers (Lewis and Pochin 1937). In human studies, laser-evoked potentials show distinct components at latencies compatible with the conduction velocities of Aδ-fibers and C-fibers, respectively, with C-fiber signals exhibiting smaller amplitudes (Treede et al. 1988; Hu et al. 2014; Iannetti et al. 2003). It was also reported that heat stimuli of low and high intensities preferentially engage cutaneous C- or Aδ- fibers, respectively (Yeomans and Proudfit 1994). In our study, despite the difficulty in calculating the accurate conduction latency, we can roughly estimate it. Supposed that the conduction length is in the order of 10 cm (estimated length from mouse hind paw to the brain, notwithstanding that the C-fiber part of the pathway is shorter) and based on the different conduction velocities, we can calculate the estimated latencies of Aδ-fiber responses as 0.003~0.03 s and C-fiber responses as 0.05~0.2s. With this course estimation, I suppose that the components of N1 followed by P1 are preferentially generated by Aδ inputs while N2 stems from inputs of C-fibers. This would imply that increased laser intensity evoked stronger potential amplitudes mainly through Aδ-fibers in naive mice, while in inflammatory pain C-fibers play a more important role in mediating evoked potential amplitude changes. Enhanced C-fiber activity during inflammatory pain is also supported by the observation of decreased

conduction failure of C-fibers, as well as reduced C-fiber activity-dependent slowing (ADS) in animal studies (Wang et al. 2016; Dickie et al. 2017). On the other hand, mechanical allodynia shows different patterns of evoked potential changes in inflammatory pain from that of laser-evoked hyperalgesia. Only the vertex amplitude of P2-N1, but not N2, expresses higher levels in contralateral S1 and PAC, indicating Aδ-fibers – and not C-fibers - play an important role. This result also indicates different mechanisms of pain processing for mechanical stimuli and laser-stimuli in inflammatory pain. However, due to the large differences between both stimuli (Cheng et al. 2017) it is difficult to reach any direct conclusion from their comparison.

Although pain signals are traditionally considered to be processed in the contralateral hemisphere, more and more studies have shown that pain processing involves both brain hemispheres. In our study, bilateral changes of amplitudes are found in laser-evoked potentials both from naive mice and mice with inflammatory pain, albeit more contralateral brain regions were involved than ipsilateral. These results suggest an integrated processing of laser-evoked pain stimuli in both hemispheres. Note that changes to mechanical stimuli in mice with inflammation were restricted to the contralateral side, indicating a different pattern of information processing between different types of stimulation.

To conclude, following either laser or mechanical stimulation, multiple brain regions show changes of evoked potential amplitudes both in naive mice and in mice with inflammatory pain. In most cases, both contralateral and ipsilateral brain structures take part in pain processing. These results underline the complex processing of evoked pain responses. Yet, I found characteristic patterns of evoked potentials for different stimuli and states: in acute laser-evoked pain, the vertex P2-N1 amplitude makes a difference, while in inflammation, N2 exhibits importance in laser-evoked potentials. Mechanical stimulation evokes changed P2-N1 amplitude in inflammatory pain. According to previous studies and our orientating calculation, P2-N1 and N2 amplitudes may represent afferent signals from Aδ- and C-fibers, respectively, indicating diverse mechanisms of laser-evoked pain in naive and inflammation states. These features could be used as electrophysiological markers for laser/mechanical stimulation evoked potentials in different pain states.

4.4 Limitations of the present study

In the present study, I have explored electrophysiological features across multiple cortical and subcortical areas in different pain stimulation paradigms in freely moving mice. In capsaicin induced tonic pain, alterations of distributed network activity were found. To study evoked pain responses in freely moving mice, we developed a custom built apparatus for simultaneous electrophysiological and behavioral measurements. By using this apparatus, I managed to find specific changes in laser and mechanical stimulation evoked potentials in both naive mice and mice with inflammatory pain.

Nevertheless, there are some limitations of our present approach. First, we investigate integrated neuronal activity in a limited set of brain regions using single wire electrodes. This leaves the question open whether the oscillations or evoked potentials are generated by the local network or are transferred from distant brain structures (Kajikawa and Schroeder 2011). Based on previous studies in our lab we assume that at least a part of the slow oscillations is generated at the sites of measurements (Yanovsky et al. 2014; Nguyen et al. 2016; Zhong et al. 2017; Tort et al. 2018). It remains, however, difficult to exclude the possibility that other slow oscillations are transferred to the reording location by volume conduction from remote regions like hippocampus.

Secondly, our custom designed apparatus has some limitations, too. Human studies have revealed a habituation of evoked potentials after stimulating the same location for several times (Greffrath et al. 2007). Yet in our study in mice, it is hard to decide whether the stimulation site is exactly the same in each trial, due to the small size of mouse hind paw. To avoid a potential habituation and to reduce animal suffering, I cut down the number of trials to a minimum, which, in turn increased the variance of the collected electrophysiological data. However, I have found a balance between habituation, data variance and ethical limitations.

Our custom made device was originally designed for both manual and automatic triggers of stimuli. In practice, only the manual trigger was performed due to the difficulty in automatically targeting the hind paw of a mouse with its almost random movements. Although it is a pity not to use the automatic trigger in the present study, it is good to have this function for potential applications in future studies with (partly?) restrained animals.

Furthermore, although our findings result from painful stimulations, it is still under debate whether the electrophysiological features do exclusively reflect pain and hence differentiate pain from non-pain states (Hu et al. 2016; Jones et al. 2016; Mouraux et al. 2009; Mouraux and Lannetti 2008). It is hard to discriminate pain from saliency. As a supplement, pain ratings from behavioral features can act as a confirmation between pain and non-pain states.

4.5 Outlook

This study has focused on exploring electrophysiological features of pain in freely moving mice.

The aim as to identify pain-specific activity patterns in distributed neuronal networks following capsaicin-induced pain as well as evoked pain in both naive and inflammatory (hyperalgesic) states. While we identified such patterns in our particular experimental design, he underlying mechanisms remain largely elusive. For example, capsaicin-induced pain was correlated with alterations in interregional coherence, indicating synchronization of neural activity across brain structures. Yet it is unclear how this synchronization is generated, and whether certain brain regions are primarily affected before recruiting others. Progress in this question requires causal analysis which was beyond the scope of the present study (Rohlfing and Schneider 2018). In addition, both laser- and mechanical stimulation led to specific patterns of evoked potential responses in multiple brain regions, both in naïve and inflammatory pain settings. However, we only investigated internal electrophysiological alterations within each recorded region. It would be interesting to apply higher order approaches such as coherence analysis and causal analysis, in order to discover underlying network processes. Moreover, systematic alterations of pain-initiating cues would be needed to find out how far our findings can be generalized.

For a causal analysis, it would also be desirable to apply optogenetic tools to manipulate the activity of selected brain structures. Besides, instead of local field potential recordings, it would also be interesting to record single unit or multiunit activity, which would yield information about cellular activity and might contribute important data to the specific pain profiles. Appropriate tools are available, e.g. the widely used tetrode recordings, depth profile acquisition by neural probes, recording with high-density microelectrode arrays and the recently developed neuropixel probes (Jun et al. 2017). Yet, analyzing such data requires highly advanced computational methods and is challenging.

Finally, the identified specific alterations of neural activities in pain may serve as starting points for translational research. For this, our findings need to be generalized (and adapted) for other species including humans, and for a broader set of stimulation conditions.

Results from such studies may then contribute to drug discovery, advanced diagnostics, and clinical monitoring of pain states.

Project-related publications

Simon Ponsel*, Jiaojiao Zhang*, Maximilian Pilz, Yevgenij Yanovsky, Jurij Brankačk and Andreas Draguhn. Alterations of distributed neuronal network oscillations during acute pain in freely-moving mice (under review; *both authors contributed equally)

Jiaojiao Zhang, Lee Embray, Yevgenij Yanovsky, Jurij Brankačk and Andreas Draguhn. Development and assessment of a new apparatus for evoked sensory testing in freely-moving mice (in preparation)

References

Ab Aziz, C. B., and A. H. Ahmad. 2006. 'The role of the thalamus in modulating pain', *Malays J Med Sci*, 13: 11-8.

Abdus-Saboor, I., N. T. Fried, M. Lay, J. Burdge, K. Swanson, R. Fischer, J. Jones, P. Dong, W. Cai, X. Guo, Y. X. Tao, J. Bethea, M. Ma, X. Dong, L. Ding, and W. Luo. 2019. 'Development of a Mouse Pain Scale Using Sub-second Behavioral Mapping and Statistical Modeling', *Cell Rep*, 28: 1623-34 e4.

Ambalavanar, R., C. Yallampalli, U. Yallampalli, and D. Dessem. 2007. 'Injection of adjuvant but not acidic saline into craniofacial muscle evokes nociceptive behaviors and neuropeptide expression', *Neuroscience*, 149: 650-9.

Apkarian, A. V., M. C. Bushnell, R. D. Treede, and J. K. Zubieta. 2005. 'Human brain mechanisms of pain perception and regulation in health and disease', *Eur J Pain*, 9: 463-84.

Basbaum, A. I., D. M. Bautista, G. Scherrer, and D. Julius. 2009. 'Cellular and molecular mechanisms of pain', *Cell*, 139: 267-84.

Benoit, B., R. Martin-Misener, A. Newman, M. Latimer, and M. Campbell-Yeo. 2017. 'Neurophysiological assessment of acute pain in infants: a scoping review of research methods', *Acta Paediatr*, 106: 1053-66.

Bliss, T. V. P., G. L. Collingridge, B. K. Kaang, and M. Zhuo. 2016. 'Synaptic plasticity in the anterior cingulate cortex in acute and chronic pain', *Nature Reviews Neuroscience*, 17: 485-96.

Bornhovd, K., M. Quante, V. Glauche, B. Bromm, C. Weiller, and C. Buchel. 2002. 'Painful stimuli evoke different stimulus-response functions in the amygdala, prefrontal, insula and somatosensory cortex: a single-trial fMRI study', *Brain*, 125: 1326-36.

Breivik, H., P. C. Borchgrevink, S. M. Allen, L. A. Rosseland, L. Romundstad, E. K. Hals, G. Kvarstein, and A. Stubhaug. 2008. 'Assessment of pain', *Br J Anaesth*, 101: 17-24.

Bromm, B., and R. D. Treede. 1984. 'Nerve fibre discharges, cerebral potentials and sensations induced by CO2 laser stimulation', *Hum Neurobiol*, 3: 33-40.

Bromm, B., and R. D. Treede. 1991. 'Laser-evoked cerebral potentials in the assessment of cutaneous pain sensitivity in normal subjects and patients', *Rev Neurol (Paris)*, 147: 625-43.

Brooks, J. C., and I. Tracey. 2007. 'The insula: a multidimensional integration site for pain', *Pain*, 128: 1-2.

Bushnell, M. C., G. H. Duncan, R. K. Hofbauer, B. Ha, J. I. Chen, and B. Carrier. 1999. 'Pain perception: is there a role for primary somatosensory cortex?', *Proc Natl Acad Sci U S A*, 96: 7705-9.

Buzsaki, G., and A. Draguhn. 2004. 'Neuronal oscillations in cortical networks', *Science*, 304: 1926-9.

Buzsaki, G., and X. J. Wang. 2012. 'Mechanisms of gamma oscillations', *Annu Rev Neurosci*, 35: 203-25.

Canolty, R. T., E. Edwards, S. S. Dalal, M. Soltani, S. S. Nagarajan, H. E. Kirsch, M. S. Berger, N. M. Barbaro, and R. T. Knight. 2006. 'High gamma power is phase-locked to theta oscillations in human neocortex', *Science*, 313: 1626-8.

Chaplan, S. R., F. W. Bach, J. W. Pogrel, J. M. Chung, and T. L. Yaksh. 1994. 'Quantitative Assessment of Tactile Allodynia in the Rat Paw', *Journal of Neuroscience Methods*, 53: 55-63.

Cheng, L., B. Duan, T. Huang, Y. Zhang, Y. Chen, O. Britz, L. Garcia-Campmany, X. Ren, L. Vong, B. B. Lowell, M. Goulding, Y. Wang, and Q. Ma. 2017. 'Identification of spinal circuits involved in touch-evoked dynamic mechanical pain', *Nat Neurosci*, 20: 804-14.

Chiang, C. L. 1966. 'On Formula for Variance of Observed Expectatioof Life - E B Wilsons Approach', *Human Biology*, 38: 318-&.

Chiappa, K. H., and A. H. Ropper. 1982. 'Evoked potentials in clinical medicine (second of two parts)', *N Engl J Med*, 306: 1205-11.

Corder, G., B. Ahanonu, B. F. Grewe, D. Wang, M. J. Schnitzer, and G. Scherrer. 2019. 'An amygdalar neural ensemble that encodes the unpleasantness of pain', *Science*, 363: 276-81.

Costigan, M., J. Scholz, and C. J. Woolf. 2009. 'Neuropathic pain: a maladaptive response of the nervous system to damage', *Annu Rev Neurosci*, 32: 1-32.

Cox, J. J., F. Reimann, A. K. Nicholas, G. Thornton, E. Roberts, K. Springell, G. Karbani, H. Jafri, J. Mannan, Y. Raashid, L. Al-Gazali, H. Hamamy, E. M. Valente, S. Gorman, R. Williams, D. P. McHale, J. N. Wood, F. M. Gribble, and C. G. Woods. 2006. 'An SCN9A channelopathy causes congenital inability to experience pain', *Nature*, 444: 894-8.

Cruccu, G., and L. Garcia-Larrea. 2004. 'Clinical utility of pain--laser evoked potentials', *Suppl Clin Neurophysiol*, 57: 101-10.

Davis, K. D., M. C. Bushnell, G. D. Iannetti, K. St Lawrence, and R. Coghill. 2015. 'Evidence against pain specificity in the dorsal posterior insula', *F1000Res*, 4: 362.

Davis, K. D., H. Flor, H. T. Greely, G. D. Iannetti, S. Mackey, M. Ploner, A. Pustilnik, I. Tracey, R. D. Treede, and T. D. Wager. 2017. 'Brain imaging tests for chronic pain: medical, legal and ethical issues and recommendations', *Nat Rev Neurol*, 13: 624-38.

de Hemptinne, C., E. S. Ryapolova-Webb, E. L. Air, P. A. Garcia, K. J. Miller, J. G. Ojemann, J. L. Ostrem, N. B. Galifianakis, and P. A. Starr. 2013. 'Exaggerated phase-amplitude coupling in the primary motor cortex in Parkinson disease', *Proc Natl Acad Sci U S A*, 110: 4780-5.

Debono, D. J., L. J. Hoeksema, and R. D. Hobbs. 2013. 'Caring for patients with chronic pain: pearls and pitfalls', *J Am Osteopath Assoc*, 113: 620-7.

Decosterd, I., and C. J. Woolf. 2000. 'Spared nerve injury: an animal model of persistent peripheral neuropathic pain', *Pain*, 87: 149-58.

DeLong, E. R., D. M. DeLong, and D. L. Clarke-Pearson. 1988. 'Comparing the areas under two or more correlated receiver operating characteristic curves: a nonparametric approach', *Biometrics*, 44: 837-45.

Deuis, J. R., L. S. Dvorakova, and I. Vetter. 2017. 'Methods Used to Evaluate Pain Behaviors in Rodents', *Front Mol Neurosci*, 10: 284.

Deuis, J. R., Y. L. Lim, S. Rodrigues de Sousa, R. J. Lewis, P. F. Alewood, P. J. Cabot, and I. Vetter. 2014. 'Analgesic effects of clinically used compounds in novel mouse models of polyneuropathy induced by oxaliplatin and cisplatin', *Neuro Oncol*, 16: 1324-32.

Dickie, A. C., B. McCormick, V. Lukito, K. L. Wilson, and C. Torsney. 2017. 'Inflammatory Pain Reduces C Fiber Activity-Dependent Slowing in a Sex-Dependent Manner, Amplifying Nociceptive Input to the Spinal Cord', *Journal of Neuroscience*, 37: 6488-502.

Dowman, R., D. Rissacher, and S. Schuckers. 2008. 'EEG indices of tonic pain-related activity in the somatosensory cortices', *Clin Neurophysiol*, 119: 1201-12.

Duncan, G. H., and M. C. Albanese. 2003. 'Is there a role for the parietal lobes in the perception of pain?', *Adv Neurol*, 93: 69-86.

Eddy, N. B., and D. Leimbach. 1953. 'Synthetic analgesics. II. Dithienylbutenyl- and dithienylbutylamines', *J Pharmacol Exp Ther*, 107: 385-93.

Engel, A. K., and W. Singer. 2001. 'Temporal binding and the neural correlates of sensory awareness', *Trends Cogn Sci*, 5: 16-25.

Foley, P. L., H. M. Vesterinen, B. J. Laird, E. S. Sena, L. A. Colvin, S. Chandran, M. R. MacLeod, and M. T. Fallon. 2013. 'Prevalence and natural history of pain in adults with multiple sclerosis: systematic review and meta-analysis', *Pain*, 154: 632-42.

Friedman, J., T. Hastie, and R. Tibshirani. 2010. 'Regularization Paths for Generalized Linear Models via Coordinate Descent', *J Stat Softw*, 33: 1-22.

Fries, P. 2009. 'Neuronal gamma-band synchronization as a fundamental process in cortical computation', *Annu Rev Neurosci*, 32: 209-24.

Frot, M., and F. Mauguiere. 2003. 'Dual representation of pain in the operculo-insular cortex in humans', *Brain*, 126: 438-50.

Fu, B., S. N. Wen, B. Wang, K. Wang, J. Y. Zhang, and S. J. Liu. 2018. 'Acute and chronic pain affects local field potential of the medial prefrontal cortex in different band neural oscillations', *Mol Pain*, 14: 1744806918785686.

Gold, M. S., and G. F. Gebhart. 2010. 'Nociceptor sensitization in pain pathogenesis', *Nat Med*, 16: 1248-57.

Greffrath, W., U. Baumgartner, and R. D. Treede. 2007. 'Peripheral and central components of habituation of heat pain perception and evoked potentials in humans', *Pain*, 132: 301-11.

Gregory, N. S., A. L. Harris, C. R. Robinson, P. M. Dougherty, P. N. Fuchs, and K. A. Sluka. 2013. 'An overview of animal models of pain: disease models and outcome measures', *J Pain*, 14: 1255-69.

Gross, J., A. Schnitzler, L. Timmermann, and M. Ploner. 2007. 'Gamma oscillations in human primary somatosensory cortex reflect pain perception', *PLoS Biol*, 5: e133.

Gu, X., Z. Gao, X. Wang, X. Liu, R. T. Knight, P. R. Hof, and J. Fan. 2012. 'Anterior insular cortex is necessary for empathetic pain perception', *Brain*, 135: 2726-35.

Hadjidimitrakis, K., S. Bakola, Y. T. Wong, and M. A. Hagan. 2019. 'Mixed Spatial and Movement Representations in the Primate Posterior Parietal Cortex', *Front Neural Circuits*, 13: 15.

Hargreaves, K., R. Dubner, F. Brown, C. Flores, and J. Joris. 1988. 'A new and sensitive method for measuring thermal nociception in cutaneous hyperalgesia', *Pain*, 32: 77-88.

Harris-Bozer, A. L., and Y. B. Peng. 2016. 'Inflammatory pain by carrageenan recruits low-frequency local field potential changes in the anterior cingulate cortex', *Neurosci Lett*, 632: 8-14.

Hartley, C., E. P. Duff, G. Green, G. S. Mellado, A. Worley, R. Rogers, and R. Slater. 2017. 'Nociceptive brain activity as a measure of analgesic efficacy in infants', *Science Translational Medicine*, 9.

Howard, C. J., N. Bashir, M. Chechlacz, and G. W. Humphreys. 2016. 'Neural Mechanisms of Temporal Resolution of Attention', *Cereb Cortex*, 26: 2952-69.

Hu, L., M. M. Cai, P. Xiao, F. Luo, and G. D. Iannetti. 2014. 'Human brain responses to concomitant stimulation of Adelta and C nociceptors', *Journal of Neuroscience*, 34: 11439-51.

Hutchison, W. D., K. D. Davis, A. M. Lozano, R. R. Tasker, and J. O. Dostrovsky. 1999. 'Pain-related neurons in the human cingulate cortex', *Nat Neurosci*, 2: 403-5.

Iannetti, G. D., A. Truini, A. Romaniello, F. Galeotti, C. Rizzo, M. Manfredi, and G. Cruccu. 2003. 'Evidence of a specific spinal pathway for the sense of warmth in humans', *Journal of Neurophysiology*, 89: 562-70.

Isnard, J., M. Magnin, J. Jung, F. Mauguiere, and L. Garcia-Larrea. 2011. 'Does the insula tell our brain that we are in pain?', *Pain*, 152: 946-51.

Jensen, M. P., K. J. Gertz, A. E. Kupper, A. L. Braden, J. D. Howe, S. Hakimian, and L. H. Sherlin. 2013. 'Steps toward developing an EEG biofeedback treatment for chronic pain', *Appl Psychophysiol Biofeedback*, 38: 101-8.

Jessberger, J., W. Zhong, J. Brankack, and A. Draguhn. 2016. 'Olfactory Bulb Field Potentials and Respiration in Sleep-Wake States of Mice', *Neural Plast*, 2016: 4570831.

Jones, M. D., J. L. Taylor, J. Booth, and B. K. Barry. 2016. 'Exploring the Mechanisms of Exercise-Induced Hypoalgesia Using Somatosensory and Laser Evoked Potentials', *Front Physiol*, 7: 581.

Jun, J. J., N. A. Steinmetz, J. H. Siegle, D. J. Denman, M. Bauza, B. Barbarits, A. K. Lee, C. A. Anastassiou, A. Andrei, C. Aydin, M. Barbic, T. J. Blanche, V. Bonin, J. Couto, B. Dutta, S. L. Gratiy, D. A. Gutnisky, M. Hausser, B. Karsh, P.

Ledochowitsch, C. M. Lopez, C. Mitelut, S. Musa, M. Okun, M. Pachitariu, J. Putzeys, P. D. Rich, C. Rossant, W. L. Sun, K. Svoboda, M. Carandini, K. D. Harris, C. Koch, J. O'Keefe, and T. D. Harris. 2017. 'Fully integrated silicon probes for high-density recording of neural activity', *Nature*, 551: 232-36.

Kajikawa, Y., and C. E. Schroeder. 2011. 'How local is the local field potential?', *Neuron*, 72: 847-58.

Karlin, L. 1970. 'Cognition, Preparation, and Sensory-Evoked Potentials', *Psychological Bulletin*, 73: 122-36.

Knotkova, H., M. Pappagallo, and A. Szallasi. 2008. 'Capsaicin (TRPV1 Agonist) therapy for pain relief: farewell or revival?', *Clin J Pain*, 24: 142-54.

Kucyi, A., and K. D. Davis. 2015. 'The dynamic pain connectome', *Trends Neurosci*, 38: 86-95.

LeBlanc, B. W., P. M. Bowary, Y. C. Chao, T. R. Lii, and C. Y. Saab. 2016. 'Electroencephalographic signatures of pain and analgesia in rats', *Pain*, 157: 2330-40.

Leblanc, B. W., T. R. Lii, A. E. Silverman, R. T. Alleyne, and C. Y. Saab. 2014. 'Cortical theta is increased while thalamocortical coherence is decreased in rat models of acute and chronic pain', *Pain*, 155: 773-82.

Legatt, A. D., J. Arezzo, and H. G. Vaughan, Jr. 1980. 'Averaged multiple unit activity as an estimate of phasic changes in local neuronal activity: effects of volume-conducted potentials', *J Neurosci Methods*, 2: 203-17.

Legrain, V., G. D. Iannetti, L. Plaghki, and A. Mouraux. 2011. 'The pain matrix reloaded: a salience detection system for the body', *Prog Neurobiol*, 93: 111-24.

Lenz, F. A., M. Rios, A. Zirh, D. Chau, G. Krauss, and R. P. Lesser. 1998. 'Painful stimuli evoke potentials recorded over the human anterior cingulate gyrus', *Journal of Neurophysiology*, 79: 2231-4.

Lewis, T., and E. E. Pochin. 1937. 'The double pain response of the human skin to a single stimulus', *Clinical Science*, 3: 67-76.

Li, L., X. Liu, C. Cai, Y. Yang, D. Li, L. Xiao, D. Xiong, L. Hu, and Y. Qiu. 2016. 'Changes of gamma-band oscillatory activity to tonic muscle pain', *Neurosci Lett*, 627: 126-31.

Li, P., E. A. Stuart, and D. B. Allison. 2015. 'Multiple Imputation: A Flexible Tool for Handling Missing Data', *JAMA*, 314: 1966-7.

Lieberman, M. D., and N. I. Eisenberger. 2015. 'The dorsal anterior cingulate cortex is selective for pain: Results from large-scale reverse inference', *Proc Natl Acad Sci U S A*, 112: 15250-5.

Luger, N. M., M. A. Sabino, M. J. Schwei, D. B. Mach, J. D. Pomonis, C. P. Keyser, M. Rathbun, D. R. Clohisy, P. Honore, T. L. Yaksh, and P. W. Mantyh. 2002. 'Efficacy of systemic morphine suggests a fundamental difference in the mechanisms that generate bone cancer vs inflammatory pain', *Pain*, 99: 397-406.

Luo, H., Y. Huang, X. Xiao, W. Dai, Y. Nie, X. Geng, A. L. Green, T. Z. Aziz, and S. Wang. 2020. 'Functional dynamics of thalamic local field potentials correlate with modulation of neuropathic pain', *Eur J Neurosci*, 51: 628-40.

Maiaru, M., C. Leese, M. Certo, I. Echeverria-Altuna, A. S. Mangione, J. Arsenault, B. Davletov, and S. P. Hunt. 2018. 'Selective neuronal silencing using synthetic botulinum molecules alleviates chronic pain in mice', *Science Translational Medicine*, 10.

Melzack, R. 1999. 'From the gate to the neuromatrix', *Pain*, Suppl 6: S121-6.

Merskey, H. 1986. 'Classification of chronic pain. Descriptions of chronic pain syndromes and definitions of pain terms. Prepared by the International Association for the Study of Pain, Subcommittee on Taxonomy', *Pain Suppl*, 3: S1-226.

Mogil, J. S. 2009. 'Animal models of pain: progress and challenges', *Nature Reviews Neuroscience*, 10: 283-94.

Mouraux, A., A. Diukova, M. C. Lee, R. G. Wise, and G. D. Iannetti. 2011. 'A multisensory investigation of the functional significance of the "pain matrix"', *Neuroimage*, 54: 2237-49.

Mouraux, A., and G. D. Iannetti. 2018. 'The search for pain biomarkers in the human brain', *Brain*, 141: 3290-307.

Neugebauer, V. 2015. 'Amygdala pain mechanisms', *Handb Exp Pharmacol*, 227: 261-84.

Nguyen Chi, V., C. Muller, T. Wolfenstetter, Y. Yanovsky, A. Draguhn, A. B. Tort, and J. Brankack. 2016. 'Hippocampal Respiration-Driven Rhythm Distinct from Theta Oscillations in Awake Mice', *Journal of Neuroscience*, 36: 162-77.

Nickel, M. M., E. S. May, L. Tiemann, P. Schmidt, M. Postorino, S. Ta Dinh, J. Gross, and M. Ploner. 2017. 'Brain oscillations differentially encode noxious stimulus intensity and pain intensity', *Neuroimage*, 148: 141-47.

Nir, R. R., A. Sinai, R. Moont, E. Harari, and D. Yarnitsky. 2012. 'Tonic pain and continuous EEG: prediction of subjective pain perception by alpha-1 power during stimulation and at rest', *Clin Neurophysiol*, 123: 605-12.

Norcia, A. M., L. G. Appelbaum, J. M. Ales, B. R. Cottereau, and B. Rossion. 2015. 'The steady-state visual evoked potential in vision research: A review', *J Vis*, 15: 4.

Ohara, S., N. E. Crone, N. Weiss, R. D. Treede, and F. A. Lenz. 2004. 'Amplitudes of laser evoked potential recorded from primary somatosensory, parasylvian and medial frontal cortex are graded with stimulus intensity', *Pain*, 110: 318-28.

Paxinos, George, and Keith Franklin 2019. *Paxinos and Franklin's the Mouse Brain in Stereotaxic Coordinates* (Academic Press).

Peng, W., L. Hu, Z. Zhang, and Y. Hu. 2014. 'Changes of spontaneous oscillatory activity to tonic heat pain', *Plos One*, 9: e91052.

Peng, W., X. Xia, M. Yi, G. Huang, Z. Zhang, G. Iannetti, and L. Hu. 2018. 'Brain oscillations reflecting pain-related behavior in freely moving rats', *Pain*, 159: 106-18.

Pitzer, C., R. Kuner, and A. Tappe-Theodor. 2016. 'Voluntary and evoked behavioral correlates in inflammatory pain conditions under different social housing conditions', *Pain Rep*, 1: e564.

Plaghki, L., and A. Mouraux. 2003. 'How do we selectively activate skin nociceptors with a high power infrared laser? Physiology and biophysics of laser stimulation', *Neurophysiol Clin*, 33: 269-77.

Ploner, M., C. Sorg, and J. Gross. 2017. 'Brain Rhythms of Pain', *Trends Cogn Sci*, 21: 100-10.

Rainville, P., G. H. Duncan, D. D. Price, B. Carrier, and M. C. Bushnell. 1997. 'Pain affect encoded in human anterior cingulate but not somatosensory cortex', *Science*, 277: 968-71.

Reinhart, R. M. G., and J. A. Nguyen. 2019. 'Working memory revived in older adults by synchronizing rhythmic brain circuits', *Nat Neurosci*, 22: 820-27.

Rohlfing, I., and C. Q. Schneider. 2018. 'A Unifying Framework for Causal Analysis in Set-Theoretic Multimethod Research', *Sociological Methods & Research*, 47: 37-63.

Rubin, D. B., and N. Schenker. 1986. 'Multiple Imputation for Interval Estimation from Simple Random Samples with Ignorable Nonresponse', *Journal of the American Statistical Association*, 81: 366-74.

Sandkuhler, J. 2009. 'Models and mechanisms of hyperalgesia and allodynia', *Physiol Rev*, 89: 707-58.

Sawamoto, N., M. Honda, T. Okada, T. Hanakawa, M. Kanda, H. Fukuyama, J. Konishi, and H. Shibasaki. 2000. 'Expectation of pain enhances responses to nonpainful somatosensory stimulation in the anterior cingulate cortex and parietal operculum/posterior insula: an event-related functional magnetic resonance imaging study', *Journal of Neuroscience*, 20: 7438-45.

Scheffzuk, C., V. I. Kukushka, A. L. Vyssotski, A. Draguhn, A. B. Tort, and J. Brankack. 2011. 'Selective coupling between theta phase and neocortical fast gamma oscillations during REM-sleep in mice', *Plos One*, 6: e28489.

Schneider, F., U. Habel, H. Holthusen, C. Kessler, S. Posse, H. W. Muller-Gartner, and J. O. Arndt. 2001. 'Subjective ratings of pain correlate with subcortical-limbic blood flow: an fMRI study', *Neuropsychobiology*, 43: 175-85.

Schulz, E., E. S. May, M. Postorino, L. Tiemann, M. M. Nickel, V. Witkovsky, P. Schmidt, J. Gross, and M. Ploner. 2015. 'Prefrontal Gamma Oscillations Encode Tonic Pain in Humans', *Cereb Cortex*, 25: 4407-14.

Segerdahl, A. R., M. Mezue, T. W. Okell, J. T. Farrar, and I. Tracey. 2015. 'The dorsal posterior insula is not an island in pain but subserves a fundamental role - Response to: "Evidence against pain specificity in the dorsal posterior insula" by Davis et al', *F1000Res*, 4: 1207.

Sestieri, C., G. L. Shulman, and M. Corbetta. 2017. 'The contribution of the human posterior parietal cortex to episodic memory', *Nature Reviews Neuroscience*, 18: 183-92.

Shackman, A. J., T. V. Salomons, H. A. Slagter, A. S. Fox, J. J. Winter, and R. J. Davidson. 2011. 'The integration of negative affect, pain and cognitive control in the cingulate cortex', *Nature Reviews Neuroscience*, 12: 154-67.

Shao, S., K. Shen, K. Yu, E. P. Wilder-Smith, and X. Li. 2012. 'Frequency-domain EEG source analysis for acute tonic cold pain perception', *Clin Neurophysiol*, 123: 2042-9.

Shen, Z., Y. Zhu, B. Liu, Y. Liang, Q. He, J. Sun, Z. Wu, H. Zhang, S. Yao, X. He, J. Fang, and X. Shao. 2019. 'Effects of Electroacupuncture on Pain Memory-Related Behaviors and Synchronous Neural Oscillations in the Rostral Anterior Cingulate Cortex in Freely Moving Rats', *Neural Plast*, 2019: 2057308.

Simons, L. E., E. A. Moulton, C. Linnman, E. Carpino, L. Becerra, and D. Borsook. 2014. 'The human amygdala and pain: evidence from neuroimaging', *Hum Brain Mapp*, 35: 527-38.

Singer, W. 2018. 'Neuronal oscillations: unavoidable and useful?', *Eur J Neurosci*, 48: 2389-98.

Sirota, A., J. Csicsvari, D. Buhl, and G. Buzsaki. 2003. 'Communication between neocortex and hippocampus during sleep in rodents', *Proc Natl Acad Sci U S A*, 100: 2065-9.

Starr, C. J., L. Sawaki, G. F. Wittenberg, J. H. Burdette, Y. Oshiro, A. S. Quevedo, and R. C. Coghill. 2009. 'Roles of the insular cortex in the modulation of pain: insights from brain lesions', *Journal of Neuroscience*, 29: 2684-94.

Tappe-Theodor, A., and R. Kuner. 2014. 'Studying ongoing and spontaneous pain in rodents--challenges and opportunities', *Eur J Neurosci*, 39: 1881-90.

Tort, A. B., R. Komorowski, H. Eichenbaum, and N. Kopell. 2010. 'Measuring phase-amplitude coupling between neuronal oscillations of different frequencies', *Journal of Neurophysiology*, 104: 1195-210.

Tort, A. B. L., J. Brankack, and A. Draguhn. 2018. 'Respiration-Entrained Brain Rhythms Are Global but Often Overlooked', *Trends Neurosci*, 41: 186-97.

Treede, R. D., A. V. Apkarian, B. Bromm, J. D. Greenspan, and F. A. Lenz. 2000. 'Cortical representation of pain: functional characterization of nociceptive areas near the lateral sulcus', *Pain*, 87: 113-9.

Treede, R. D., S. Kief, T. Holzer, and B. Bromm. 1988. 'Late somatosensory evoked cerebral potentials in response to cutaneous heat stimuli', *Electroencephalogr Clin Neurophysiol*, 70: 429-41.

Treede, R. D., J. Lorenz, and U. Baumgartner. 2003. 'Clinical usefulness of laser-evoked potentials', *Neurophysiol Clin*, 33: 303-14.

Uhelski, M. L., M. A. Davis, and P. N. Fuchs. 2012. 'Pain affect in the absence of pain sensation: evidence of asomaesthesia after somatosensory cortex lesions in the rat', *Pain*, 153: 885-92.

Uhlhaas, P. J., and W. Singer. 2006. 'Neural synchrony in brain disorders: relevance for cognitive dysfunctions and pathophysiology', *Neuron*, 52: 155-68.

Wager, T. D., L. Y. Atlas, M. M. Botvinick, L. J. Chang, R. C. Coghill, K. D. Davis, G. D. Iannetti, R. A. Poldrack, A. J. Shackman, and T. Yarkoni. 2016. 'Pain in the ACC?', *Proc Natl Acad Sci U S A*, 113: E2474-5.

Wang, X., S. Wang, W. Wang, J. Duan, M. Zhang, X. Lv, C. Niu, C. Tan, Y. Wu, J. Yang, S. Hu, and J. Xing. 2016. 'A novel intrinsic analgesic mechanism: the enhancement

of the conduction failure along polymodal nociceptive C-fibers', *Pain*, 157: 2235-47.

Yanovsky, Y., M. Ciatipis, A. Draguhn, A. B. Tort, and J. Brankack. 2014. 'Slow oscillations in the mouse hippocampus entrained by nasal respiration', *Journal of Neuroscience*, 34: 5949-64.

Yeomans, D. C., and H. K. Proudfit. 1994. 'Characterization of the foot withdrawal response to noxious radiant heat in the rat', *Pain*, 59: 85-94.

Yoburn, B. C., R. Morales, D. D. Kelly, and C. E. Inturrisi. 1984. 'Constraints on the tailflick assay: morphine analgesia and tolerance are dependent upon locus of tail stimulation', *Life Sci*, 34: 1755-62.

Zhang, X., W. Zhong, J. Brankack, S. W. Weyer, U. C. Muller, A. B. Tort, and A. Draguhn. 2016. 'Impaired theta-gamma coupling in APP-deficient mice', *Sci Rep*, 6: 21948.

Zhang, Z. G., L. Hu, Y. S. Hung, A. Mouraux, and G. D. Iannetti. 2012. 'Gamma-band oscillations in the primary somatosensory cortex--a direct and obligatory correlate of subjective pain intensity', *Journal of Neuroscience*, 32: 7429-38.

Zhong, W., M. Ciatipis, T. Wolfenstetter, J. Jessberger, C. Muller, S. Ponsel, Y. Yanovsky, J. Brankack, A. B. L. Tort, and A. Draguhn. 2017. 'Selective entrainment of gamma subbands by different slow network oscillations', *Proc Natl Acad Sci U S A*, 114: 4519-24.

Zou, H., and T. Hastie. 2005. 'Regularization and variable selection via the elastic net (vol B 67, pg 301, 2005)', *Journal of the Royal Statistical Society Series B-Statistical Methodology*, 67: 768-68.

Acknowledgements

My PhD study was accomplished in Institute of Physiology and Pathophysiology, Heidelberg University, with financial supports by China Scholarship Council (CSC), SFB 1158 and the research group of Prof. Andreas Draguhn.

I would like to express my deepest gratitude to all those who have offered me help and support in the whole process of my dissertation writing and my PhD study.

First of all, my heartiest thanks flow to my Supervisor, Prof. Andreas Draguhn, for offering me the opportunity to do neuroscience studies. I'm always grateful that he accepted me, a student with little neuroscience background, to be a member of his research group. From here, I took my first step to learn and arm myself with knowledge, techniques and multiple skills to be a neuroscience researcher. I appreciate it a lot for his tremendous help and support of both my PhD studies and my life in Germany. Besides, his excellent leadership deeply impresses me, and for me he is the model of a good lab leader. I'll always look up to him and hope that I can be a scientist like him one day.

Secondly, particular thanks go to my supervisor, Dr. Jurij Brankačk for his constant guidance, valuable advices and massive support on my projects and studies, even after his retirement. His scientific insights and rigorous scientific research attitude benefits me a lot.

I also want to thank Dr. Yevgenij Yanovsky (Genia) and Lee Embrey for giving me substantial technical support on building up the electrophysiological devices and on developing the custom made apparatus. Many thanks go to Simon Ponsel and Maximilian Pilz, who made great efforts together with me on my first project in electrophysiology.

Sincere thanks go to Katja Lankisch, Nadine Zuber and Tina Sackmann for their massive technical support. Thanks also go to Dr. Alexei Egorov, Dr. Claus Bruehl and Dr. Matin Both for assistance and support during my PhD study.

Many thanks go to my TAC committee, Prof. Thomas Kuner and Dr. Andre Rupp, for providing me valuable and helpful suggestions and comments on my studies. I also would

like to thank Prof. Rohini Kuner, Dr. Anke Tappe-Theodor and Dr. Linette Tan for their kind help on my project.

I would like to express my sincere gratitude to Susanne Bechtel, who gave me tremendous help in life when I moved to Heidelberg and though my whole PhD study. Thanks go to Weiwei Zhong for teaching me experimental skills and data analysis methods, as well as all the help and accompany in my daily life. I'd like to thank all Draguhn Lab members for sharing the past years together with me.

Particular thanks go to my dear friends in Germany, especially Xiaoli Shen (申晓莉) and Wei Huang (黄薇) for sharing so many happy hours together. I appreciate it a lot for the deep friendship of 小贝，圆圆 and 大爷 during the whole time since we first met each other in college, and hope that our friendship will last forever.

I would like to address special appreciation to my boyfriend Baifeng Qian (钱柏锋), for his care, accompany and support on my daily life as well as on my study.

Finally, I would like to thank my family who always support me and give me strength.

感谢我的父母对我的辛勤养育和教诲，和一直以来的包容、保护、理解与支持，让我能够健康成长，安心在德国学习和科研，并有勇气追求理想，努力成为更好的人。